Comparison of Technologies for Nano Device Prototyping with a Special Focus on Ion Beams - A review

Bruchhaus, L.; Mazarov, P.; Bischoff, L.; Gierak, J.; Wieck, A. D.; Hövel, H.;

Originally published:

January 2017

Applied Physics Reviews 4(2017), 011302-1-011302-52

DOI: https://doi.org/10.1063/1.4972262

Comparison of Technologies for Nano Device Prototyping with a Special Focus on Ion Beams - A review

L. Bruchhaus[1,a)], P. Mazarov[1,b)], L. Bischoff[2,c)], J. Gierak[3,d)], A. D. Wieck[4,e)], and H. Hövel[5,f)]

[1]Raith GmbH, Konrad-Adenauer-Allee 8, 44263 Dortmund (Germany)

[2]Helmholtz-Zentrum Dresden-Rossendorf, Institute of Ion Beam Physics and Materials Research, Bautzner Landstrasse 400, 01328 Dresden (Germany)

[3]LPN-CNRS, Route de Nozay, 91460 Marcoussis (France)

[4]Angewandte Festkörperphysik, Ruhr-Universtät Bochum, Universitätsstr. 150, D-44780 Bochum (Germany)

[5]Fakultät für Physik / DELTA, Technische Universität Dortmund, Otto-Hahn-Str. 4, 44221 Dortmund (Germany)

[a)]corresponding author: Lars.Bruchhaus@raith.de

[b)] Paul.Mazarov@raith.de

[c)] l.bischoff@hzdr.de

[d)] jacques.gierak@lpn.cnrs.fr

[e)] Andreas.Wieck@ruhr-uni-bochum.de

[f)] heinz.hoevel@tu-dortmund.de

Keywords: nanotechnology, nano device protoyping, nano patterning, nano fabrication, focused ion beam, electron beam lithography, self-organized 3D epitaxy, atomic / scanning probe nano patterning, magnetics, photonics, fluidics, implantation

Abstract

Nano device prototyping (NDP) is essential for realizing and assessing ideas as well as theories in form of nano devices, before they can be made available in or as commercial products. In this review, application results patterned similarly as in the semiconductor industry (for cell phone, computer processors or memory) will be presented. For NDP some requirements are different, thus different technologies are employed. Currently, in NDP, for many applications direct write Gaussian vector scan electron beam lithography (EBL) is used to define the required features in organic resist on this scale.

We will take a look at many application results carried out by EBL, self-organized 3D epitaxy, atomic probe microscopy (STM / AFM) and in more detail ion beam techniques. For ion beam techniques there is a special focus on those based upon liquid metal (alloy) ion sources (LM(A)IS), as recent developments have significantly increased their applicability for NDP.

Table of contents

I. Preface

Nanotechnology is a term for analyzing or artificially creating features with at least one physical dimension below 100 nanometer (nm), which is $1 \cdot 10^{-7}$ m or 10 millions of a meter [1] down to even the 1 Ångstrom (Å = $1 \cdot 10^{-10}$ m) level [2]. The general public can sometimes find it hard to grasp these dimensions. For purpose of "public outreach" consider the examples shown in FIG. 1 below. FIG. 1 a) is a hair from a typical human head, having a diameter of about 120 micrometers (µm) (or $120 \cdot 10^{-6}$ m), which is 1200 times larger than the 100 nm height of the triangular-shaped nanostructured object of FIG. 1 b). This same relative, vast difference in scale factor is depicted between the living objects of FIG. 1 c) and d): A giraffe (which can be up to 6 m high [3]) is compared to a Lasius (or moisture ant, about 0.005 m long [4]). Another possibility to visualize atomic, nano, mikro up to our makro world is shown in FIG. 1 e).

With a resolution of 5 nm, on a 170 mm long human hair, the whole bible could be written (pages in the same quality like an A4 laser printer with 300 dpi, assuming 1000 pages)!

a)

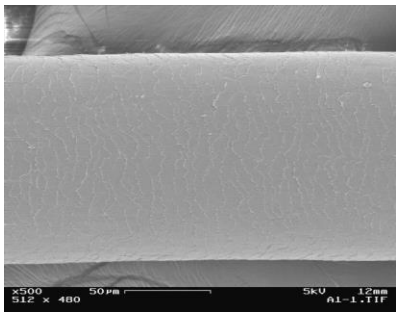
x500 50µm 5kV 12mm
512 x 480 A1-1.TIF

b)

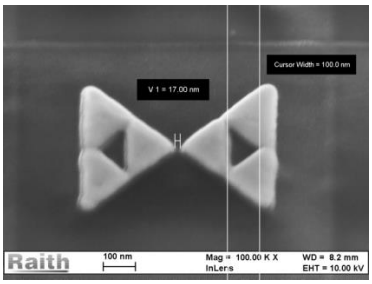
V 1 = 17.00 nm
Cursor Width = 100.0 nm
Raith
100 nm
Mag = 100.00 K X
InLens
WD = 8.2 mm
EHT = 10.00 kV

c)

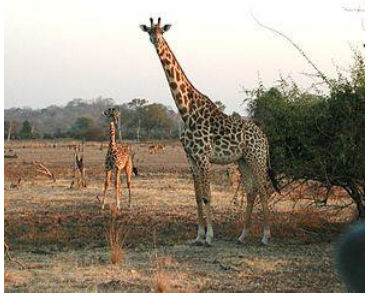

d)

e)

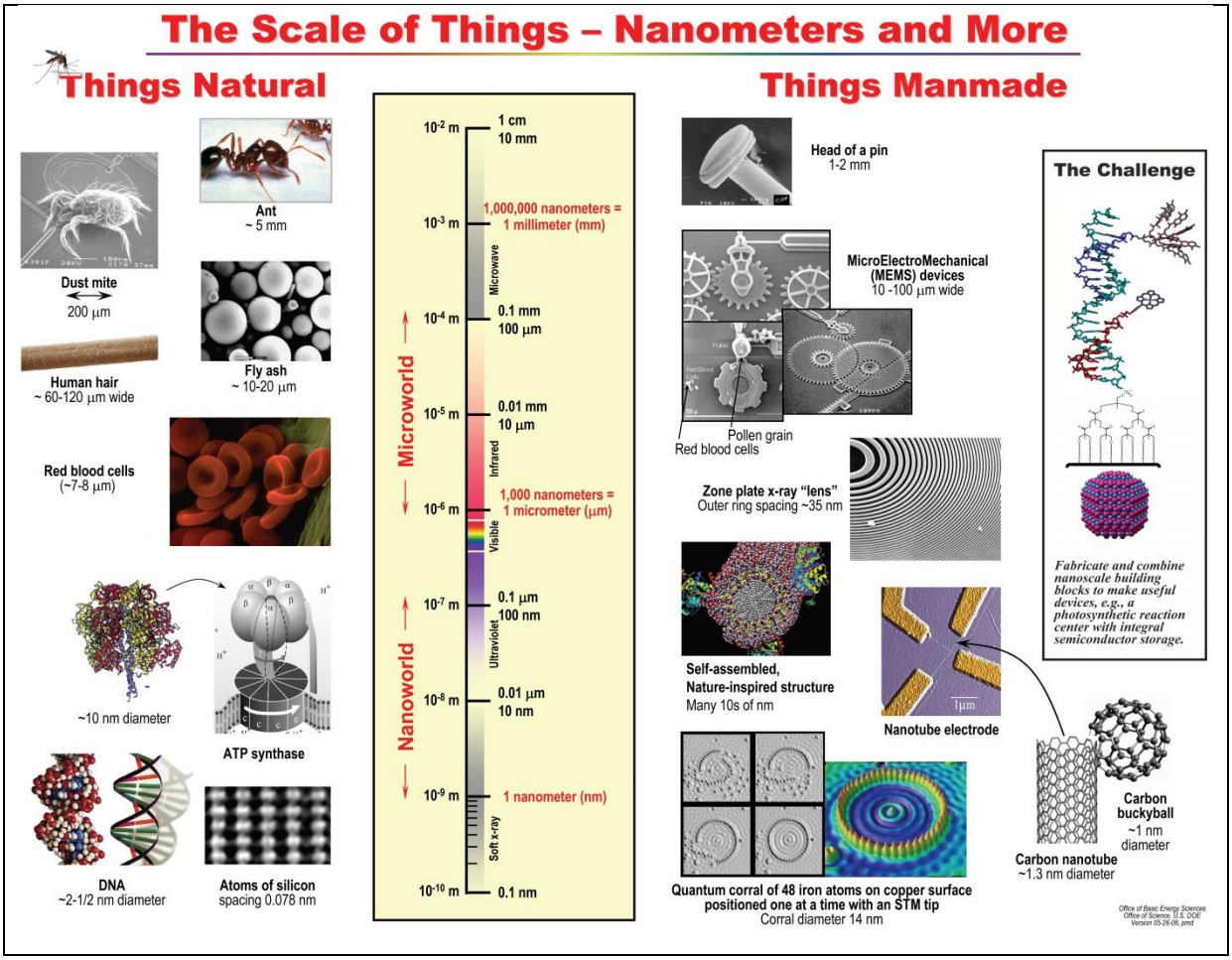

FIG. 1. a) SEM image of a hair of head (diameter about 120 µm),
Reprinted with permission from, courtesy of and copyright Univ. of Rochester / URnano [5]
b) SEM image of the inner part of a fractal bow tie (about 100 nm wide, patterned by a Ga LMIS into 5 nm Cr, 35 nm Au on a SiO_2 substrate),
Reprinted with permission from, courtesy of and copyright A. Elezzabi – Uni. Alberta and Application lab Raith GmbH More details of this work can be found in section V.E.2)
c) photograph of a giraffe (height can be up to 6 m) [3]
Reprinted with permission from public domain, courtesy of and copyright PD images John Walker - Images of Africa, taken from German Wikipedia
d) photograph of a Lasius (moisture ant, length up to about 5 mm) [6]
Reprinted with permission from GNU Free Documentation License, courtesy of and copyright Sarefo Wikipedia
e) sketch: "from atoms, nano, mikro to the makro world ", used with permission and copyright Office of Basic Energy Sciences (BES) for the U.S. Department of Energy (2006) [7]

Another definition for nanotechnology "is the study of the control of matter on an atomic and molecular scale…." [8]. Ensembles of nanoparticles can display new and extraordinary properties [9], for example optical, electronic and magnetic ones. They depend on the size, period and elemental composition, which are different from bulk surfaces or discrete nanoparticles [10], [11], [12], [13], [14]. The properties are a result of interactions between the excitons, magnetic moments, surface plasmons of individual nanoparticles [10] or the surface. Nevertheless care has to be taken not all small ensembles "… exhibit no unusual properties in the nanoparticle regime…" [15].

Nanotechnology is a key enabling technology [16] for the following tasks: First analyzing naturally occurring structures or features on this scale or those created artificially, to verify theories, device concepts, or generate new ideas. Second, it can be employed "… to create many… new materials … with wide-ranging applications in medicine, electronics, energy production …" [8], energy storage, reduction of device energy consumption or higher device speed as well as efficiency (of solar cells [17]), quantum mechanics, optics, or biomimetics [18] (or bionics [19]), so models can be further refined or new ones created. Third nanotechnology can be used to further study these ideas and theories or to convert them into new devices (machines, ideas, theories …) realizing functionalities. The order of these 3 steps will vary.

In nanopatterning there exists the differentiation between so called top-down and bottom-up approaches. Bottom-up means placing specific nano components, molecules or atoms in desired periodicities exploiting atomic forces and growth interactions to get the desired features, without human interaction [20]. "Assembly of small building blocks such as atoms, molecules and nanoparticles into macroscopic structures—that is, 'bottom up' assembly—is a theme that runs through chemistry, biology and material science" [21]. "Bacteria, macromolecules and nanoparticles can self-assemble, generating ordered structures with a precision that challenges current lithographic techniques." [21].

Top-down or lithography means creating features of a designed shape on the sample surface [9]. Some regard (lateral) pattern definition or lithography on this scale as the most crucial step [22]. It has to be taken into account, that feature definition inside organic resists is in many process chains only one step. Especially with increasing requirements as shrinking feature sizes other process steps also can become crucial. Top-down examples are techniques like optical lithography [23], [24], nano imprint [25], [26] or electron beam lithography (EBL) [27], [22]. They employ a hardware mask / template or a software design to create features on the sample surface directly or via a transfer process. "A key difference from the bottom-up approach is that, in the top-down approach, the parts or chips are both patterned and built in place, so that no assembly step is needed" [28]. "Assembly of nanoparticles as a controlled fashion also provides a link between 'top-down' and 'bottom-up' strategies for the construction of functional devices as well as flexible scaffolds for the introduction of chemical functionality" [9].

The scope of this review is to take a look at application results in **n**ano **d**evice **p**rototyping **(**NDP), which is similar to the feature definition in semiconductor volume production (for cell phone, computer processors or memory). We have categorized these by different fabrication techniques and processes. Accessible feature dimensions shall be smaller than 5 nm (at least in one dimension). R&D is an abbreviation for research and development. The term device is meant literally for any kind of function (electronic, magnetic, optical devices or surface morphologies ("tribology" [29]) created artificially to fulfil a task. We use prototyping to describe necessary process steps between the idea and the act of characterizing or measuring the device.

The ability to fabricate tiny features often follows an analytical ability and technique to see things on this scale [30], e.g. the current possibilities to resolve features on an Å level (such as transmission electron microscopy (TEM), He ion microscopy, or atomic probe microscopy (STM / AFM)). As a result, new analysis techniques can enable next generation fabrication ones. Sometimes they evolve directly from the analysis technique. In addition, analysis and patterning interdependently influence each other. Analysis techniques can be used to (in situ) control the patterning or improve theories. Nevertheless, it has to be taken into account that fabrication usually has different requirements than analysis.

Craftsmen and artists have a need for (complementary) tools as well as processes. So does applied fundamental research and nano device prototyping (NDP), especially as some fabrication processes have become quite complex [31]. Different technologies can be employed for arbitrary shape, high placement accuracy, or lateral nano pattering. Some are parallel (thus fast), like optical lithography [23], [24] (routinely employed in the semiconductor industry) and nano imprint [25], [26]. However we think these are not ideally suited for NDP in our definition, because of their high initial equipment, mask or template costs, the long times needed until first prototype devices are ready for measuring, and their high costs for small device (design) modifications, which belong to the prototyping phase. NDP requires flexibility and cost efficiency taking a small to mid-number of devices into account. For example a maskless technology has no need for expensive masks / templates, as CAD designs can be easily and quickly modified. These techniques are often serial (thus too slow for volume production applications), but less expensive and more flexible, so more often used in NDP environments. Some of the techniques presented here are capable in finishing the complete fabrication process in one instrument or even producing devices in only one process step.

A first example is a direct write serial focused charged particle beam technology called direct write electron beam lithography (EBL). Since decades it is the main tool for lateral nano patterning in research and development. However for EBL some over all process chains have become quite complex. In addition some application related requirements are difficult to fulfil (like perfect interfacing to the substrate).

Second, we take a look at two promising additional candidates: Atomic probe microscopy (STM / AFM) based patterning techniques and self-organized 3D epitaxy [32].

A third detailed example –which is the main focus of this work- are ion beam technologies (with a focus on liquid metal (alloy) ion source techniques). Already in 1959 Feynman announced this vision to use ions for nano fabrication in his talk ("There's Plenty of Room at the Bottom", later published under [33]). About 3 years later S.P. Newberry suggested ion beams for micro fabrication [34]. Recent technology breakthroughs in ion beam technologies have significantly improved their applicability for NDP. As the main focus of this review are nano device prototyping applications, further ion beam processes (also industrial ones) like circuit edit, cross sectioning, TEM lamella preparation and analysis applications will not be discussed.

We will briefly describe historical roots for each technique and involved processes. In addition the resulting applicability for NDP will be checked for each technology family with respect to the following criteria: the application resolution; minimum periodicities; interfacing to the surface; freedom for arbitrary geometry and shape; produce features at dedicated sample positions / locations, with a high accuracy; 3 dimensional objects; areas of coverage which exceed an instrument's single field of view; time required to develop a new process; the process know-how accessibility to the community ("standardization"); process and instrumentation maturity; over all time and efforts necessary to create devices which can be tested and measured ("time to device"); time required for design changes; versatility of the technology for all kind of applications and material systems; costs from idea to device ready for testing and the reproducibility for structuring more than a few devices up to the feasibility to run small scale production lines, Table II of section VI attempts to group and rank these various metrics. Depending on the application some of these capabilities are necessary during the prototyping phase, when devices and circuitry are often altered [35].

If a certain application is limited by, or perhaps even impossible to achieve, using conventional processing steps, exploring non-conventional technologies with unique capabilities may be a rewarding alternative. Firstly

though, as a starting point, we start –as a reference- with the most often applied technique: electron beam lithography (EBL).

II. Electron beam lithography (EBL)

II.A. Introduction

A technology for lateral pattern definition in nano device prototyping (NDP) is Gaussian beam vector scan [36] electron beam lithography (EBL) on organic resist [37], [38], [27]. Here, at least a sample preparation process step to cover the sample surface with resitst is needed, initially. Further on a development as well as a pattern transfer process step afterwards are required. The instruments employ acceleration energies from about 20 V to 125 keV [39] and [40], respectively. Different electron / matter interaction regimes in this energy range take place and further ones could be employed for NDP. Electron beam lithography is well suited for NDP, whereas optical lithography is widely used for semiconductor devices volume production [41] (for cell phone, computer processors or memory). Both possess a long history (EBL [42], optical lithography [43]), thus there exists dedicated instrumentation. They are currently the most commonly used top-down lateral pattern definition techniques allowing feature sizes in the regime of interest in organic resists, for the respective applications.
Now we will take a look at the history of EBL.

II.B. History

Electron beam lithography (EBL) possesses analytical roots to, the scanning electron microscopes (SEM) and the transmission electron microscopes (TEM). Early focussing attempts of “cathode rays” (electrons) were carried out by Hittorf (1869) and Birkeland (1869). They applied the rotationally symmetric field lying in front of a cylindrical magnet pole for focusing the rays [44]. In 1924 de’ Broglie discovered the wave nature of the electron [45]. This has been a starting point of the scientific field of electron diffraction (later called charged particle optics, CPO). Already in 1926 H. Busch has been able to calculate trajectories in an electron ray bundle and found that the magnetic field of a short coil has the same effect on an electron bundle as the convex glass lens with a defined focal length on a light bundle [44], [46]. Based on these calculations the first lenses have been created by Busch, Davisson and Calbick [44].
In 1933, Ruska has managed to overcome for the first time- the resolution barrier of an optical (visible light) microscope, employing electrons (magnification of 12,000 with an edge resolution of 50 nm) [47]. Almost at the same time, a competing group at AEG research labs in Germany (Brüche, Scherzer and Recknagel) managed to fabricate a similar electron microscope instrument. Differently to Knoll and Ruska, they have applied electrostatic lenses [46]. Later on, Ruska commercialized the SEM with the company Siemens. More about the history can be found in [48], [46], [49] and [50]. At the end of the 1930s technology advanced quickly due to the similar fundamental technology of electron microscopes, oscilloscopes and television sets. In 1932 applying de ’Broglie’s theory Knoll and Ruska estimated the resolution limit for a 75 kV electron microscope to 2.2 Å [51], this has been reached about 40 years later [44]. Today, leading-edge transmission electron microscopes (TEMs) employing special “correction lenses” -based upon K. Urban’s work [52], [53]- can resolve features below 1.6 Å with an acceleration voltage of 1 MV [54] or 300 kV [55]. A comprehensive overview about the history of micro and nano patterning is given in [56].

Already in the 1930s P. H. Carr has studied the electron recording properties of various materials. As possible image formation process he suggested the creation of deposited layers [57]. According to Schmallenberg [56] and Owen et al. [37] Buck and Shoulder's paper "An approach to microminiature printed systems" is among the first papers suggesting an electron beam patterning process creating devices in 1958. They suggested to locally deposit the gas tetraethoxysilane as silicaceous resist [58]. In 1967 M. Hatzakis and R.F.M. Thornley, (researchers from IBM) have published the fabrication of solid state devices employing an organic resist electron beam exposure technique [59]. They have used a resist called poly(methyl-methacrylate) (PMMA, a thermoplastic and transparent plastic) [60], also known under the name of "Plexiglas". PMMA is a high resolution organic resist which is sensitive to electron exposure and is still used by researchers today. In 1976 Broers et al. published remarkable 8 nm feature sizes reached by a deposition lithography process [61]. They deposited layers by extracting molecules from "the process" (sample handling contaminants of earlier process steps, vacuum chamber residuals, ...). Today dedicated process gases are intentionally and controllably injected by gas injection systems [62], [63]. Broers used the deposited layers as etch masks, so the uncovered areas could be etched away and the covered ones remained.

From the resist exposure process fundament by IBM researchers [64], [59], [60] and the various instrument development branches, electron beam resist lithography started its success story which still continues.

II.C. Fundamentals

II.C.1. Fundamental Instrument set-up

Electron beam lithography is either carried out in raster or fixed beam vector scan, variable shaped beam, projection or mixed modes [36], [27]. We'll focus here on Gaussian beam vector scan electron beam writers and their applications as they are the most commonly used ones in nano device prototyping (NDP).

Scanning electron microscopes (SEMs), focused ion beam (FIB) instruments, vector scan electron beam writers and vector scan focused ion beam nano patterning instruments all share a similar fundamental instrument, and column set-up. Depending on the application, the columns are equipped with different elements. In SEMs: lenses, deflection and stigmation are usually carried out electromagnetically, since all electrons are indistinguishable and have thus exactly the same mass. EBL writer have usually more than 2 lenses. For ions, this is different, they consist of several isotopes and possess a non neglible energy width. As magnetic fields disperse the momentum of different particle masses: lenses, deflection and astigmators are purely electrostatic in FIB – columns. Displayed in FIG. 2 is an ion beam column with such electrostatic lenses, deflection and stigmation, as all fundamental functions are represented and LM(A)IS FIBs are the main focus of this review article. A charged particle optics column is assembled on top of a vacuum chamber with for example electrons in normal incidence. In an EBL instrument they are optimized for maximum instrument resolution at reasonable probe currents (< 5 nm or guaranteed feature sizes below 10 nm [65], [66], [67], [68], [69]) and large calibrated write-fields (fields of view, deflection fields; illustrated by FIG. 3) with little beam shape and size deterioration away from the optical axis.

Electron extraction area	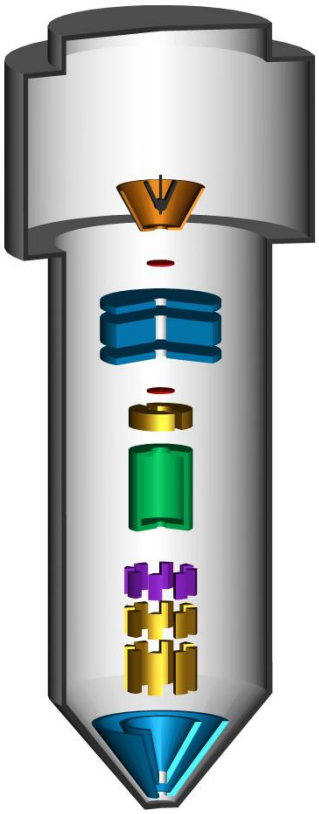
First lens	
Beam defining aperture	
Beam blanking	
Stigmation correction	
Beam deflection	
Final lens	

FIG. 2. Schematic of basic focused charged particle column set-up, courtesy of and copyright Raith design team

Electron sources are optimized for long term beam current stability and the instruments offer a selection of possible probe currents depending on the application, e.g. high resolution patterning. This is usually done with the assistance of an automated beam defining aperture exchanger, allowing to select the suitable probe current.

The software in EBL instruments has five major tasks: first an interface to the instrument hardware (adjust lenses, stigmator, vacuum control...), second carry out imaging of the sample surface, third design basic features, fourth pattern the features with a predefined dose and fifth program and execute complex unattended computer aided design (CAD) based patterning sequences, including the necessary machine parameter control loops (probe current, focus, dose,... which were just explained above). Some have the additional capability to design and store CAD patterns. If a pattern design (CAD structure) exceeds one write-field, the instruments can stitch several write fields together. Here the design is automatically cut into sub structures called write-fields (compare above). Then the content of the first one will be patterned at the desired position, followed by a sample stage movement to the next position, here a second write-field will be patterned and so on [41], alternatively the stage can be moved underneath the beam during patterning. Stage position sensing is usually realized employing a laser interferometer, with high precision. Consequently, complex and unattended batch nano structuring sequences can be programmed, like patterning sequences “over night” or “over week-end”, thus large areas with small features can be covered, well above one write-field. During the patterning sequence

different tool settings (for instance probe current and size) can be employed suiting different patterning requirements.

In addition the high positioning reproducibility can be used for multi-level patterning on top of existing patterns, generated by also by EBL or other techniques, for example imprint or optical lithography. Here the stage is driven to the desired sample position and an automatic mark recognition sequence including write-field recalibration is carried out.

II.C.2. Writing strategy

Fixed beam vector scan instruments step the electron beam within a designed geometry employing a selectable exposure grid (step size, "s" in FIG. 3) and dwell time. Between different features the electron beam is blanked to create well separated, defined features with incident electrons only inside the designed feature frames (for example a square) FIG. 3 illustrates how example geometries could be written [36]. Here the circles sketch the digital exposure steps; the electron beam is addressed to and waits here one dwell time long, before it is deflected to the next position (usually unblanked). The arrows indicate possible pathes ("line mode") how the electon beam could be moved along the sample surface within the designed geometry. Obviously the beam could travel any number of different directions or employ different strategies to effectively "fill in" the geometric shapes. Usually the stage is moved between different write-fields with the accuracy of a laser interferometer stage.

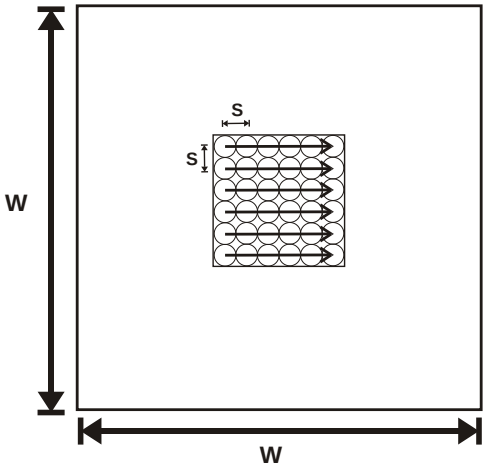

FIG. 3. Sketch of an exposure a write-field of edge length and height w, a vector scan process for a square., the circles indicate the exposure grid / step size (s) and the lines with arrows possible exposure paths ("line mode")

II.C.3. Interaction regimes

If electrons accelerated by 30 keV, hit the sample surface, then they transfer a momentum of about $9 \cdot 10^{-23}$ kg·m / s ($1.027 \cdot 10^{8}$ m / s · $9.1 \cdot 10^{-31}$ kg, relativistic corrections still being small [41]) and energy to it. This energy and momentum transfer result in different electron matter interaction regimes [27], [70]: atoms can be excited, molecules break or cross link, heat can be locally generated, the energy at the surface can be employed to cause chemical reactions between a precursor gas and the sample surface. These offer fascinating complementary possibilities [62], [63]. A gas injection system (gas supply) intentionally injects a precursor gas for a certain time. The energy transferred by the electron beam to the sample surface initiates a chemical reaction of components of the precursor gas with the sample surface. This is for example exploited for industrial applications like high end mask repair for optical lithography masks [71]. In addition the incident electrons can be backscattered out of the sample again.

II.C.4. Processes

Although different electron matter interaction regimes [27] are exploitable for NDP (nano device prototyping), the most commonly applied application is the exposure of organic resists. The lateral pattern definition inside the resist is followed by a development process step. In addition sample preparation and pattern transfer technologies are required [72]. Here the flux of the e^- deposits energy inside the resist. This can on one hand cause more resist molecules to be cut into shorter chains. This “chain scission” is the mechanism behind positive tone resist exposures, see FIG. 4 b). The shorter molecular chains are more soluble in a developer [38], [73]. As a result, exposed resist areas are removed during development. On the other hand, resist molecules can link to form longer molecule chains. This “cross linking” is used to define features in negative tone resists, see FIG. 4 c) [38], [73], rendering the exposed areas insoluble to developers, leading to a removal of the non-exposed areas during development. For some resists like PMMA the exposure dose defines whether it behaves like a positive tone resist or negative one (in case of PMMA a lower dose results in positive behavior and a very large dose to a negative one).

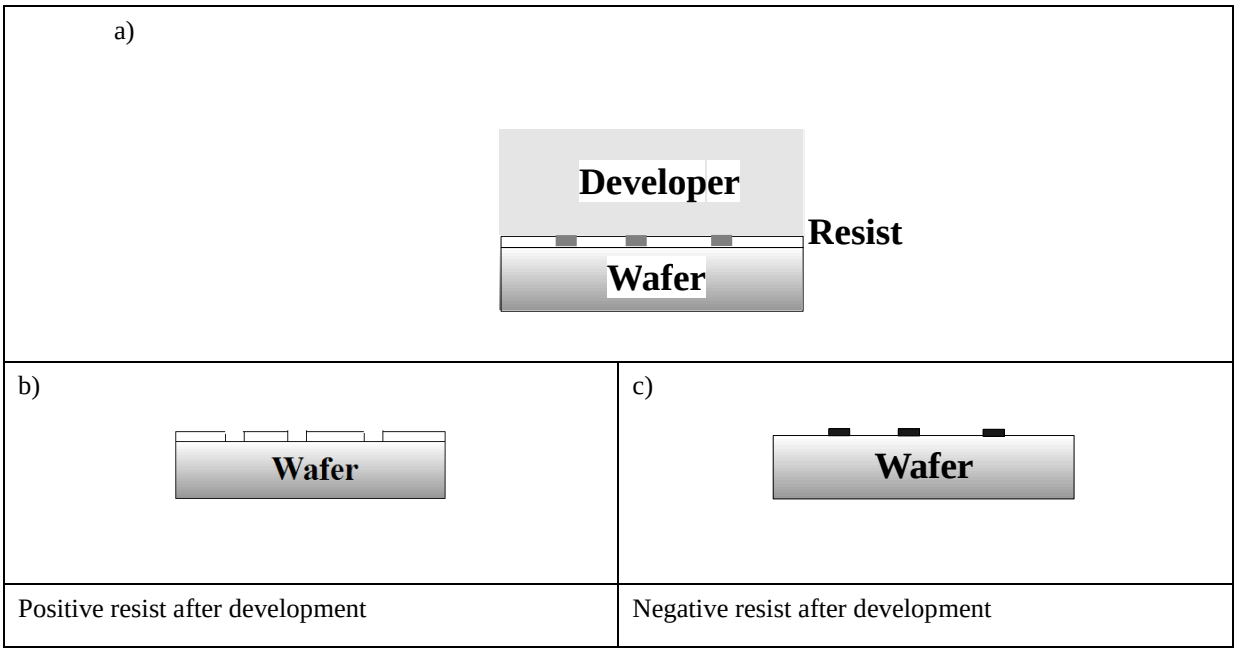

FIG. 4. Sketches (black rectangles ■ indicate irradiated regions) of a) exposed resist, b) diluted by the developer in the positive case or c) remain after developing in the negative case [74]

Electron beam resist based patterning techniques possess several limitations. First, in 3D patterning, as the standard resist exposure technique is a lateral feature definition one, so 3D patterning requires complex and dedicated processing [75] or exploiting a different electron matter interaction regime like electron beam deposition techniques. Second, electron sample interaction regimes lead to a relatively large interaction volume and electron backscattering, causing the so called proximity effect [37], making the accurate replication of the design complicated with the neccisity for a proximity correction. Third, it is usually an indirect technique with the need for pattern transfer. This can lead to multi step process chains [72], depending on the application. In addition creating interface defect free (for details see section III.C) devices -like quantum dots- can be difficult [14] and it can be challenging to find an appropriate resist for the resolution level or application of interest [22].

II.D. Examples of applications

First, a resist exposure example applying one of the oldest and still employed resist called PMMA in the positive mode is presented. It has been exposed by a 100 keV TEM, pattern transfer has been carried out by a lift-off process [77]. The electron beam has been blanked for a few (7 to 11) pixel in between the about 30 nm wire to create the necessary energy distribution inside the resist exploiting the proximity effect to reproducibly fabricate a very thin gate [77], see FIG. 5.

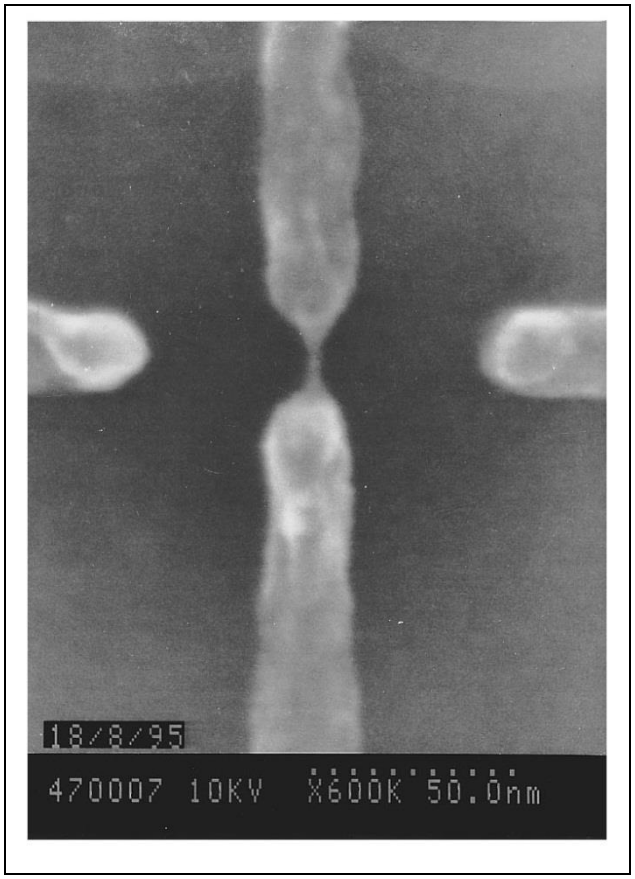

FIG. 5. SEM micrograh of a 3 nm wire close to other structures
Fig. 4 in [77], Reproduced with permission from Appl. Phys. Lett. **68**, 322 (1996). Copyright 1996 American Institute of Physics

Second, FIG. 6 shows a different example utilizing a promising, much younger, negative tone resist called hydrogen silsesquioxane (HSQ). In this case exposure was carried out with a 10 keV electron beam. Similar feature sizes have been reached by exposing the features classically, without the blanking pixels technique described above. There they applied a special development process: 4 min in aqueous 1 wt% NaOH, 4 wt% NaCl [78].

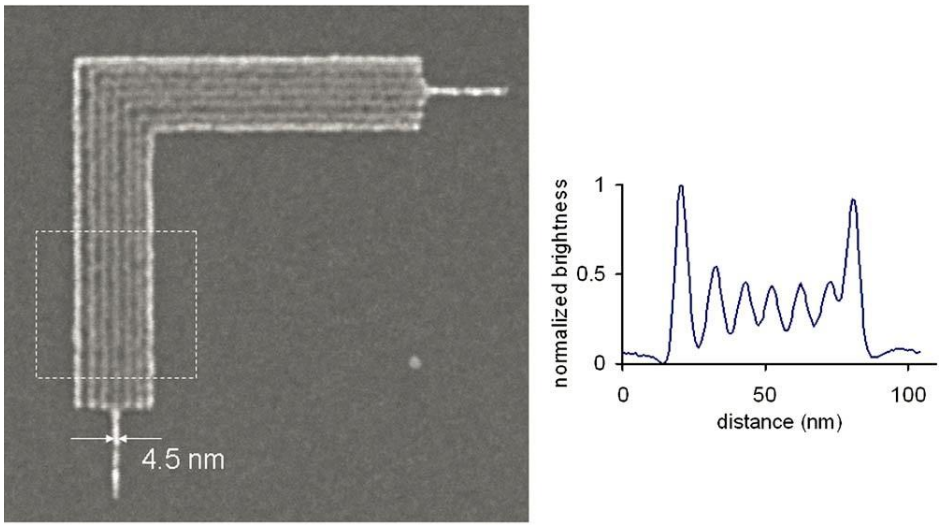

FIG. 6. SEM micrograph of 9 nm pitch structures in 10 nm thin HSQ resist, patterened at 10 kV
b) resulting brightness level averaged lines plot perpendicular to the features inside the dashed box of a)
FIG. 1 in [78], Reproduced with permission from J. Vac. Sci Technol. B **27**, 2622 (2009). Copyright 2009 American Vacuum Society

Third, as mentioned above electron beam induced deposition can be used as complementary patterning technique. An exemplary high resolution result by Dorp et al. is displayed in FIG. 7 a). It has been created utilizing a 200 keV scanning transmission electron microscope (STEM, spot size of about 0.35 nm) with $W(CO)_6$ as precursor. It has been imaged within the same instrument utilizing the high angle annular dark field (HAADF) mode [79]. An exemplary result for direct 3D micro patterning is shown in FIG. 7 b), using a SiO_2 precursor [80].

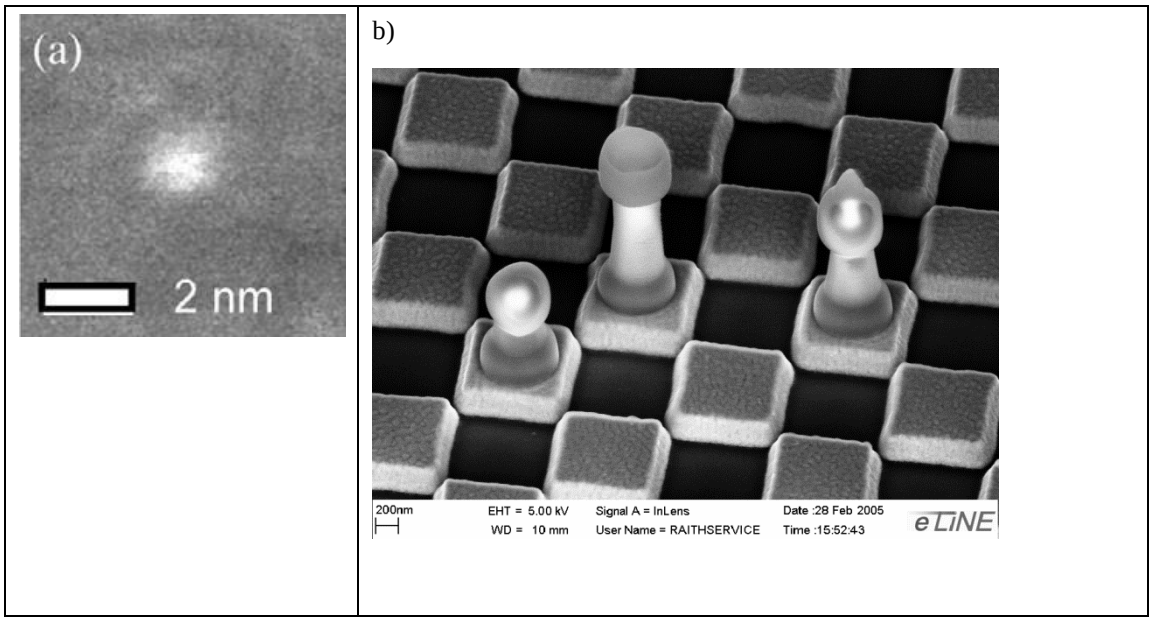

FIG. 7. (a) HAADF STEM micrograph of a dot patterned with a 0.35 nm spot size and $W(CO)_6$ as precursor, Fig. 10 in [79] © IOP Publishing, Reproduced with permission. All rights reserved
b) SEM micrograph of an electron beam micromachining example employing a SiO_2 precursor, deposited chess pieces on a Au / Si check board sample [80], courtesy of and copyright Raith Application team

Another focused electron beam-induced-deposition (FEBID) result is shown in FIG. 8: magnetic 3D structures [81]. In addition it displays a sketch of the experimental configuration and magneto-optic Kerr effect (MOKE) hysteresis loops from a 3D wire [81]. The MOKE configuration shown in Fig. 8(g) used on a tilted nanowire as displayed in Fig. 8(e) gave evidence of a 3D magnetic functionality of the nanowire by square hysteresis loops (see Fig. 8(h)). A deformation of the nanowire by laser-heating during the MOKE experiment (Fig. 8(f)) could be reduced by focusing the laser on the nanowire base close to the substrate [81].

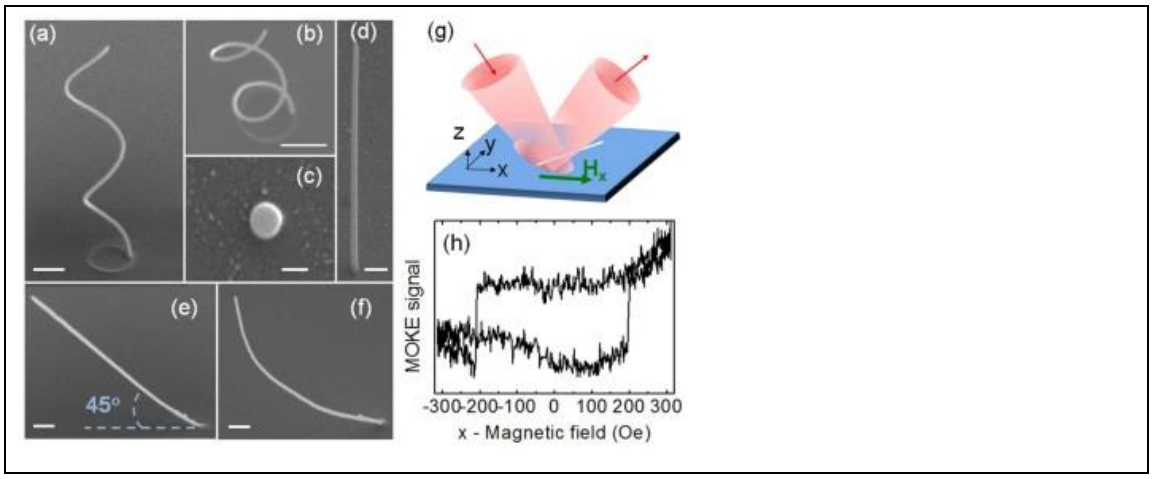

FIG. 8. "3D magnetic nanostructures grown by FEBID.
(a)-(f) SEM micrographs, The scale bar is 500 nm in all images, except for (c)
(a) and (b) Different views of a double-loop nano-spiral.
(c) Top-view of a straight NW, scale bar 100 nm
(d) and (e) Lateral view of NWs grown at 0 and 45 degrees, respectively, to the substrate plane.
(f) Curved NW after MOKE measurements.
(g) Sketch of the experimental configuration used to obtain MOKE hysteresis loops of 3D-NWs at 45 degrees.
(h) magneto-optic Kerr effect (MOKE) hysteresis loop of a 3D wire."
Fig. 1 in [81], Reproduced with permission from Scientific Reports **3**, 1492 (2013), Copyright 2013 Creative Commons

II.E. Capabilities for nano device prototyping

Focused electron beam analysis tools can be upgraded to patterning capabilties at moderate costs, if an adequate transmission or scanning electron microscope is available in the lab. They can be used for dedicated patterning applications, for example on the few devices, single field of view (FoV) level, without the requirement for high precision sample manipulation. Dedicated EBL writers have reached an unprecedented level of stability and maturity, thus they are expensive.

It has to be taken into account, that (electron) beam resist lithography usually covers only one process step in a device fabrication process. The developed resist pattern inside an organic resist has to be transferred, which can be challenging and time consuming depending on the application in addition the realizability of interface defect free (for details see section III.C) features depends on the other process steps.

If the other necessary process steps are fast and only a few nano devices needed, the overall time to device can be adequate for NDP, however EBL is a rather slow technology compared to optical projection lithography, so not suitable for volume production.

Large area patterning for prototyping applications is possible with high end instruments which offer: stability, placement accuracy, and reproducibility. As a result features < 10 nm can be patterned over large areas (> cm^2) or at different dedicated sample locations. In addition future device characteristic research can be carried out in semiconductor R&D sites, with instrument stage travel ranges of 200 mm (with 12" wafer handling capability) or larger [82]. This is in conformance with the current semiconductor fabrication process, and thus gives the

opportunity to partially pattern R&D wafers with this instruments and otherwise process them in the normal semiconductor production line [82].

As it is a top-down lithography technique which employs SW designs (no need for masks), the features can be easily and quickly altered, however the rest of the process to get finished devices has to be repeated. Little design modifications can only be realized expeditiously, if the rest of the process has not been changed.

EBL possesses significant advantages: its high resolution capabilities, half a century of usage and thus technology evolution with a resulting wide spread standardized process know-how, instrumentation as well as process maturity, a large technology flexibility by applying different pattern transfer techniques [83] and versatility for many applications, also utilizing different electron matter interaction regimes applicable to NDP. Although challenges applying EBL exists (examples given in section II.C.4); it is since decades the most commonly applied technology in nano device prototyping and for some special applications also for small scale production.

As the electron beam is a charged beam, the charge has to be removed from the sample surface, thus charge removal is necessary either by a somehow conducting sample, resist surface or by other means. Most applications and material systems can accommodate this, as many substrates are (semi) conducting and for high resolution small beam currents are required.

The techniques' capabilities for nano device prototyping will be summarized and compared with the others - covered in this article- in Table II.

II.F. Conclusion

With about 50 years of instrument and process development as well as evolution [84], the EBL technique and instrumentation have reached a high level of maturity (stability, pattern placement accuracy, resolution down to the sub 10 nm regime [78]) [83]. As a result the electron beam writer is the main lateral nano patterning tool in R&D and an essential part of many nano structuring activities. It is the first choice for nano device prototyping (NDP) [35], and for photo mask generation (however employing usually a different type of electron beam lithography, than Gaussion beam vector scan) [85]. These masks are necessary for optical "stepper" instruments in the semiconductor industry (for cell phone, computer processors or memory). It is ideally suited for a large range of complex lateral batch nano pattering tasks directly from CAD designs. It is capable in delivering the necessary resolution for many applications. Electron matter interaction regimes are mostly non-destructive to inorganic sample materials. The instrumentation gives flexible process control and can be realized with a high automation level for unattended batch nanofabrication. It is possible to select from a variety of commercially available EBL equipment solutions from attachments for SEMs / TEMs to dedicated >200 mm travel range Gaussian beam vector scan electron beam writers, suitable for a large range of applications, however these are not adequate for full 12" wafer exposure tasks. Challenges can occur if (pattern transfer) processes get too complicated or interface defect free features (for details see section III.C) are required. However, it is well suited for many R&D type nano device prototyping applications, which is the scope of this article. In addition many successfully applied processes in many different labs around the world are routinely applied; some of them with sub 5 nm resolution capabilities [78].

We now take a look at applications carried out by alternative techniques, starting with self-organized 3D epitaxy.

III. Self-organized 3D epitaxy

III.A. Introduction

A nano patterning technique -with fascinating potential- is a solid film crystalline growth process called self-organized 3D epitaxy. This bottom-up approach is a very efficient and parallel thus quick way of nanopatterning. Epitaxy is one important root of nanotechnology [86]. Epitaxy can be used to fabricate sharp monolayers- but initially it has not been used for lateral pattern definition. As a high quality layer deposition technique it is a central part of the standard process for semiconductor device fabrication for decades. These high quality films are employed to produce: solid state electronics, optoelectronics (high brightness LEDs), photonic devices [87], [14] like quantum wells or lasers, discrete bipolar transistors [88], high frequency transistors [20], random excess memory (RAM) [88], CMOS ICs [88] and thermoelectric modules [89], [20], [14]. "…The field spans the subnano to the macroscale, and covers both equilibrium and far-from-equilibrium systems with timescales that can vary from microseconds or less, to many years…" [15].

If certain process parameters are applied, regular three dimensional features can evolve, instead of thin films. This is called self-organized 3D epitaxy. Self-organized 3D epitaxy is a bottom up lateral pattern definition process, thus very different from commonly applied top-down nano patterning techniques.

Thin layer creation as well as self-organized 3D epitaxy can allow the realization of dedicated, and sometimes even unique physical properties. In the last two decades a prominent application for ordered nano structures with lattice matched growth and feature sizes smaller than 10 nm in three dimensions has evolved: The growth of interface defect free quantum dots, with many potential device applications, for example opto electronics [90], including lasers [91], [15], and single-electron transistors [20]. Quantum dots feature sizes have to be around 10 nm [14], so the charge can be confined in 3 dimensions [14], leading to 0-dimensional electronic systems. These can be charged via tunnel processes with a small and well defined number of electrons or holes. Thus, they are often referred to as "artificial atoms". Here the charge carriers occupy quantum states like in atoms, following the same Aufbau-principle in shells dominated s-, p-, d- shell and so forth [92].

III.B. History

This technique is a pure patterning one, without analytical roots. Early successful thin layer deposition experiments with controlled crystal grow have already been published in 1836 by Frankenheim [93]. He studied liquid phase epitaxy of sodium nitrate on calcite. First sputter metal deposits have been reported by Grove employing a glow discharge plasma in 1853 [94]. Four years later Faraday evaporated thin films by "…exploding fuselike metal wires in an inert atmosphere…" which is a different deposition technique [94]. From 1877, early applications have been to coat mirrors by sputtering [94]. At the end of the 1960's evaporation became also a wide spread deposition technique [94].

In 1938 Stranski and Krastanov published a theoretical paper about seed formation and nucleation during oriented growth processes [95], this is the theoretical fundament of the aforementioned self-organized 3D epitaxy. Since this time, the parallel progress in vacuum technology (surface quality), epitaxy equipment and

analysis techniques (like in situ control of the growth process) or improved models for layer quality; have altogether contributed to today's remarkable growth layer quality [87], [94]. In 1952, H. Welker of Siemens company extended the elementary –periodic table group IV- semiconductors by compound ones from group III and V, for example GaAs [96]. At that time, these have been created by melting the elements together and opened a huge application field for epitaxy. 1970 Esaki and Tsu suggested to tailor electronic band structures by creating epitaxial layers (1D layer growth) [97], [98]. This led to the possibility of "bandgap-engineering" employing epitaxy, which is today a common way to create heterostructures, quantum wells, and quantum well lasers, pioneered by H. Kroemer [99] and Zh.I. Alferov [100]. In 1978, H. Störmer invented the discipline of modulation doping. Here a heterostructure is exclusively doped in the higher band gap layer, yielding a transfer of the mobile carriers into the adjacent lower bandgap layer [101]. This allowed –for the first time in semiconductor history- a spatial separation of mobile carriers from their ionized ("parent") impurities, atoms otherwise limiting the mobility by Coulomb scattering. In this way, the room temperature mobility was enhanced by typically a factor of 2 and at low temperatures, this enhancement exceeded a factor of 1000 [102]. This opened the path to exciting research in fundamental transport physics, leading to the discovery of the integer quantum Hall effect (1980 K. v. Klitzing, initially on Si [103]) and the fractional quantum Hall effect (1997, by H.L. Strömer, D.C. Tsui and A. C. Gossard [104], as well as R. B. Laughlin [105]). In 1985 Goldstein had been among the first to describe growth parameters (substrate temperature, arsenic pressure and film thickness) at the transition between 2 and 3D growth and showed examples for both. In addition they analyzed the 3D nucleation by x-ray diffraction, STEM, and photoluminescence for 2D quantum wells and 3D clusters [106]. Around 1990 more and more researchers started to grow islands as a potential 3 dimensional lateral nano patterning technique [14]. During the last two decades many different multidisciplinary techniques to synthetize nano particles and new materials have evolved [15]. In 1995, operational quantum dots have been successfully fabricated and their optical response proven by Shchukin, see FIG. 11 [91], [107], or Ge quantum dots have been deposited by strain engineered Ge vapor phase epitaxy (VPE) on Si (001) [108].

III.C. Fundamentals

Epitaxy is a form of controlled phase transition leading to single crystal solid layers [109], [87]. A new crystalline phase (called "epilayer" or **"**crystallization interface") is created on top of the substrate surface [87]. The substrate surface serves as seed crystal [88]. The atoms of the next atomic layer (epilayer) adapt to the crystal structure of the surface of the substrate [87]. When the first monolayer is formed, atomic ordering takes place. The epilayer crystal quality normally does not exceed that of the substrate surface, often it is inferior [88]. However, thick buffer layers can lead to a reduction of the lattice defect density which is particularly important if there is no (nearly) lattice-matched substrate available. This is the case for GaN on sapphire, widely used in the light emitting diode industry today. Epitaxy is a surface kinetic process and depends on the structure and the chemical activity of the substrate surface [87]. A thermodynamic description of growth is given in this reference [109]. In general, to give a chance to find the lowest possible energy and thus build up an epitaxial layer the mobility of the adatoms must be enhanced. For this purpose, the substrate is usually heated to temperatures between about 300° C and 1000° C, so for example the the hexagonal (atomic) lattice ordering can be reached, representing the highest density packaging, depending on the material. Another way to enhance the surface

mobility of the adatoms to form epitaxial layers is to shine very intensive light on the wafer instead of heating. Photons close to the visible spectral region of some eV are able to transfer enough energy to surface atoms, to move them, so adatoms find a regular lattice position. In some cases, a mass transport from the substrate to the growing epilayer takes place ("segregation") [87]. This is often an unintentional phenomenon, since the growth of thick buffer layers should lead to to a dilution of the unintentional impurity density during growth and thus to gradually cleaner epitaxial layers. Segregated atoms have a statistical tendency to stick at hetero-interfaces. That is why, short-period superlattices (SLs) with some ten periods (like 2 nm GaAs / 2 nm AlAs, for example) are often grown to filter out segregating atoms. These SLs are called "couches poubelles" (French for "garbage layers") and often precede the growth of a thick (≈ 1µm), further cleaning buffer layer.

Assembling nanoparticles in a controlled manner by epitaxy is a kind of a link between "top-down" and "bottom up" [9]. "Self-assembly (SA) is the process in which a system's components –be it molecules, polymers, colloids, or macroscopic particles- organize into ordered and / or functional structures without human interaction" [110] (bottom up definition can be found in the preface, section I). "This can be referred to as guided (self-) assembly." [20]. This technique, allows precise control of physical properties like doping profiles, tailored band gaps, conductivity, and magnetic properties. Some are different from the ones of the substrate and some cannot be created by other techniques [88].

Different techniques can be applied to carry out epitaxy. They can be classified based on the involved physical or chemical processes [111] or other means [10]. An exemplary overview can be found in [109], [112] or [87]. Layers can grow from amorphous solid deposits (solid phase epitaxy), liquid phases (solution, melt, liquid phase epitaxy) or vapor / gas (vapor phase epitaxy) [87]. We will describe three sub-groups and for two of them we present examples of successfully created 3D nano features. Liquid phase epitaxy (LPE) [87] techniques have been employed for 3D nano feature creation. This is historically the first epitaxy technique and possesses a potential for low cost and large area nano patterning. In addition, colloids or dry ligands with different geometries can be added to the liquid, as a tool to influence the geometry of the resulting self-organized features. Another popular technique is called molecular beam epitaxy (MBE), which is the cleanest epitaxy technique, and two self-organized 3D epitaxy application examples are described below. MBE is not a vapor phase technique because it operates in the extreme ballistic limit. In contrast to vapor or a gas, the evaporated particles do not interact in between them. The residual gas pressure p of for example 10^{-12} mbar yields to an mean free paths for N_2 (air) of about l=0.07 cm / p(mbar) = $7 \cdot 10^8$ m, which is two times longer than the distance to the moon (!) and much larger than the dimensions of the UHV-vessel. Of course, formally also a ballistic molecular beam could be considered as a "gas" or "vapor". However, this ballistic beam is totally non-interacting, neither in between its own particles nor with the residual gas particles and thus not a gas in thermal equilibrium. In MBE, the source material is evaporated [88] in an ultra-high vacuum instrument and directed in a ballistic path to the sample surface employing Knudson cells or electron evaporation. Todays instruments have reached a high level of maturity. They generate thin layers of very high purity and ultra-high crystalline quality, dedicated process parameter control and in situ analysis are possible. The sample is positioned facing all cells in the working distance and in that way the epitaxial layer grows on its surface [114]. Examples of the mechanisms between the sample surface (Si) and the epilayer (Ge) during a MBE growth process can be: material is deposited on the sample surface, nuclei are formed, islands evolve, atoms desorb into the vacuum chamber and diffuse on the surface (as illustrated in FIG. 9).

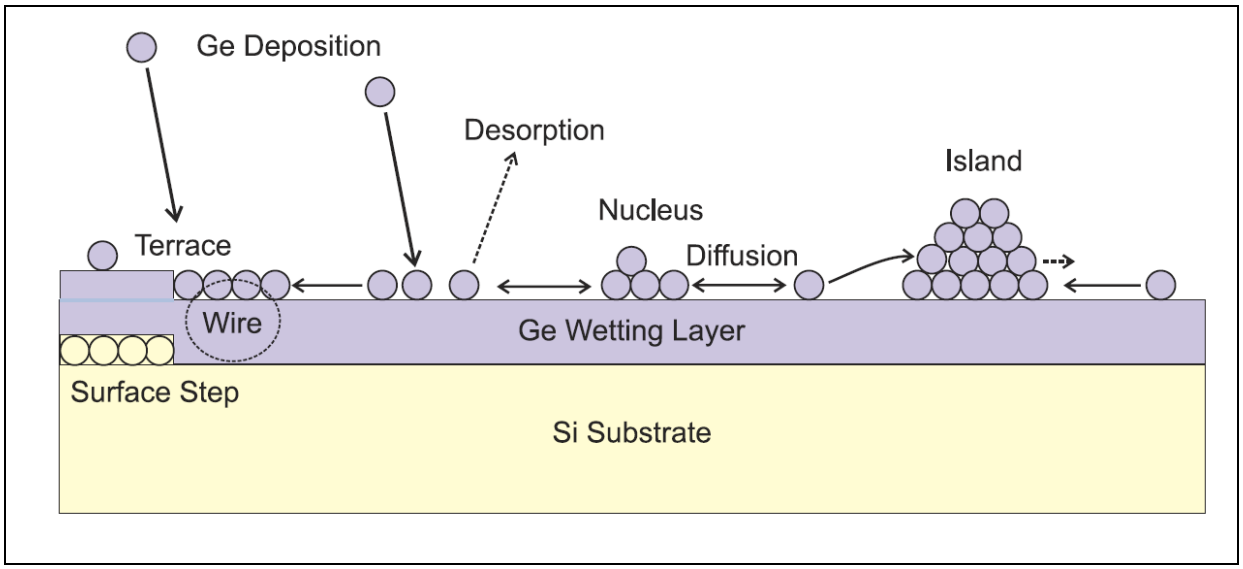

FIG. 9. sketch of involved processes in a Ge or SiGe layer on Si MBE growth process (substrate temperatures T > 400 ◦C), including step flow, accumulation of SiGe as wires and dots, gathering of material at steps and nucleus
Fig. 1 in [97] © IOP Publishing. Reproduced with permission. All rights reserved

The most applied technique in industry is MOVPE (metal organic vapor phase epitaxy) or, more generally the MOCVD (metal organic chemical vapor deposition). It works at a slight underpressure (close to atmospheric pressure) and with a relatively high throughput of carrier gases whose molecules transport the desired atoms to the heated substrate wafer. There, the gas molecules are cracked into even more volatile fragments, leaving on the wafer the desired atoms which arrange themselves to make up the epitaxial layer. With this technique, most of the blue GaInN-LEDs are fabricated today.

Different growth types can be differentiated, three of which will be summarized here, depending on the crystal / lattice properties of the epilayer and the "crystalline phase" (substrate). First, homoepitaxy ("isochemical phases") takes place, if the epilayer consists of the same material as the substrate [87], which is the ideal epitaxial situation because there is a natural perfect lattice match. The surface adatoms fit perfectly on the substrate, making up their own crystalline lattice (for example GaAs on GaAs). They arrange themselves with the same lattice constant on the substrate surface as the one of the substrate itself. This is then called lattice matched growth, which we call "defect free interface to the surface", since the crystalline lattice of the host material (substrate) matches the one of the adatoms. In addition, two techniques with different chemical components from the epilayer exist [87]: heteroepitaxy and graphoepitaxy. Second, in heteroepitaxy, the crystal of substrate surface and the epilayer differ [87] and microscopic factors dominate (monoatomic steps, etc [87]). Third, graphoepitaxy is based on macroscopic factors (macrosteps, macro particles, etc) [87]. Hetero- and grapho epitaxial growth have much in common: the described effects can act simultaneously during growth and the mechanisms can have the same nature [87].

Self-organized 3D epitaxy resulting in regular nano features can be realized by heteroepitaxy (strain engineering). Self-assembly in hetereoepitaxial growth can evolve due to topographical conditions, stressor guidance or vertical organization [20], as islands preferably nucleate at steps or on amorphous areas [87]. Both kinetic as well as thermodynamic effects can lead to ordering [87], [115], [116].

Regular ripple formation is an effective strain relaxation mechanism [14]. In strain engineering, natural lattice constant differences can be exploited (for example between Si / Ge). Strain engineering of Ge growing on Si has many advantages and the subsequent feature forming sequence can be observed within a MBE process. The process parameters (like the Ge deposition rate and / or the Si substrate temperature) can be found to generate nanostructures and to control the size and position distribution [14]. Alternatively an intentionally tailored parameter (for example employing alternating III/V semiconductor layers) can be employed for nano patterning feature growth. Possible geometries if Ge is evaporated onto Si are pre-pyramids, hut clusters, pyramids, domes [117] and ripples [116]. Different material systems 3D crystals growth has been reviewed for example in this reference [10]. Many applications for these epitaxial grown nano features have evolved: injection lasers (InAs / GaAs) [14], magnetic nano features (by evaporation from a target [118]), sensors (exploiting changes in the plasmonic wavelengths of metal nanoparticles, changes in the photoluminescence of semiconductor nanoparticles, or variations in the magnetic relaxation of magnetic nanoparticles in different chemical or biological environments), nanoscale thermometers and pH meters, summarized in this reference [10], [9]. However, it has to be taken into account that self-organized 3D nanoparticles don't grow automatically it requires external support [15], [119]. For example, nanoparticles are not thermodynamically stable and can disintegrate into elongated hut clusters [115]. Intermolecular and interparticle forces in nanoparticle assemblies are particularly complex. Because of this complexity the processes are still not completely understood, most of the advances have been empirical. In addition, dots can for example have a random distribution, whis is sufficient and adequate for some application [20]. Nevertheless the recent advances in synthesis and characterization of nanoparticles show, more and more aspects are understood, now [15].

III.D. Examples of applications

During the last two decades, interesting regular nano features have been created. Three exemplary ones will be mentioned here created on vicinal substrates, by hetero or strain epitaxy employing: electron evaporation, MBE and colloid LPE. Gambardella grew two monolayers of Ni on Pt(997), a vicinal surface of (111) terraces, resulting in an impressive period of about 2 nm (T = 300 K; I = 0.9 nA, V = 24 mV) [120]. Vicinal steps are created by miscut and followed by an annealing processes. Then the lines are formed by step bunched factors [32]. "Ni was deposited by means of an e-beam evaporator. After evaporation, the sample was cooled to 77 K; all STM images have been recorded at this temperature." [120]

Further periodic pattern examples from vicinal substrates are: Men et al. CaF_2 on Si(111) (64 nm period) [32]; Rohard et al. grew a Co nanodot array on Au(788) (3.8 nm / 7.2 nm array) [121]; and ViolBarbosa et al. grew Fe on "alternate parallel stripes of Cu(111) terraces and (110) oxidized facets …" (4 nm period) [122].

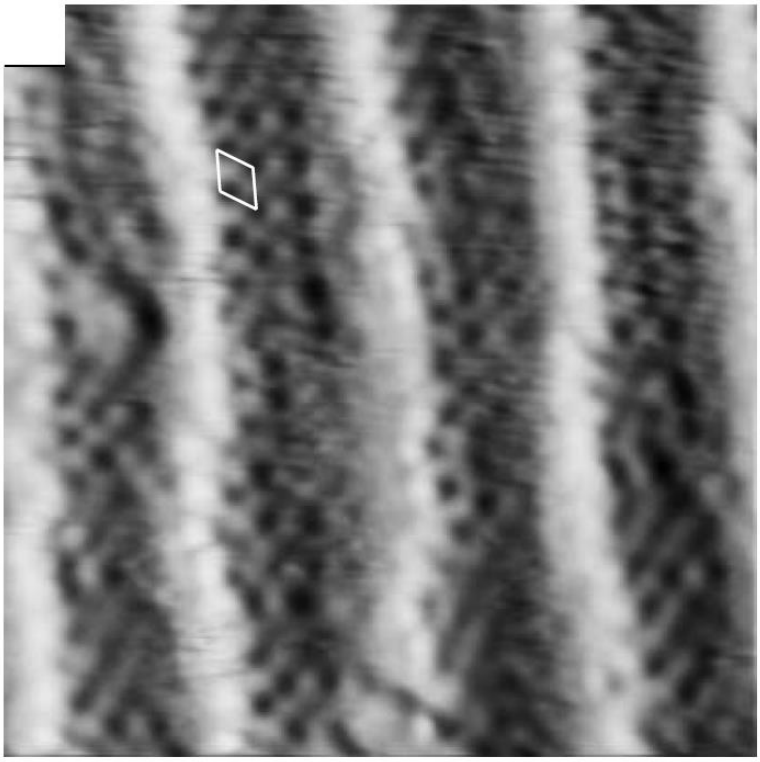

FIG. 10. „STM images recorded after deposition of 0.2 ML Ni on Pt(997) at different temperatures. Step down direction is from right to left. … (c) T = 300 K; I = 0.9 nA, V = 24 mV. The … image is displayed in $\partial z/\partial x$ mode to enhance the contrast on the terraces. The solid line represents a (2 x 2) unit mesh."
Fig. 1c in [120] ("c" removed), Reproduced with permission from Surf. Sci. Lett. **575** / Elsevier, L229 (2009). Copyright 2009 Elsevier

An example for the creation of pyramidal shaped quantum dots by epitaxy with a narrow size distribution is displayed in FIG. 11 (a typically dot has a size at the base of 12 ± 1 nm and a height of 4-6 nm) [91]. A fraction of the dots could be excited by spatially and spectrally resolved cathodoluminescence, proving the operational capability [91]. A series of ultrasharp lines has been measured (FWHM < 0.15 meV), each originated from a separate single InAs quantum dot [91]. Further examples of successful quantum dots fabrication employing MBE are [115] and [108], in addition the spin locking of electron spin coherence has been analyzed [123].

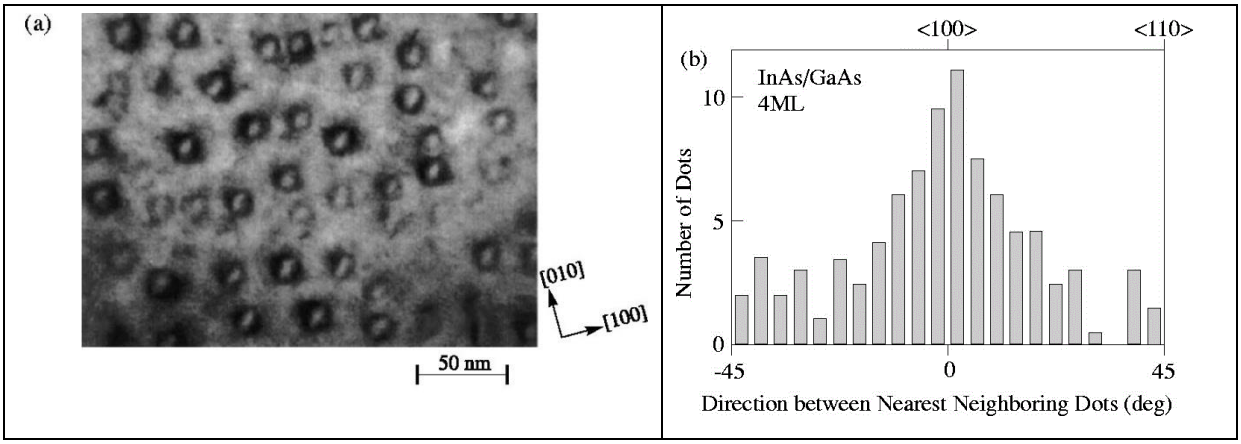

FIG. 11. 3D – MBE, "Ordering of quantum dots: (a) plan-view transmission electron microscopy (TEM) micrograph of a single sheet of InAs dots grown in molecular beam epitaxy by four-monolayer deposition of InAs. Dots are preferentially aligned in rows parallel to <100>. (b) Histogram of the direction between the nearest neighboring dots."
FIG. 18 in [107], Reproduced with permission from Rev. Mod. Phys. **71**, 1125 (1999). Copyright 1999 American Physical Society

Langmuir–Blodgett films are a promising LPE pattern creation technique from pre-existing nanoparticles in a solution. It possesses low cost and high throughput potential, at high resolution [10]. Complex regular feature geometries can be created by self-assembly from colloidal solutions from LaF_3 triangular nanoplates and Au nanocrystals, an example is displayed in FIG. 12 a) [119], [21]. Another fascinating example is employing DNA as "dry ligand" [124]. In a dewetting process, Au nanoparticles surrounded by DNA result in regular features [124] here an example can be seen in FIG. 12. b).

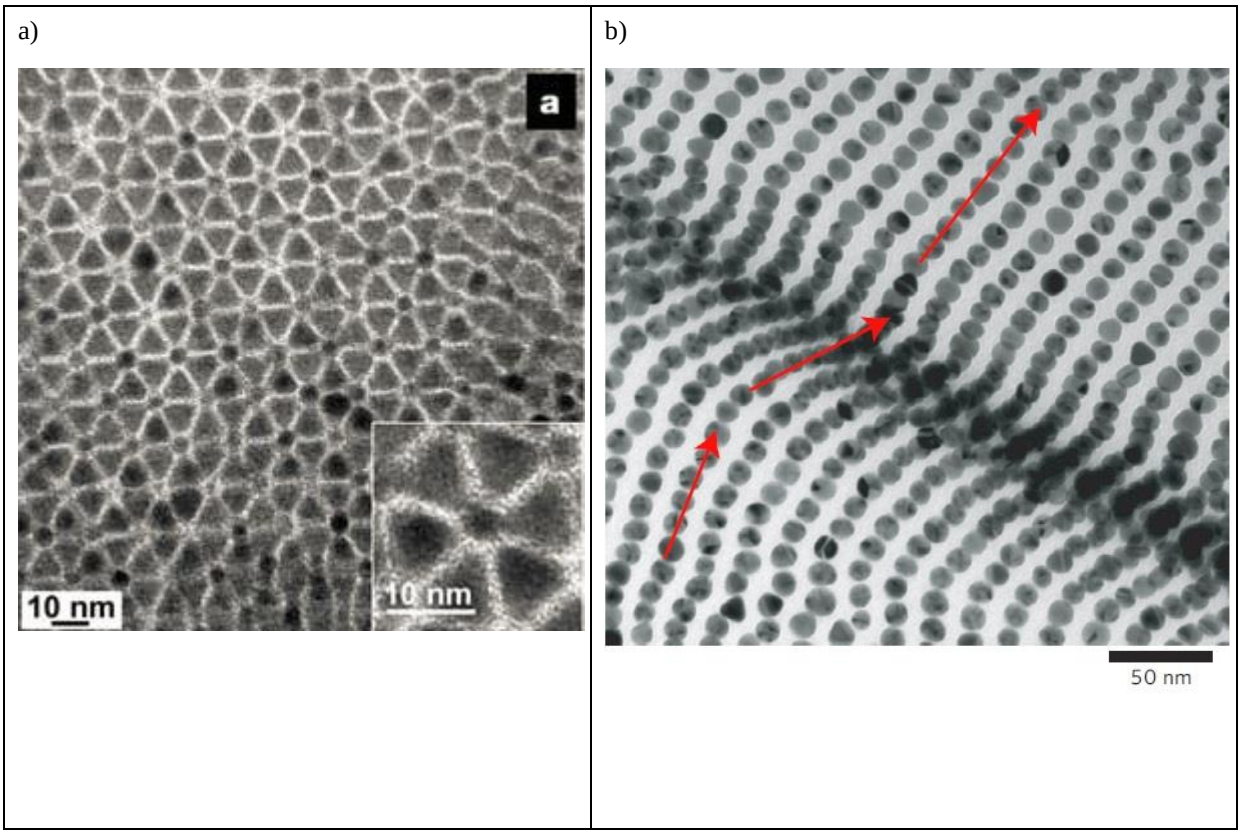

FIG. 12. a) "TEM images and proposed unit cells of binary superlattices self-assembled from triangular nanoplates and spherical nanoparticles. Self-assembled from LaF_3 triangular nanoplates (9.0 nm) and 5.0 nm Au nanoparticles." [21] The structure shown is formed on a silicon oxide surface. Figure 4a in [21], Reprinted by permission from Macmillan Publishers Ltd: Nature, **439**, 55-59, copyright 2006
b) "Crumpled, nanoparticle superlattice sheet. High-resolution TEM micrograph of a ridge in a, showing that nanoparticles remain aligned even when the sheet is bent." [124]
Figure 3b in [124], Reprinted by permission from Macmillan Publishers Ltd: Nature Materials **8,** 519-525 (2009)

III.E. Capabilites for nano device prototyping

Self-organized 3D epitaxy is suitable for many nano pattering applications. Liquid phase derivatives allow nano feature creation at very low overall costs [119], [21]. However if dedicated ultra high vacuum (UHV) equipment and sophisticated in situ layer grow process control techniques are required, then the necessary equipment is similar in expense to dedicated electron beam lithography (EBL) writers. Initial process development time (i.e. overall time to result) as well as design modifications can be a challenge and take a long time compared to SW design based top-down techniques. Some processes have the potential to produce operating devices in one single process step [125]. It is a bottom-up parallel therefore fast growth technique which can cover large areas (>1 cm²), [14]. Consider one monolayer on a 3" wafer with a surface of about 180 cm^2: every cm^2 of almost any solid contains in its first monolayer about 10^{15} atoms, which makes 3 10^{17} atoms on our 3" wafer. If we would like to position all these atoms with a speed of typically 1 atom / s, we would need 3 10^{17} seconds (equalling about $3.5 \cdot 10^{17}$ days or 9.5 billion years). This demonstrates the power of massive parallel, self-organized 3D

growth, in which one monolayer is epitaxially deposited in typically 1 s, thus 3×10^{17} faster than by direct and sequential manipulation of single atoms. It means that epitaxy is the only way to create macroscopic crystal layers in practice, taking profit of the power of self-organization. This is possible at the resolution level of interest (see for example FIG. 12.) and with the potential for interface defect free features (for details see section III.C) [88]. In addition 3D features with < 10 nm lateral resolution are naturally possible. Vertically even down to monolayer height control is possible, at least to the UHV growth techniques.

State of the art periodicities are possible, on vicinal substrates periods down to 2 nm have been reached, see FIG. 10 [120].

However, feature placement at very specific locations with high positioning accuracy is difficult to realize on the level known from EBL writers. Self-assembly processes have emerged that appear capable of satisfying these needs, at least to some extent [20]. In addition regular periods in one direction can be realized, an example being aligned stripe patterns [126] and for two different materials [21]. This is sufficient for many applications. There does not yet exist one single epitaxy technique for 3D nano pattering, with commonly applied recipes. Currently there exist many different techniques –where different equipment is sometimes required. However the large variety of epitaxy techniques leads to a large versatility, but not usually in one single instrument.

Progress has been made in particle size and shape control [126], however it is still a challenge [127] compared to top-down techniques. Special arbitrary shapes are difficult to realize. Features grow / evolve because of the materials and process conditions (stress, kinetics), which cannot be tailored in a way as SW designs, masks or templates in top-down techniques. However different kinds of shapes can be realized by adding adequate geometry colloids, “dry ligands” in LPE (an example is shown in III.D, FIG. 12b), special sample cutting followed by annealing or by combined processes with top-down methods, such as local substrate pretreatment. These allow controlled feature placements and periodicities in the substrate plane [126].

The techniques’ capabilities for nano device prototyping will be summarized and compared with the others -covered in this article- in Table II.

III.F. Conclusion

“Self-assembly provides a simple and low-cost method for producing ensembles of nanoparticles in a controllable manner,…” [10], “low-cost” for some liquid vapor derivatives. The technique possesses reproducible and fast parallel large area processing capabilities. In addition it can create features with a perfect interface to the substrate (for details see section III.C) and tailor physical properties, some not obtainable by other techniques [88]. However, although better understanding of the fundamentals and tighter process control has managed to narrow the size and height distribution [14] results are not yet as reproducible as by conventional top-down techniques within their resolution limits. Thus, “At present, … most nanoparticle-based optoelectronic components are made with top-down nano fabrication techniques rather than bottom-up self-assembly approaches” [10]. For high placement accuracy, arbitrary shapes or specific periodicities top-down techniques might be more feasible.

Design modifications can take quite long. In nano device prototyping, the design has to be often altered and other techniques (with software designs) might be more suitable. However once the process is established the same features can be reproduced over and over again easily.

Currently, self-organized 3D epitaxy is not so frequently used as nano patterning technique in nano device prototyping (NDP), except for quantum dot applications. The research is mainly focused on developing potential techniques for large area mass production applications with moderate feature uniformity and no pattern placement requirements. Self-organized 3D epitaxy is a promising technique for applications with large area but not so strict feature shape and position requirements, like adding regular nano features to solar cells to enhance their efficiency [128], [125]. Finally using a combined process the sample surface can be locally functionalized or sacrificial features can be placed at dedicated sample positions, with desired periodicities and outer shapes (geometries), before the self -organized 3D epitaxy step. Then mediated growth due to intended local surface modifications ("defects") can take place at these locations, leading to the required results.

Next we take a look at applications and methods carried out by atomic probe techniques.

IV. Atomic probe microscopy (STM and AFM) derivates for nano patterning

IV.A. Introduction

Atomic probe nano feature creation [129], [130], [131], [2] and [28] is a versatile nano patterning field with remarkable resolution and placement accuracy capabilities. On one hand atomic probe patterning can be a human interaction induced bottom-up single atom manipulation or on the other hand it can be used as a top-down one like low voltage electron beam resist exposure with the apex of the tip acting as field emitter. Also mixtures of both are possible. These techniques are very different from epitaxy. They all allow, within their specific capabilities, tailoring nano feature shapes and dimensions similar to EBL by transferring SW designs onto the sample surface.

IV.B. History

These patterning techniques possess analytical roots. Already in 1929 an instrument called “stylus profiler” has been used to image sample surface topography [132]. In 1972 R. Young published the usage of a similar set-up. He developed it as non-contact instrument, detecting the field emission current between the tip and the sample calling this instrument the “Topographiner” [133]. Later on, in 1982, Binnig, Rohrer, Gerber and Weibel published their invention the “scanning tunneling microscope” (STM). The STM can visualize atomic lattices of some conducting surfaces, in an ultra-high vacuum environment [134]. A few years later Binnig et al. [135] have published results from a similar technology, capable in operating also on insulating surfaces at ambient conditions. It is called the atomic force microscope (AFM) and senses surface forces. Today many derivates exist and are employed also at ambient conditions. Then researchers started to employ these techniques also for patterning.

IV.C. Fundamentals

Most atomic probe microscopy techniques are equipped with a very accurate piezo electric positioning stage which moves a tip or probe along the sample surface. These piezo crystals allow positioning down to the sub Å level and travel ranges up to about hundred µm if not combined with for example an encoder stage, so employing them alone larger travel ranges are not possible, like those available in EBL writers. In addition they allow sub Å vertical positioning or sensing capabilities. The inverse piezo effect is employed for positioning (certain ceramics expand if a voltage is applied). However the expansion is not linear to the applied voltage, therefore position measurement can be used to correct this.

In addition atomic probe microscopy techniques either sense the tunneling current between the apex of the probe to the sample surface (STM) or the deflection of a cantilever (AFM) to control the tip sample distance. An AFM detects surfaces forces by measuring the deflection of a cantilever with a laser diode or by self-actuated piezo resistive cantilevers [136]. The piezo resistive method can be employed if laser alignment is difficult in the desired set-up or space is limited. In atomic force microscopy different atomic forces are involved: long range mostly attractive van der Waals (down to about 4 Å apex sample distance), short range forces mostly repulsive

(short distances < 4 Å). In addition, capillarity-, Coulomb-, and further forces are involved [137]. Under certain conditions it is possible to visualize surface atom lattices [138]. The surface force serves as feedback loop to keep the distance constant, while rastering the sample surface. Two fundamental modes are differentiated the non-contact regime (mostly attractive forces) and the contact mode (repulsive forces). Forces (mostly repulsive) can be visualized by the Lennard Jones potential Φ:

$$\Phi(r) = 4 \cdot \varepsilon \left(\left(\frac{\sigma}{r} \right)^{12} - \left(\frac{\sigma}{r} \right)^{6} \right)$$

Equation 1: Lennard Jones potential Φ, r being the distance between the apex of the tip and the surface [139]

In the STM analysis case the tunneling current between an atomically sharp tip and a conducting sample surface is used for detecting the sample topography, often in an ultra-high vacuum (UHV) environment. The sensitivity allows resolving atomic lattices.

Today many additional derivates of this fundamental surface analysis methods (STM and AFM) exist: magnetic force microscopy (MFM, sensing magnetic fields); scanning near field optical microscopy (SNOM, here evanescent electromagnetic fields, often in the visible spectrum, as created by a sub-wavelength diameter probe, the transmitted or reflected electromagnetic field can be detected); scanning thermal microscopy (SThM, the tip is either used as a nm sized resistor thermometer or thermocouple) and many other variants.

A possible classification scheme for patterning applications has been suggested by Staufer [130]. It differentiates four different quantities exploitable for patterning: energy flux, forces, energy quanta and potential barriers. These can be directly regulated by control parameters like electron / ion beam current, the applied electric fields as well as additional environmental ones like gas / fluid supply or additional external energy sources (radiation) [130]. This large variety of possible interaction regimes and techniques result in many different exploitable processes for nano patterning [129], [140], [141], [142], [131], [2]. The techniques can locally modify the sample by: exposing resists (serve as emitter [2]), mechanical machining, depositing, treating the sample thermally, decomposing organometallic gases, manipulating molecules and atoms, carrying out electrochemical and photo-electrochemical processes, transferring material [141] or etching with the assistance of ions and electrons.

IV.D. Examples of applications

Most sub 10 nm results have been published utilizing STM or AFM so far, some exemplary results will be briefly described here. With basic environmental requirements, AFM can nanofabricate sub 10 nm features [143], [144]. With a converted commercially available AFM [143], Moon et al. imprinted ultra-sharp tungsten and carbon like tips into poly(methyl methacrylate, PMMA) reaching down to the sub 10 nm resolution level (an example is shown in FIG. 13 a). Here they worked in the repulsive (contact) mode and locally displaced the resist by applying the appropriate forces. In addition they have suggested a nano meter precision pattern registration technique for this set-up [143], [145]. Another group exposed a molecular resist (calixarene derivate C-Methylcalix [4] resorcinarene (C-MC4R, $C_{32}H_{32}O_8$, Sigma-Aldrich) by the energy delivered by electrons and

successfully patterned < 10 nm pits, the result is displayed in FIG. 13 b) [144]. They employed the following exposure parameters: tip bias voltages < 20 V and a dose of 1 µC / cm [144]. Further on, Wilder et al. have analyzed different resist exposure mechanisms taking place in EBL and atomic probe microscopy exposure [146].

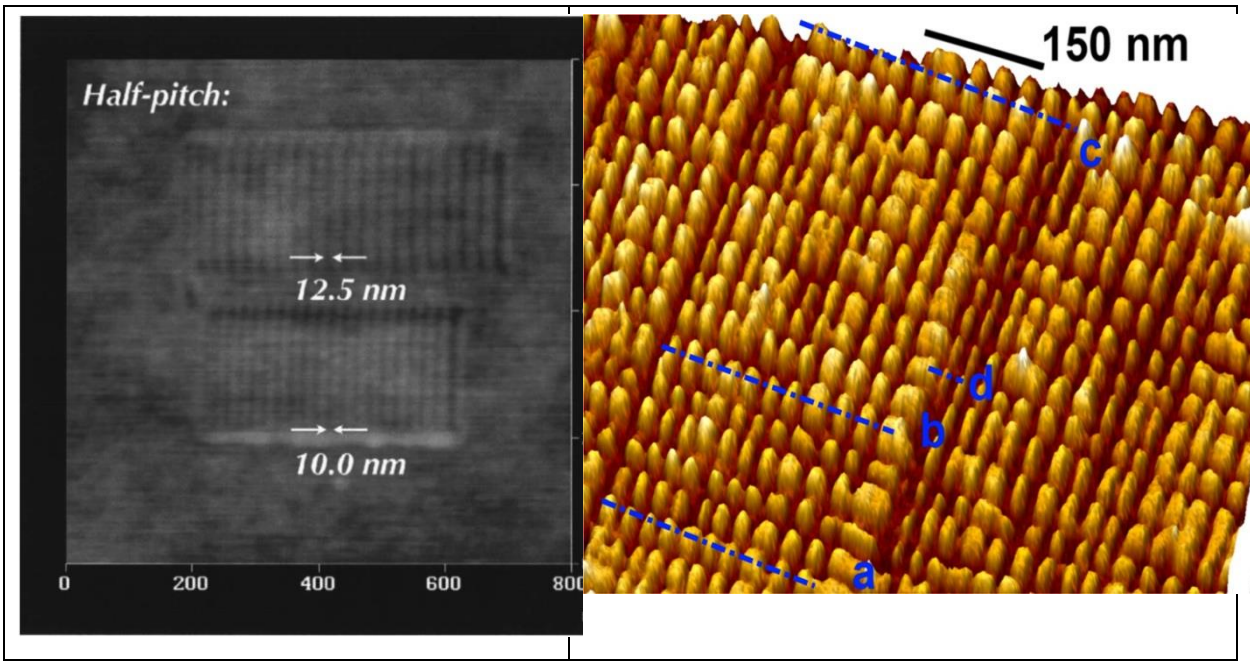

FIG. 13. a) AFM scan of gratings written with a tungsten tip in PMMA. Grating half pitches are 12.5 and 10.0 nm in the upper and lower gratings, respectively.
Fig. 7 in [143], Reproduced with permission from J. Vac. Sci Technol. B **8**, 519 (2009). Copyright 2009 American Vacuum Society
b) "AFM topography image (proving 7 nm resolution) … demonstrating the patterning of small features into 9.5 nm thick CMC4 resist with an electrochemical etched tungsten tip."
FIG. 6. in [144], Reproduced with permission from J. Vac. Sci Technol. B **29**, 06FD02-1 (2011). Copyright 2011 American Vacuum Society

In a second example, a STM has been used to create single electron transistors by quantum dot fabrication [147], employing hydrogen resist lithography [148], [149] and [150], [151]. "Patterning occurs when electrons field emitted from the probe locally desorb hydrogen, converting the surface into clean silicon." [148]. In this way the source (S) and Drain (D) electrodes as well as the small dot in the centre were structured. After PH_3 dosing and annealing phosphor atoms are incorporated in the surface. A single phosphorous atom in the centre shows up with the single Si atom ejected in the incorporation process. Here energy flux in the form of electrons from the tip are the exploited interaction regimes.

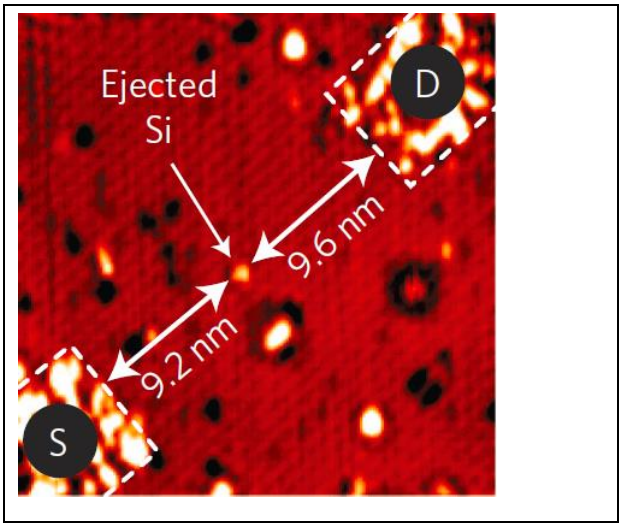

FIG. 14: "Single-atom transistor based on deterministic positioning of a phosphorus atom in epitaxial silicon. … STM image … of the inner device area …, where the central bright protrusion is the silicon atom, which is ejected when a single phosphorus atom incorporates into the surface."
Fig. 1 b in [147], Reprinted by permission from Macmillan Publishers Ltd: Nature Nanotechnology **5**, 502-505 (2012), copyright 2012

A third example is individual atom manipulation. It has been demonstrated already in 1990 by Eigler and Schweizer [152]. They managed to position individual Xe atoms on a Ni surface using a STM and afterwards read out the results with the same instrument, displayed in FIG. 15 [152]. The STM tip exchanges mainly van der Waals and electrostatic forces with the sample surface, which could also be delivered by a conducting AFM tip. These forces can be tailored by the distance and the applied voltage. The actual tunnelling current is often negligble in view of the acting forces [153] it is only employed as a feedback loop to keep the distance constant. Usually, less force is needed to move an atom along a surface than to extract it from the surface [154]. As a result the Xe atoms could be moved along the surface and positioned to dedicated locations. Here manipulation forces are larger than the lateral forces of the Xe atoms to the surface.

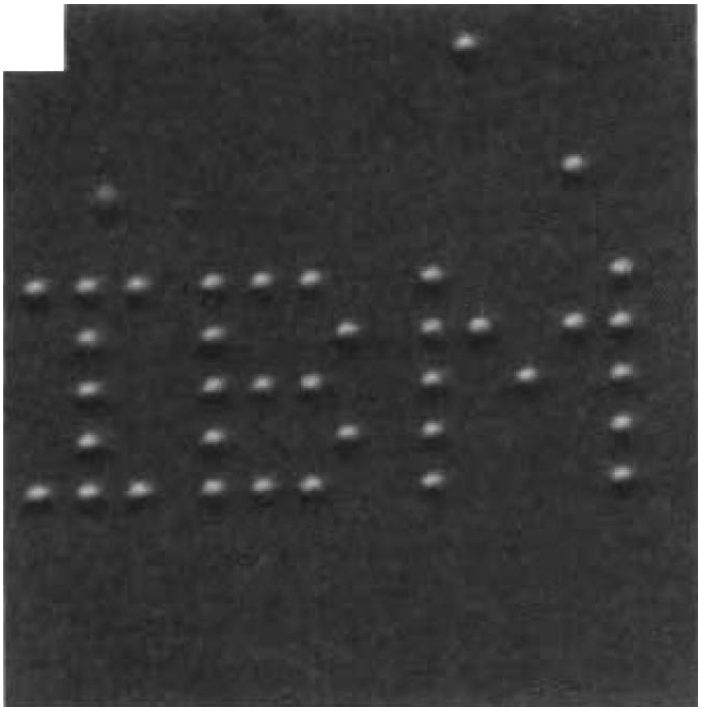

FIG. 15. STM image of individual Xe atoms on Ni (110), arranged to write “IBM”,
Fig. 1f in [152] (“f” removed), Reprinted by permission from Macmillan Publishers Ltd: Nature **344**, 524-526 (1990), copyright 1990

Later on, Eigler together with Heinrich et al. have managed to position large assemblies of CO molecules to create operating devices. They acted as a three-input sorter that uses several AND gates and OR gates [155].
Nevertheless single atom manipulation is currently only possible in very specific material systems and mostly under UHV and cryogenic temperatures [2]. In another technique employing electric fields with an STM feature sizes down to the 1 nm level [149] can be reached at room temperature. In addition a few nm feature sizes can be patterned with an AFM at ambient conditions [156], increasing the usability of the technology family for more applications. Individual atom placement has also been carried out in a room temperature environment [157]. However the selection of the molecule is important, as the binding energy must be larger than the ambient thermal energy (“kT about 25 meV”) conditions and small enough that it can be moved [158].

IV.E. Capabilities for nano device prototyping

The fascinating capability of tailoring individual atoms and molecules is about the ultimate resolution and pattern placement accuracy we can think of today. Already individually, but especially in combination this resolution, pattern placement accuracy, and resulting shape tailoring capabilities are unique [2].
In the case of pattern placement accuracy, for new features with respect to existing ones already on the sample, it can be realized on 3 different levels: down to the atomic level by placing an individual P dopant atom [150], on the 1 nm level by an interferometric special phase imaging technique [145], [143] or on similar levels as accessible for EBL writer. This is possible, because the placement accuracy of the piezo positioning stage can be

quite high and reproducible [159]. The master is usually a design in software, so modifications can be carried out quickly and at low costs, in addition the feature shape can be controlled pretty well.

For individual atom arrangement, patterning has been shown only laterally so far, as one atom thick features. 3D patterning similar to self-organized 3D epitaxy or top-down techniques is so far only accessible to other atomic probe microscopy patterning techniques. Nano device interface to sample surface depends on the technique, individual atom placement can create perfect interfaces (for details see section III.C), for other AFM based techniques a perfect interface can be difficult to realize (similar to EBL).

Many SPM techniques are available at low to mid-price regimes [2]. However dedicated cryogenic UHV (STM) with patterning adequate positioning stage travel ranges and sample preparation devices are similar in expense todedicated SEM lithography attachment solutions with laser stages or entry level EBL writers. With the large variety of different techniques and accessible interaction regimes [2], atomic probe microscopy derivates are very versatile nano patterning techniques. They can be used for many nano patterning applications. However this is usually not possible within one single instrument. In addition dedicated process know-how, especially of the leading edge results, is not very wide spread yet (not "standardized") inside the community. This might be because of the existence of so many different (competing) techniques and the necessity for different equipment. As a result it can take quite long to develop a new process for a specific application, so the initial process development time (i.e. overall time to device) depends strongly on the technique and how well the associated process is known.

Creating nano features over larger areas is not feasible employing individual SPMs (because of the limited raster / scan area [160]. Employing a single AFM tip, "… SPM methods are very time consuming and not suitable for large-scale assembly of nanostructures" [12]. The patterning speed for larger areas can be increased if it is combined with other techniques or by the idea to employ parallel techniques where more than one tip is active [2], [136], for data storage [161]. Especially with the parallel versions, the speed limitations can be overcome and the technology advantages kept. Thus the technology family is currently not so well suited for setting up a R&D nano patterning production line. However large area patterning speed contributes only partially to the overall process time in nano device prototyping (NDP) and is not required for the creation and studying of ultra-high resolution proof of concept devices [155].

The techniques' capabilities for nano device prototyping will be summarized and compared with the others - covered in this article- in Table II.

IV.F. Conclusion

Atomic probe microscopy derivates are well suited for NDP, because of the combination of currently unprecedented feature shape fidelity, pattern placement accuracy and resolution. Creating a few ultra-high resolution devices, the rather slow pattern definition step is tolerable, as the capabilities are currently not accessible via other techniques and contribute only as one part to the over-all time to device. Thus, the necessary time to result in NDP can still be quick to moderate if only the ultra-high resolution step is carried out applying one of these techniques. In addition further non-conventional techniques exist like dip pen lithography [162] and

further commercial developments Zyvexlabs [163] and SwissLitho [164]. Further on, its mid-price availability of some derivates make it accessible to many research groups.

Next, we take a look at applications and methods carried out by ions.

V. Ions

V.A. Introduction

Ion beam implantation has been for decades a crucial fabrication step in the semiconductor industry, where silicon regions are doped p-type or n-type, altering the electrical properties [165] to allow the manufacturing of diodes and transistors. Nano device prototyping is the scope of this review article, so this classical ion beam implantation and standard applications of point ion source instruments like circuit edit, cross sectioning and TEM lamella preparation are not described here, examples can be found in: [167], [168], [169], [170], [171]. Already, 1959, Feynman in his famous talk ("There is plenty of room at the bottom") at Caltech [33] and 3 years later S.P. Newberry [34] published the ideas that ions can be used for patterning of small things. Later on Townsend summarized its unique power to create materials "...not obtainable by normal thermodynamic processes..." [166]. Today we know a large variety of ion matter interaction regimes, which are exploitable for nano patterning. Ion matter interaction regimes can be applied utilizing different instrument types.

Recent technology breakthroughs improving the instrument performance for focused ion beam nano patterning are:

- improved liquid metal ion source (LMIS, including beam current stability) [172],
- gas field ion sources (GFIS) for lateral high resolution analysis [173],
- improved plasma sources [174], [175]
- (single) focused ion beam implantation [176], [177], [178], [179], [180], [181], [182], [183]
- dedicated nano patterning instruments based upon an electron beam writer instrument architecture [184], [41]

We will summarize the fundamentals, explain techniques employed so far, take a look at five example applications in detail and briefly introduce further ones, proving their applicability as complementary (lateral) nano patterning technique by different ion beam instrument types. If an application is limited by conventional processing, exploring one or the other ion matter interaction regime with unique capabilities may be a rewarding alternative.

V.B. History

Ion beam technologies possess analytical roots. A few years after Ruska and Knoll (compare to EBL history in section II.B) in 1937 E.W. Müller invented the field emission microscope [185]. First he had used electrons for a special kind of projection imaging of a sharp tip surface material. In 1955 he has been able to visualize individual atoms and the tip metal high index net planes by employing the "Field Ion Microscope", with a resolution of 2.3 Å [185]. Drummand et al. [186] have realized a scanning ion microscope with 20 keV Ar ions focused to a 1 µm probe and a beam current density of 0.6 A / cm^2. They also cut a grid to image it and estimated the sputter rate. In addition they have noticed that the cutting "…is considerably slower than obtainable by electron beam techniques, but the use of ions has the advantage that, for reasonable current densities, the process is non-thermal…" [186]. However their source technology suffered from a low beam current inside a dedicated (small) spot size, thus the beam brightness of the available ion source has not been high enough [187], [188], [189]. Fifteen years later Levi Setti published first results from a scanning transmission ion microscope using hydrogen ions from a field ionization source [190]. Further details about ion beam techniques and ionization processes can be found in [188]. Among the first reported applications of ion beams for the fabrication of small things, have been carried out by K. Kanaya et al. in 1965 [191], according to Schmallenberg [56]. The paper title is "Micro color recording, etching and machining by means of high voltage ion beams". They cut a 20 µm diameter hole into a thin Ni sheet and discussed possible advantages of ion beams over electron beams due to their smaller particle wavelength and higher momentum. In the 1960's a brighter and promising source technology called liquid metal ion sources (LMIS) was starting to be used, for the historical background see for example [192], [193], [194], [41], [195]. It became applicable for FIB applications in the 1970's [196]. During the 1980 and 1990s further groups evaluated focused ion beams employing LMIS for patterning, MIT [197], NEC [198] and Hughes research lab [199]. They summarized and tested various techniques and applications and reached state of the art results like those visible in FIG. 16. 1983 LaMarche et al. [200] showed that FIB Ga implantation into Si acts as an etch-stop for an anisotropic KOH etching at elevated temperatures. This process has been used to fabricate sensors or MEMS (Microelectronic Micromechanic Systems) structures [181], [201].

At the beginning of the 1970s Seliger and his team [202], [203] added an "Einzel lens" to an ion implantation system. The instrument was capable to create ions by different techniques, radio frequency plasma, surface ionization, sputtering or electron bombardment [188]. They doped a Si sample by a boron focused ion beam and exposed an electron beam lithography resist (PMMA, described in the EBL fundamentals section II.C) using 60 kV He ions. The 300 keV instrument applied during these experiments is described in [188]. They reported a beam diameter of about 3.5 µm. In addition they employed LMIS technology which showed a significantly higher beam brightness of $3.3 \cdot 10^6$ $A / cm^2 sr$ than the formerly used plasma ion sources (up to 100 $A / cm^2 sr$), thus the probe current in the fine beam is significantly higher [187]. At about the same time J.H. Orloff, and L.W. Swanson studied a field ionization source and performed micro etching [204]. In 1991 Kubena et al. succeeded to pattern sub 10 nm features (see FIG. 16) in Polymethyl-methacrylate (PMMA), an electron beam lithography organic resists (for more details see EBL history section II.B). The resist film (60 nm thin) has been patterned using an acceleration voltage of 50 kV, employing Ga LMIS technology [205].

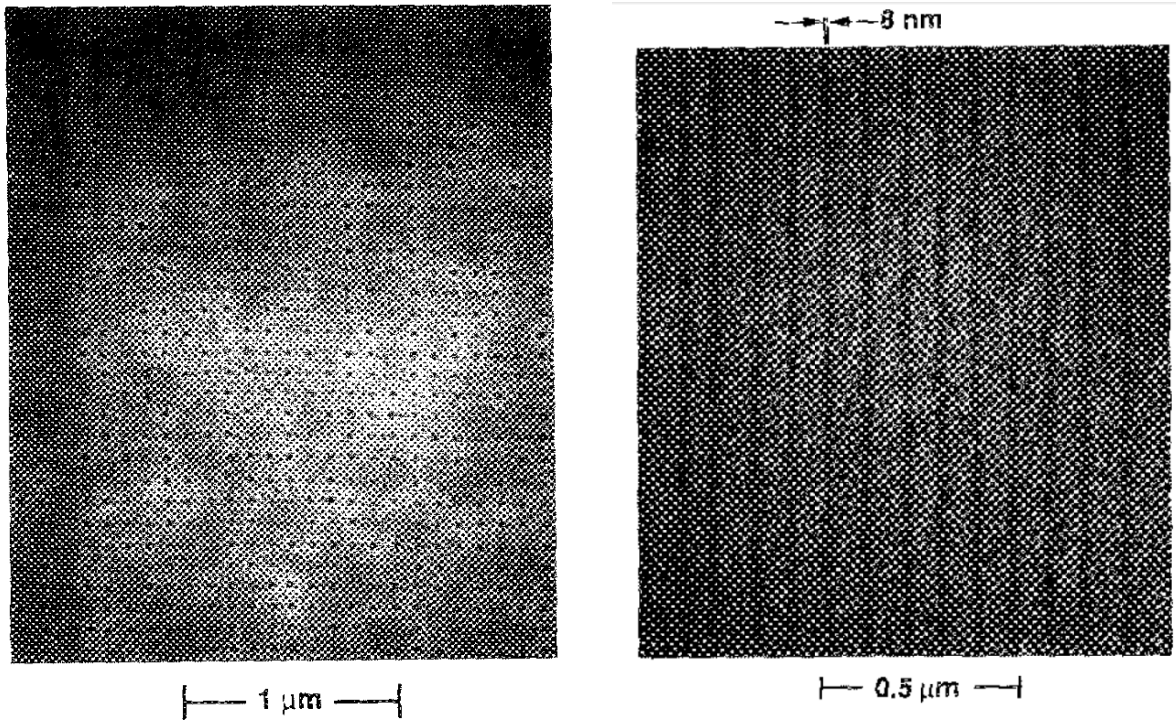

FIG. 16. SEM micrographs

a) down to 7 nm dots (in 60 nm PMMA, 50 kV Ga, 8 nm spot, 8 µs dwell time), Fig. 6 b in [205]
b) 8 nm thin lines (in 30 nm PMMA, 50 kV Ga, 8 nm spot, $2.4 \cdot 10^{-7}$ Ga^{+} / cm), Fig. 5 a in [205]
Both reproduced with permission from J. Vac. Sci Technol. B **9**, 3079 (1991). Copyright 1991 American Vacuum Society

Although „…the potential elegance of the technique was clear then.…" [197], challenges have been encountered like:

- Organic resist related ones:
  discontinued lines (exposure process, shot noise, limited angular intensity LMIS ...) [206], [207], [197], [205], [208], as well as lower penetration depth ones (of Ga ions compared to electrons) like: thick resist is only exposed at the surface [83] and marks are not visible for the ion beam [209].
- The employed incident ions are deposited into the sample surface and might cause unwanted contaminations to the sample material system [210], [83], [211].
- Unintended damage at places next to the area that has been patterned, because of imaging / milling coincidence [210].
- LMIS resolution degrades significantly for high beam currents [212]
- The lack of stability and adequate automated control and feedback mechanisms for nano patterning without user interaction even during long sequences [83]. For example in 2004 Marrian has compared ultra-high resolution vector scan electron beam lithography (EBL) instruments (explained in section II) with flexible ion / electron beam combined instruments available at that time, the conclusion has been: "…But, and perhaps most telling, the available tooling for electron beam lithography (EBL) is much more sophisticated, which is perhaps the single-most reason it is much more widely used..." [83]. "Sophisticated" with respect to (unattended) nano patterning requirements.

More details can be found in [41].

Today, almost all of these challenges can be overcome by the summarized technological breakthroughs (explained in section V.A). For organic resist exposure there exists one drawback which might limit applications: discontinuous lines (caused by shot noise or the different nature of the exposure process) [208]. If this is limiting an application, we suggest to employ a different technique or process (examples will be given in section V.D or V.E). Since pure resist exposure by ion beam lithography (IBL) is still a relatively new technique compared to the significantly longer history and experience of EBL resist processing, it will (for now) not be on equal footing especially as FIB organic resist exposure experimentshaven't revealed significant advantages compared to EBL, yet. Further challenges reported for organic resist exposure can also be present in other processes like: incident ion residuals, damaging at unintended sample locations or where the pattern shall be defined. These are due to patterning or imaging side effects like milling or implantation. Further, marks cannot be registered (are not visible) because of the small penetration depth of (Ga) ions into the sample. Some of them vanish if a high precision stage is used [213], like those employed in EBL writers. This has already been implemented in a FIB instrument in 1988 [198]. Such a stage allows incident ions only at desired areas.
Recently commercialized technology breakthroughs will be mentioned here and briefly explained in the following section:
First, a very promising high resolution ion microscope with a high angular source intensity. It employs a gas field ion source (GFIS) technology (He or Ne, for more details see section V.C.1) [173], [214], [215], [216].
Second, a Xe plasma ion source column has been developed [217], [215], [218] and entered resolution regimes so far only accessible to LMIS with significantly higher probe currents than LMIS and GFIS [219], [217].

Third, we have realized a dedicated instrument for NDP by integrating some of the recent technology breakthroughs (described in section V.A), especially in liquid metal focused ion beam techniques, into an optimized focused ion beam column [184] and LMIS source [172] on an EBL writer architecture instrument platform [184], [41], [220] and [221].
All three will be further described in the following section.

V.C. Fundamentals

V.C.1. Sources and instrument types

A large variety of incident (process) ion species are available for ion beam technologies. Ion species are atoms as well as conglomerations (clusters) of atoms with at least one additional or missing electron. Some instruments allow to switch quickly between species with the aid of a Wien filter (with crossed E and B field, “ExB filter”) [222] or inducing a different source gas. A periodic table with exemplary available ions for different source types is shown in FIG. 17 [195], alternatively a periodic table especially for LM(A)IS can be found here [223]. Source parameters and more detailed descriptions of LMAIS are described in [194], [195].

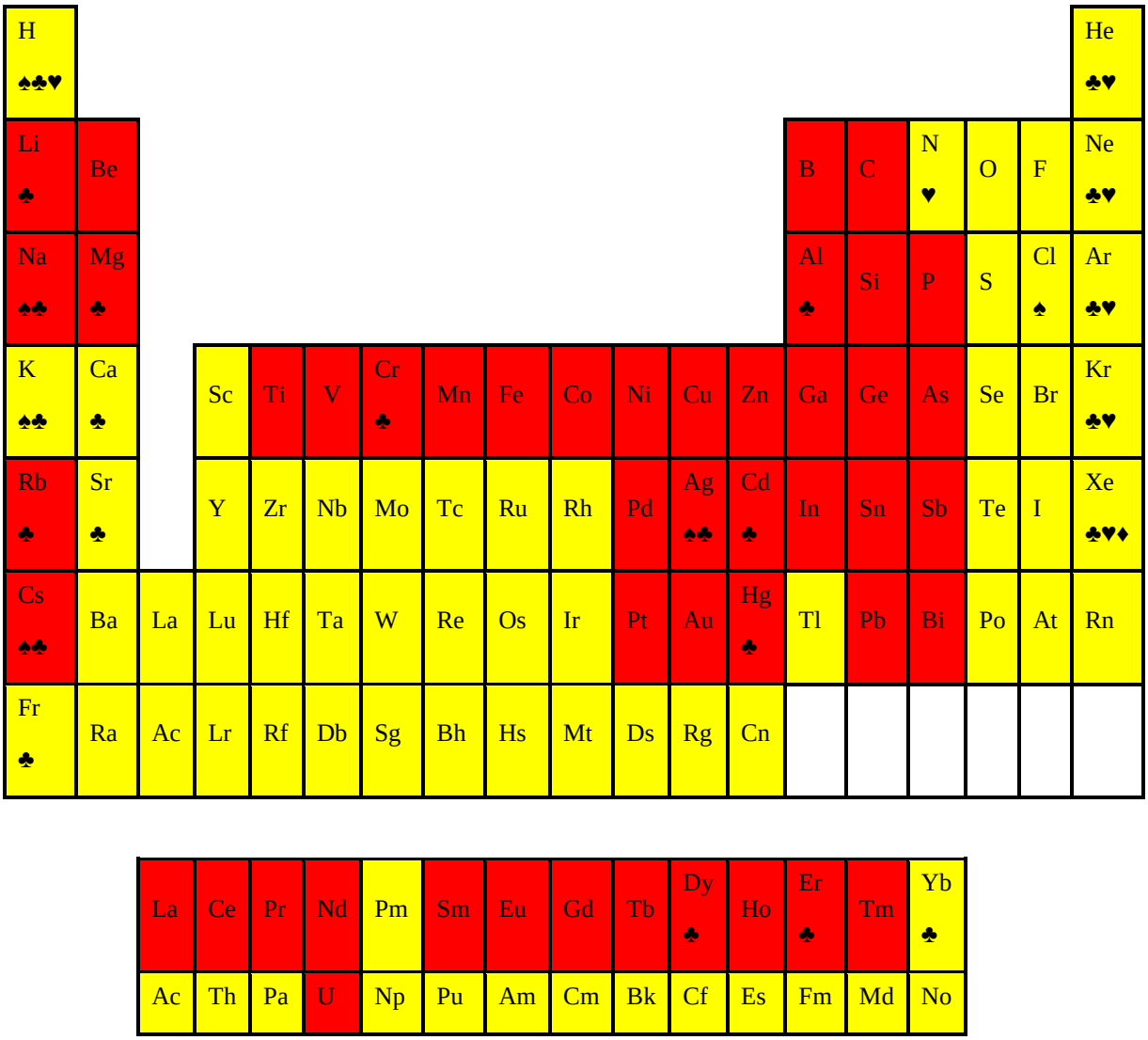

FIG. 17. periodic table, available ion species for LMAIS and other ion sources,
LMIS and LMAIS: The red marked elements in the periodic table can be provided as single or doubly charged mono- or even as heavy polyatomic ions (cluster),
Further or same ions may be used employing different source types like ionic liquid ion sources (ILIS) ♠ [224], magneto-optical trap ion source (MOTIS) ♣ [225], GFIS ♥ [214] or others ♦, in particular high current Electron cyclotron resonance (ECR) [226] or Xe plasma sources [227].
Fig. 53 in [195], to be published, Reproduced with permission from Appl. Phys. Rev. (2016).

This large variety of accessible incident ions and ion-matter interaction regimes [166], [228], [229], [230], opens an enormous application space for ion beam nano patterning. (Lateral) nano patterning is carried out, employing mainly 7 fundamentally different ion source or instrument techniques. Two of them use a larger (> 50 nm) spot size on the sample surface to create thin surface films or dope the surface (altering the electrical properties):

1. The first instrument (“sputter coater”) [114] surrounds the specimen with an ionized process gas atmosphere (plasma) environment. This can be used for area surface treatment.

2. The second instrument type is used in the semiconductor industry for large area ion implantation. Dopant atoms in a vapor atmosphere are accelerated towards the silicon substrate and scanned over the surface by electrostatic deflection plates [165]. The implantation depth is controlled by the acceleration voltage, the silicon crystal structure is afterwards recovered by an annealing process [165]. The dopant concentration can tailor the electrical properties of a semiconductor layer as described in section V.A.

In addition five point ion source types with smaller spot sizes on the sample surface (below 50 nm) will be described. These can be employed for vector scan ion beam nano patterning, which is the main scope of this work [215], [41], detailed instrumentation descriptions can be found in [167], [168], [169], [184], [231]. The fundamental instrument set-up is similar to the one described in the EBL section (see FIG. 2 in section II.C.1). The following ion source parameters and characteristics are important for ion beam nano patterning [188]: Energy spread, virtual source size, angular intensity, beam brightness, source life time, source stability (last two [41]) and a choice between different ion species [232]. Especially for fine spot sizes the source emission stability is an important parameter for the usability, if more than a few nano features requiring the same dose (number of ions per pixel) shall be created. The lifetime has to exceed at least the time to carry out the patterning job. More details about ion beam generation mechanisms can be found in [188], [193], [214], [233], [234], [235], [236], [237].

3. The recently commercialized ultra-high resolution ion microscope, equipped with a gas field ion source (GFIS) [173], [214], [215], [233]. It can become a complementary patterning technique with < 1 nm potential instrument resolution capability. Early 10 nm and below pattering results in resists -used also for electron beam lithography- have been published by Sidorkin [238] and Winston [239], exemplary results can be found in section V.E.4 and V.E.7. Gas field ion sources are based on the field ionization process. It takes place at high electric fields (≥10 V / nm). Around 1940 Müller employed this ion generation technique in his field ion microscope [185] (as described in section V.B). The tip is operated in a noble gas environment applying electric extraction fields [173]. GFIS is capable to resolve sub nm features in imaging [215] and to pattern sub 5 nm minimum feature sizes [240]. The source possesses a small virtual source size (0.3 nm), high reduced beam brightness ($1 \cdot 10^9$ A / $(sr \cdot m^2 \cdot V)$ [173], calculated from an angular intensity of 2.5 µA / sr) [173]. The energy spread was estimated to 0.25 to 0.5 eV [173]. More details about the operation principle can be found in [233], [173], [193]. Available ions for this technology are He and Ne, currently employed [241], further possible ones are: H_2, N_2, Ar, Kr and Xe [195], as illustrated by "♥" in FIG. 17.
4. Instruments utilizing a new generation of inductively coupled plasma (ICP) ion sources ([217], [215], [41], [218]), as well as Electron Cyclotron Resonance (ECR) ion sources [242] have entered resolution regimes so far only accessible to LMIS, with much higher beam currents. In these ion sources the ions are extracted through a small aperture. The virtual source size can be altered by selecting different beam defining apertures. The polarity of the emitted ions can be selected by the polarity of the extraction electrodes [233]. Typical parameters for Xe are a few eV energy spread [219], a spot size depending on the beam current from 50 nm to about 1 µm and a reduced beam brightness of 10^4 A / $(sr \cdot m^2 \cdot V)$ [219] with mostly single charged (ionised) ions in the beam [219], [217]. The described plasma ion sources are well suited for µm

scale milling applications. With larger beam currents of more than 1 µA Xe ions this technique is up to 50 times faster for milling applications than liquid metal ion sources using Ga (an example application can be found in V.E.6) [219]. Available species for this technology are: inert gas ions, such as He, Ne, Ar, Xe and in addition O^- or O_2^+ [215], [195], as illustrated by "♦" in FIG. 17. An exemplary application result is given in section V.E.6.

Instruments employing liquid metal ion sources (LMIS), are well suited for a large range of applications. Since about the 1980s this ion source technology is dominating focused ion beam (FIB) applications [218]. They are wide spread and routinely used in a large number of nanotechnology labs, mostly as two beam and columns workstations, consisting of a Ga LMIS FIB and a SEM column (the instrument description is given by type 6 below). As a result many ion beam nano patterning experiments are currently carried out in these labs employing LMIS. From a broader point of view, we take a look at the fundamentals (applicable also to other ion instruments), necessary processes development steps and application results for different instrument types, because some promising interaction regimes currently apply different fundamental instrument set-ups (here the instrument description is given under type 1 and 2 above). With additional and beneficial capabilities some of these interaction regimes can also be tried employing point ion source technologies. Although (Ga) LMIS possess a mid-range reduced beam brightness of $2 \cdot 10^6$ A / $(sr \cdot m^2 \cdot V)$ [243] and energy spread (few eV) [244], it is a well matured source technology [215] and spans a wide range of applicable beam currents [0.1 pA; 1 nA] at competitive resolution, for some applications below the 5 nm level [245]. Starting with their invention at the beginning of the 1960's, with its more than 50 years of evolution [84], they are very well suited for high resolution patterning applications, especially with the improvements described in [172]. For LMIS ar large variety of incident (process) ions are available, red marked elements in FIG. 17, [195]. In case of LM(A)IS instruments three further fundamental instrument types can be differentiated:

5. Automated and dedicated ones for a single (industrial) application like mask repair or circuit edit [246].
6. Versatile ones sometimes equipped with two charged particle optics (CPO) columns, one with electrons usually from the top (electrons hit the sample surface with normal incidence), the other one with Ga ions for patterning and analysis applications, at an angle. These SEM / FIB or FIB / SEM systems are often employed for analysis, cross sectioning or TEM lamella preparation applications [167], [168]; and can also be used for patterning, a recent overview can be found in [247].
7. A dedicated one for nano patterning (NanoFIB, LPN CNRS, Marcoussis France joinedly developed within an EC growth project [248]). It is equipped with the improved LMIS technology mentioned above [172] [195], and optimized for long time (> 12 h [72]) patterning processes. In addition it has been realized inside an electron beam writer instrument architecture [41] with a sample stage controlled by a laser interferometer positioning signal, which can be employed, for write-field (for details see sections II.C.1 and II.C.2) calibration, absolute stage positioning information and automated drift correction, using a dedicated SW.

   Thus, unattended batch nano fabrication jobs are possible. Patterning process reproducibility is obtained by the stable probe current [172] (stable dose), in combination with automatic correction and control schemes. Sub 5 nm lateral resolution patterning has been proven utilizing this instrument (this is shown in section

V.D.3) [249]. A recent overview is [220].

In addition the technology has been commercialized [221] and offers a choice of liquid metal alloy ion sources. An ExB filter is available [250]. In addition processes can be catalysed by inserting gases into the process chamber [62], [63] or an annealing process can be added. All this can be selected from a large variety of ion matter interaction regime processes. Thus, desired interaction volumes and ion matter interaction regimes fitting the application and material system (fundamentals described in section V.C.2) can be selected by the incident ion types, cluster types and charge states of the particles. Both will be further explained in the following section.

V.C.2. Ion matter interaction regimes

Ga ions accelerated by 30 keV hitting the sample surface transfer a momentum of about $3 \cdot 10^{-20}$ kg m / s ($1.16 \cdot 10^{-25}$ kg, resulting speed 288 km / s, i.e. non relativistic [41]). In addition, they hit the sample surface with a higher energy density [251], than electrons of the same energy. As a result (Ga) ions offer a large variety of ion matter interaction regimes, which are accessible to ion beam processing (analysis and patterning), thus also to vector scan point ion instruments. For Ga^+ (and ions of a similar mass), a so called linear cascade regime has been defined (accessed by acceleration voltages from 5 to 50 kV) [230], because the majority of the available Ga FIB instruments inside nano patterning labs operate in this regime. As a result many researchers have access to them and carry out nano patterning experiments with them. Ga possesses a low melting temperature (303.05 K which is equivalent to 29.9° C) and -depending on purity and environmental conditions- a large undercooling behavior down to about -8° C [252]. As a result it is liquid at room temperature inside the instrument and can emit [253] if heated before. During operation no steady heating is required. In addition, Ga LMIS sources produce mainly single charged ions (> 99%) [194] and [254]. This means each ion carries the elementary charge of $1.6 \cdot 10^{-19}$ As (or Coulomb).

Interaction mechanisms -as a first approximation [255]- can be analyzed separately, as elastic (nuclear) and inelastic (electronic) interactions, because of the large mass difference between the incident ions or surface atoms with respect to electrons [229] and the resulting different respond times to impacting ions [256]. Ions interacting with other atoms cause elastic and nuclear interactions often referred to as radiation 'damage' [230], [229]. Following Townsend we will employ the term radiation interaction instead; "... One should repeat that the prejudice invoked by the words damage or defects is unfortunate since the changes in structure produced by the passage of fast ions enables us to make materials which were not obtainable by normal thermodynamic processes. It is also true that the "damaged" material may have superior properties to the original solid..." [166].

Incident ions transfer momentum to target surface atoms and loose initial kinetic energy until they come to rest, within the so called collision cascade region [230] or interaction volume. The interactions with the surface depend for example on the acceleration energy, mass of the incident particle and mass of the substrate. Most theoretical work has been carried out so far for Ga^+ as these are most commonly used, if light incident ions like He, Ne or Si are employed the interactions are significantly different. For example lighter ions like Si would result in an interaction volume significantly larger than that of Ga^+ ions, but still significantly smaller than electrons. Employing an instrument with an ExB filter, ions with different charges can be separated, so for example Si^{++} ions will be accelerated faster than Si^+ ions employing the same acceleration voltage (in the same instrument), thus resulting in an even larger interaction volume.

The extension of ion matter interaction regimes are called collision cascade region can be modelled by Monte Carlo computer programs like "SRIM" (The stopping and range of ions in matter) by Ziegler at al. [257], [256], which simulates statistical interaction events. SRIM takes direction changes due to binary collisions into account together with nuclear and electronic energy loss. If the energy deposit into the target is small enough, Monte Carlo simulations predict experimental results quite well [229]. In SRIM only amorphous substrates are taken into account, so an effect like channeling is neglected. Exemplary interaction volumes for 40 keV Ga^+ ions impacting into an amorphous silicon substrate have been simulated by SRIM as well as for electrons by Casino (details about the Casino SW can be found here [41]). For 40 keV kinetic energy the interaction volumes have been simulated:

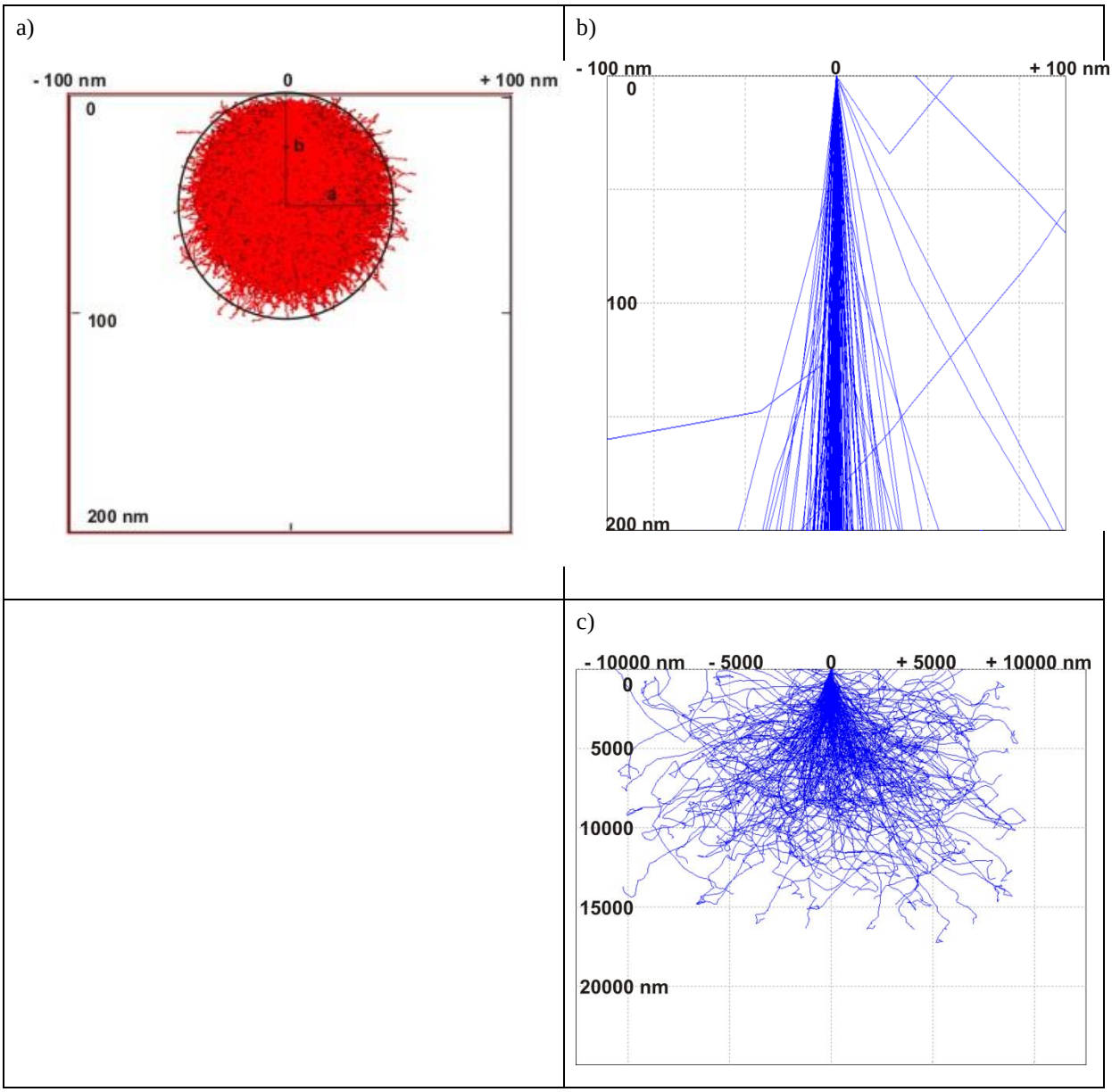

FIG. 18. a) Ga ions simulated interaction volume (40 kV, Si sample, SRIM, 1,000,000 trajectories)
b) electrons upper part, same scale as for the Ga ions (40 kV, Si sample, Casino, 1000 electrons, 200 displayed)
c) and complete interaction volume for electrons (40 kV, Si sample, Casino, 1000 electrons, 200 displayed)
for details see [41]

The SRIM simulation results of primary Ga ions are displayed in FIG. 18 a), they induce radiation interactions in the range of a few tens of nanometers in 3 dimensions (approximated by an ellipse with a = 44 nm (about 8µm for electrons) and b = 48 nm (about 6 µm for electrons). The interaction volume is 3.9 10^{-22} m^3 or 0.00039 μm^3 (without backscattering and collision cascade effects, which would enlarge the interaction volume for Ga ions). Further interaction volumes for different atom and ion species can be found in [258], [231] and [232]. For electrons the interaction extension for all three dimensions is each about two orders of magnitude larger than for Ga ions. Although the interaction volume is much larger than for ions the surface imaging or

pattern definition resolution can be higher than for ions. This can be estimated from the high particle density entrance channel in FIG. 18 b) near the surface (at the top).

Ion interaction regimes with electrons of the target atoms are called inelastic or electronic interactions (see for example [228], [230], [229]). This process can be regarded as a continuous viscous drag between the incident ions and the sea of electrons [228]. The nuclear contribution usually dominates the stopping power [228] in the linear cascade regime. At higher ion acceleration voltages the electronic stopping power increases, too and is usually observed at energies of several hundred keV. In addition channeling can occur [230], it describes incident ions travelling along a low particle density trajectory inside a sample crystal lattice. Here ion interaction regimes with the surface atoms are the same as in the non-channeling case, at sub surface crystal layers they have less interactions with the crystal and thus travel longer.

Possible interaction regimes are visualized in FIG. 19. Incident ions can interact as described above with the surface atoms and electrons as well as groups of surface atoms (molecules). In addition they can participate in chemical reactions either with surface atoms or precursor gas molecules [62], [63], [259]. Table I gives an overview about matter interaction regimes for ions and electrons.

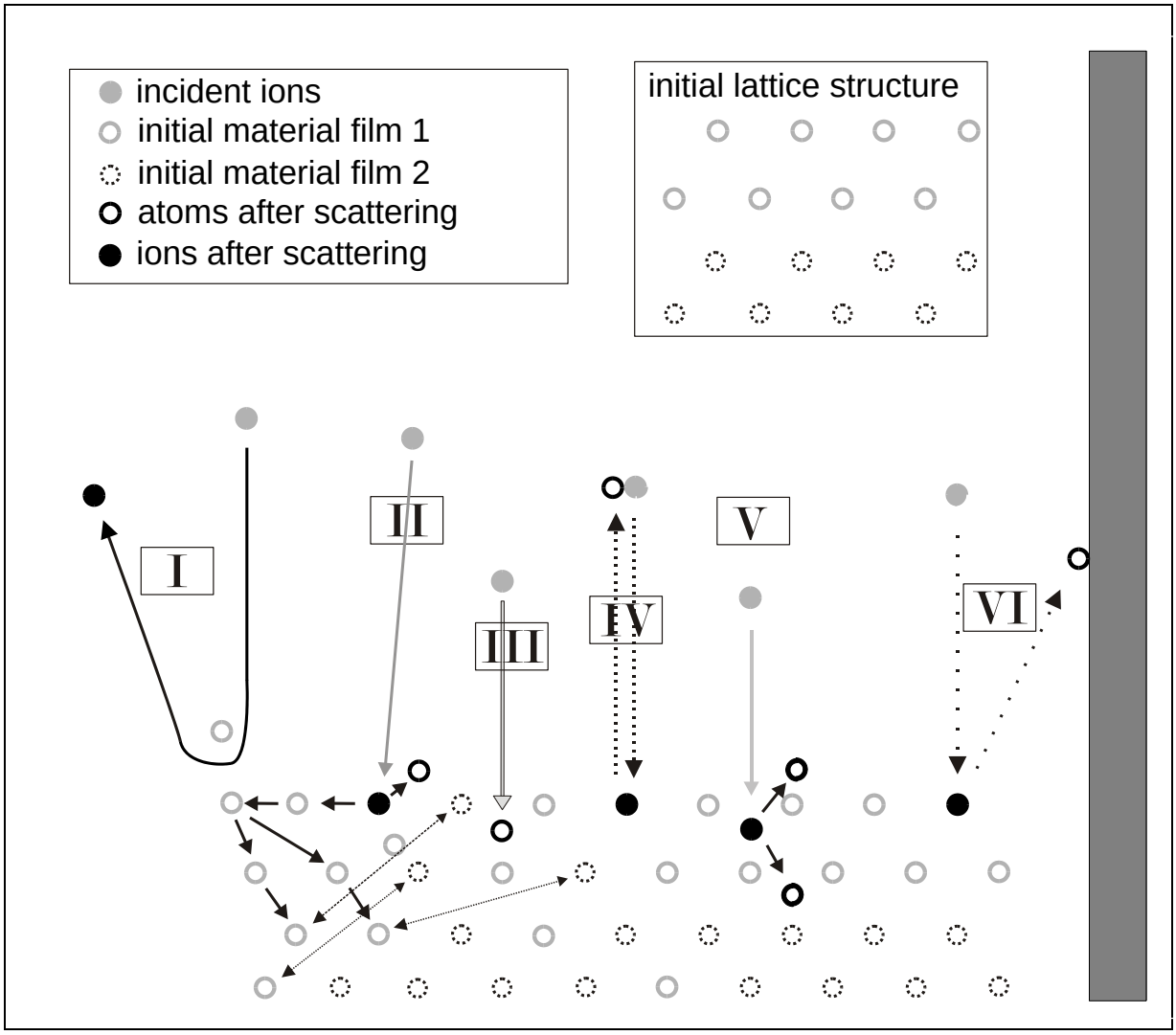

FIG. 19. Overview of exemplary ion matter interaction regimes. Incident ions are: I) backscattered, II) implanted at lattice sites (and cause further interaction regimes like atom intermixing with a 2nd material layer), III) implanted at interstitial sites and come to a rest, IV) target atoms are milled out of the sample, V) implanted at interstitial sites, influencing the original crystal structure, VI) target atoms are milled out of the sample and redeposit at a surface in the vicinity.
from [41], modified

Table I: Ga^+ and electron matter interaction regimes (Roman numerals, refer to those in FIG. 19) adapted from [41].

Ga^+ ions can	**Electrons can**
cut / crosslink organic molecules	cut / crosslink organic molecules
excite atoms	excite atoms
generate heat	generate heat
be backscattered (these become charge neutralized at the surface, becoming an atom, and get re-ionized leaving the surface again, making them the same as the incident ions) (**I**)	be backscattered
initiate gas assisted processes	initiate gas assisted processes
participate in gas assisted processes	-
implant at interstitial (**III, V**) or lattice places (**II, IV, VI**) in crystalline or into amorphous surfaces (get charge neutralized at the surface, thus become atoms)	-
cause surface modifications, move surface atoms to other positions (**II, V**), these can also be ones from a buried layer below, which can than intermix with ones in a thin surface layer, giving access to unique concentration profiles	-
remove surface atoms ("milling"), these atoms can either "redeposit" (**VI**) at surfaces in the vicinity or escape into the vacuum chamber (**IV**)	-

The interaction regime called atom intermixing or chemical alloying is mentioned in Table I and illustrated by "II" in FIG. 19). It can place atoms from a layer below a thin surface layer into the latter. This atom transport from a lower substrate layer into the thin surface layer takes place at the interface between them [228], [213]. This effect can be exploited as complementary pattering / implantation processes. First to achieve a larger concentration of impurity atoms in a thin surface layer than possible by direct implantation, which is limited by the steady state condition [228]. Second thin magnetic films can be locally separated by the formation of domain walls already at a low ion dose and with high resolution capabilities (an example is given in section V.D.4).

Interactions between incident ions and inorganic materials like milling (or sputtering), ion implantation and thin layer atom intermixing have been successfully applied for nanopattering (here application examples are described in sections V.D and V.E). In addition organic resist exposure has been studied already from the very beginning (as explained in the history section V.B), however the definite exposure process is not completely understood yet [208]. Further routinely employed techniques are employing additional process gases. They can be initiated into the vacuum chambers resulting in many additional capabilities, a comprehensive overview

about precursor gases for deposition and etching with focused ion and electron beams are given in [62], [63]. The gas can interact directly with the incident ions and the sample surface (initiate gas assisted processes by the incident energy), both listed in Table I.

In addition to the ion matter interaction regimes described in Table I another fascinating mixed ion matter effect exists. It is initiated by broad ion sources (type 1 in section V.C.1) with large beam currents eroding a surface area in a way that self-organized regular nano structures evolve [229] (an application example is given in section V.E.15). These 3D nano features arise, on amorphous semiconductor surfaces and can be explained by similar processes on metal surfaces: "…in metals, the surface curvature dependence of the sputtering yield and the presence of an extra energy barrier whenever diffusing adatoms try to descend step edges, produce a similar surface instability, which builds up regular patterns. " [90]. In addition rapid amorphization (surface diffusion [160]), mass redistribution and modifications to the surface curvature contribute [260]. The feature size can be influenced for example by the acceleration energy [261] and angle of incidence. Here different areas (different components) of the surface are milled with different speeds. Further details can be found in [262], [230], [229], [263]. Although the large variety of ion-matter interaction regimes open fascinating patterning opportunities and Seliger has proven the practical feasibility of resist exposure already in 1973 [202], [203], still only two Ga^+ ion matter interaction regimes are routinely employed: milling and gas assisted processing.

In the next section, another important parameter which can influence ion matter interaction regimes and interaction volumes will be briefly described.

V.C.3. Ion dose

Together with other research groups we explore non-conventional patterning applications. Especially for these applications the dose plays a significant role. In addition to varying the incident ion species and acceleration energy. The dose is another parameter which can be used to alter ion matter interaction regime (results) and interaction volumes. Dose is the quantity of particles absorbed by a medium within a certain area [230]. Dose is proportional to the probe current (I_p), point dwell time (T_d) and inverse proportional to the square of the "step size" (as illustrated by.Equation 2). Depending on the process, a definition of area or line dose is used.

$$D = \frac{I_p \cdot T_D}{s^2},\ D_L = \frac{I_p \cdot T_D}{s}$$

Equation 2: Area and line dose

D = area dose

D_L = line dose

I_P = probe current

T_D = point dwell time (time the beam rests at a point of the discrete pattering grid)

s = distance between two points in the discrete patterning grid ("(exposure) step size")

FIG. 20 shows experimental cross sectional AFM results from different ion doses irradiated onto silicon (100) wafer surfaces, surface bumps and milling are visible, due to local amorphisation and surface modifications [264].

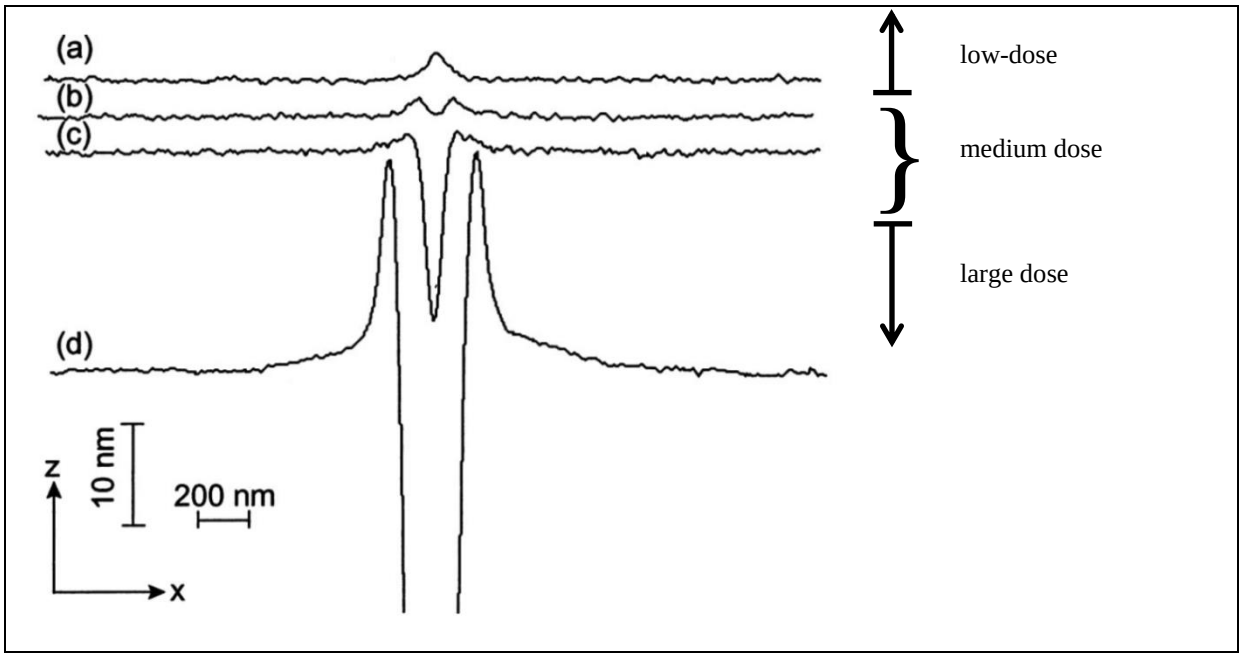

FIG. 20. Left: Cross sections of a Si (100) surface applying different doses (50 keV Ga^+ ions)
a) $1.3 \cdot 10^{15}$, b) $8.6 \cdot 10^{15}$, c) $8.6 \cdot 10^{16}$, d) $1.7 \cdot 10^{19}$
Fig. 1 from [264], Reproduced with permission from J. Vac. Sci Technol. B **21**, 927 (2003).
Copyright 2003 American Vacuum Society
Right: definition of dose regimes following [184]

The ion dose can be classified into three regimes: low / medium / large (for Ga^+ ions in the linear cascade regime), causing different surface effects [255] which can be exploited for different applications (implantation, amorphisation, milling).

In the low ion dose regime (10^{11} to 10^{15} ions / cm^2), the surface damge generation dominates. The crystal to amorphous transition is initiated at the surface (few monolayers), the global crystallographic order of some materials (metals, metal alloys and oxides) will not be modified. Stress is accumulated and afterwards relaxation occurs, resulting in "bumps". If ions hit solids with covalent bonds the surface phase can be rendered locally into the amorphous phase and if they hit amorphous oxide surfaces they may become locally crystalline [255]. The depth concentration profile of implanted ions can be characterized by a Gaussian distribution around the projected range R_p [228]. Significant milling does not take place in this dose regime, but other effects like atomic lattice modification, atom mixing, phase transitions, surface cleaning, ... occur.

FIG. 20 illustrates that in the medium ion dose regime (intermediate, 10^{15} to 10^{17} ions / cm^2) milling effects progressively take place, "volcano crater shape" features evolve. If the dose is further increased, multi-dimensional atomic lattice modifications and complex configurations can be generated [230].

The high dose regime (>10^{17} ions / cm^2) milling and redeposition of sputtered material effects are dominant, thus material ejection is limited and also the aspect ratio for a small hole. It is usually applied for material removal applications, however the other effects are still present. Milling effects in the linear cascade and the high dose regime can be modelled with the linear cascade model and the binary collision approximations [256]. It is a quite well understood and studied regime, because of the commercial interest of the semiconductor

industry, for applications like circuit edit [246]. However, the medium and low-dose regime has so far been relatively little studied and applied for patterning applications.

In the following section we take a look at different concepts for resolution.

V.C.4. Resolution

Resolution can describe on one hand the minimum distance between two objects in analysis or imaging, which can still be differentiated [265]. On the other hand in fabrication other concepts are more adequate like the minimum distance (period) between two artificially created objects or the smallest feature size, which can be intendedly created. The smaller the resolvable features or periods are, the higher the resolution.

In the fields of charged particle optics and ion matter interaction regimes some aspects of resolution can be modelled, resulting in numbers for the beam diameter, current distribution, or lateral scattering (primary and collision cascade effects).

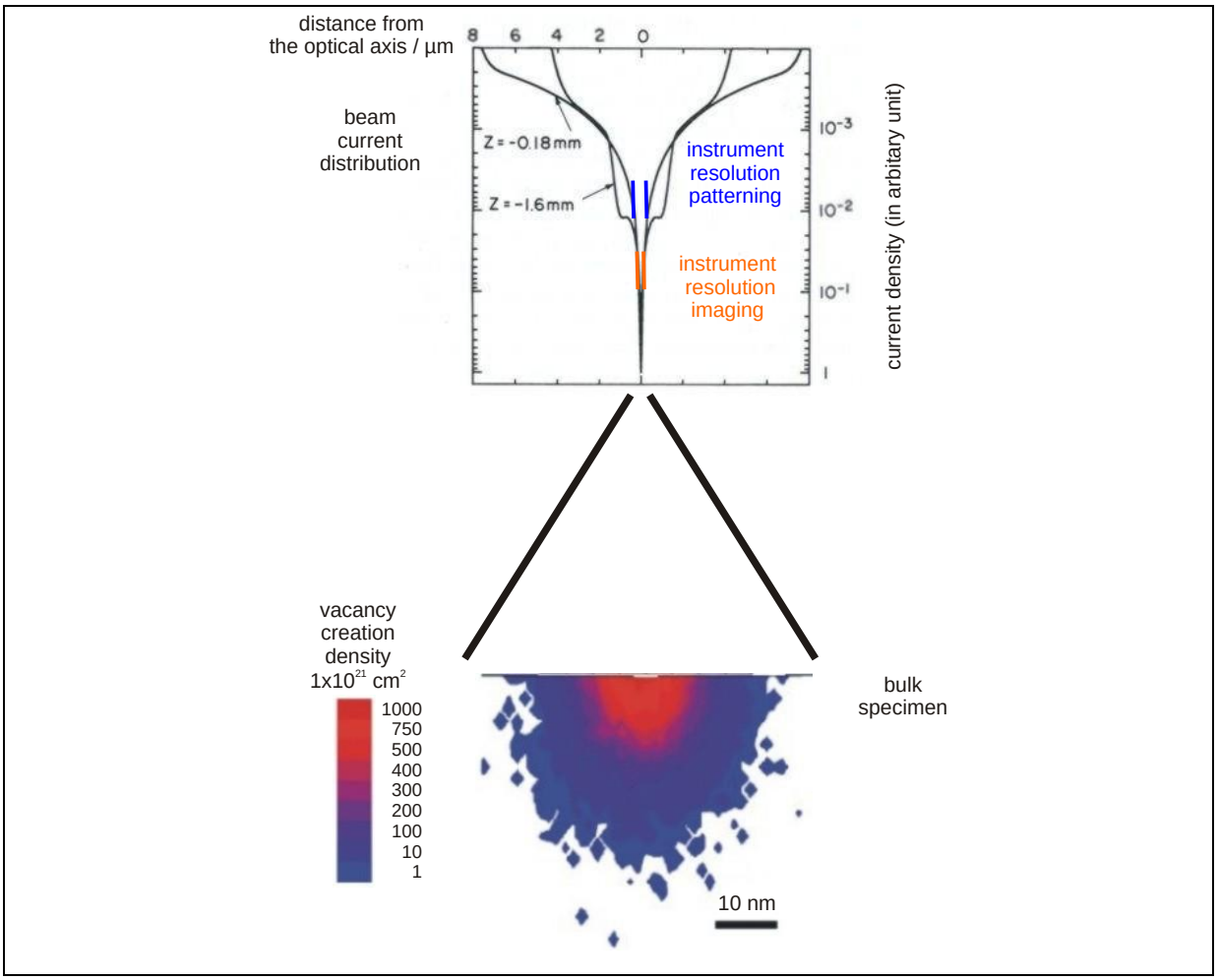

FIG. 21. Combining a modified calculated beam current distribution plot for two objective lens excitations (Z = -0.18 and Z = -1.6), with suggested possible patterning and imaging resolutions for certain applications and material systems
modified Fig. 2 in [254] with permission from the author J. Orloff, Reproduced with permission from J. Vac. Sci Technol. B **9**, 2609 (1991). Copyright 1991 American Vacuum Society
with a modified TRIM simulation of the energy deposited by the ion beam and the collision cascades of a 35 keV Gabeam with a bulk target showing the damage localization.
Fig. 3 a) in [245] (modified), Reproduced with permission from Ultramicroscopy **109** / Elsevier, 457 (2009), Copyright 2009 Elsevier

Four different inter-related fundamental resolution concepts can be differentiated: beam diameter (instrument resolution), beam profile (current distribution), interaction volume (collision cascade regimes) and application resolution.

A first resolution concept, the instrument resolution, can be simulated (beam diameter calculations: finite elements methods, trajectories analysis, Barth Kruit formula [266], wave optics, …) based upon charged particle optics (CPO) theory [267], [49], [268], [269], [46]. At the beginning of this field first analytical and nowadays numerical models have been developed based upon experimental verifications [267]. The value for the beam diameter is often advertised by instrument manufacturers and proven on special selected and ideal samples. Today's point liquid metal ion source (LMIS) optical systems are mainly limited by spherical and chromatic aberrations [262] as well as charge effects [263]. Which one of these actually dominates, depends on the "column operation mode" [194]. For patterning applications with large write-fields, aberrations due to the deflection of the beam away from the optical axis have also to be taken into account.

A second resolution concept is called ion trajectories or beam current distribution. It is also studied in the field of CPO theory which allows for example to simulate the beam diameter in the surface plane [254], [266]. The ion trajectories, the current distribution and the beam profile, thus the application resolution can be influenced by the position of the sample surface in the image plane (working distance (WD), which can be influenced by the objective lens excitation or the vertical sample position). There exists a specific working distance for the optimum imaging resolution the Gaussian plane and a different value is needed to mill the smallest features the plane of least confusion, which is illustrated in FIG. 22 a). This results in different beam current distributions or beam profiles illustrated in FIG. 22 b), Orloff et al. [254]. In addition it has to be taken into account that "…the spherical aberration coefficient increases rapidly with working distance (as the fourth power), a short working distance will decrease the amount of current carried in the tail of the distribution" [254]. FIG. 22 c) and d) illustrate this different optimum foci for the two cases.

a)

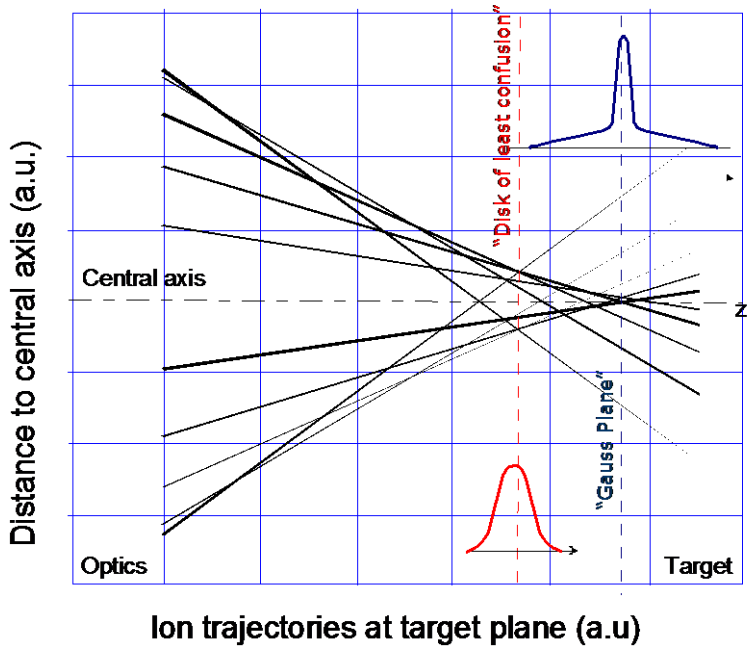
Distance to central axis (a.u.)
Central axis
"Disk of least confusion"
"Gauss Plane"
z
Optics
Target
Ion trajectories at target plane (a.u)

b)

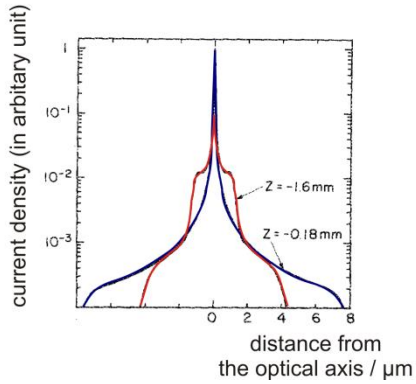
current density (in arbitary unit)
Z = -1.6mm
Z = -0.18mm
distance from
the optical axis / µm

c)

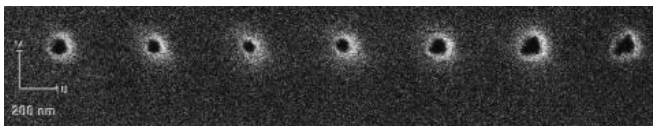
200 nm

d)

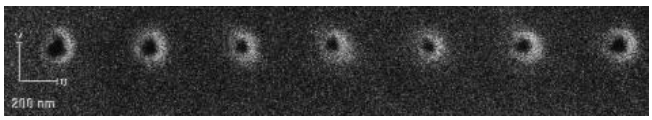
200 nm

FIG. 22. a) “Schematic representation of the trajectories of ions at the exit of an electrostatic lens with aberration. (1) Geometrical plane of the “Gauss optimum” with a profile presenting not only a narrow peak but also side wings. (2) Optimum plane for FIB writing experiments (“circle of least confusion”) giving a bell-shaped profile for the current distribution.” [271]
Fig. 3.12 in [271],
b) Calculated current density distribution profiles for the case of large aberrations (at different focus positions Z, Spherical aberration referred to image side C_{si} = 20,000 mm, Chromatic aberration referred to image side C_{ci} = 240 mm [270]), modified (colors matched to FIG. 22 a)
Fig. 2 in [254], Reproduced with permission from J. Vac. Sci Technol. B **9**, 2609 (1991). Copyright 1991 American Vacuum Society
c) Part of an ion SE micrograph (scale bar has been copied into this part of the image from the original), taken with a lens setting for optimum image focus (ΔWD = 0 µm), the holes have been drilled with different WDs, starting with the left one: -40 µm, -20 µm, 0 µm, +20 µm , +40 µm), sharp image and the smallest hole is one left to the centre at -20 µm
d) Part of an ion SE micrograph (scale bar has been copied into this part of the image from the original image), taken at lens setting for optimum patterning focus (ΔWD = -20 µm), the holes have been drilled with different WDs, starting with the left one: -60 µm, -40 µm, -20 mm, 0 µm , +20 µm), unsharp image and smallest hole in the center at -20 µm

A third resolution concept, interaction volumes, can also be modelled, in this case by Monte Carlo particle scattering simulations [256], [257] or molecular dynamics [229], [272] (more details can be found in section V.C.2). Ion matter interaction regime processes are usually complex many body interactions, so being able to model certain aspects for some applications is essential for users and mandatory for opening new application fields. The interaction volume can be influenced by the selected ion species, probe current, angle of incidence and acceleration voltage.

The fourth resolution concept, application resolution, effective interaction volume or voxel is well suited for practical applications [194], [273]. It includes the ones above, the achievable signal to noise ratio [262] in imaging, contrast creating or structuring mechanisms [262], as well as the chemical or physical processes including their corresponding process sensitivities, interaction volumes (ranges) and contributions from the environment (vibration, electromagnetic fields, ...) [263]. Application resolution is a result-oriented concept and has to be figured out experimentally for each application. Imaging or patterning “ideal” material systems which can proof the instrument resolution is very different from using such an instrument to fabricate certain structures or devices in the material system of interest. Since the end of the 1970s liquid metal ion source (LMIS) instruments carry out patterning as well as analysis applications, both rely on and influence each other. Acceleration energies between 5 and 50 keV in Ga LMIS point source ion beam instruments induce near surface processes with a few tens of nm penetration depth / interaction volume. A high “instrument resolution” enables small lateral spot sizes (a few nm). However, if the interaction volume for the target application is of the order of a few tens of nm or more this will dominate the effective usable resolution.

In high resolution imaging all interaction processes have to be taken into account. An incident ion matter interaction phenomenon is called milling or "sputtering" (as described in section V.C.2). The relatively large material removal rate for 5 to 50 keV Ga^+ ions limits the resolving capability of an ultra-sharp edge, because the edge is removed / smoothed out during the imaging process: “For extended small features (like layered structures), rearrangements, redepositon, and differential milling rates may limit the resolution in some cases” [262], [274]. For high dose ion matter interaction regimes, the resulting patterning application resolution can be lower than for low-dose ones, due to the beam current distribution of the ion beam [220]. In addition, features

without interface defects produced by the ion impact can also be realized by ion beam nanopatterning (similarly as in the self-organized 3D case, section III.C), for example by selecting the incident ion species according to the sample material system, sometimes an additional annealing process is required.

For some applications ion beam imaging / structuring can be more suitable than electron beam imaging / patterning, although the instrument resolution is often lower (LMIS). Clever processing can allow to pattern with an application resolution better than the actual instrument resolution (a nanopore application example is given in section V.D.3).

V.D. Examples of applications

The prevalent FIB instruments (almost every nano patterning and analysis lab is equipped with one), are more and more used to evaluate a large variety of patterning applications (ion matter interaction regimes), also beside the two main stream ones (milling and gas assisted processing). In this first section a modified version of the versatile FIB instrument (No. 6 in section V.C.1) as well the dedicated nano patterning ones (described under point 7 in section V.C.1) have been used to create leading edge application results. These are thought to stimulate testing of further ion matter interaction regimes for all kinds of applications. Some of them can create operating devices (or preliminary stages of them) already within one process step. Different possibilities to categorize them exist by: ion matter interaction regimes, material systems, instrument technology or application fields.

At five application results we take a closer look: (single) ion implantation for local doping, preparation for graphene nanoribbon growth, nanopores for DNA manipulation, small magnetic domains and the fabrication of a X-ray zone lens. This will be done with a focus on:

- ion matter interaction regimes exploitable for nano pattering
- precision
- process times / (instrument) stability
- resolution
- the current nano application challenges in this specific application field

V.D.1. (single) ion implantation I

Single ion events represent the minimum dose (1 ion) and in combination with the ion matter interaction regime implantation give access to small interaction volumes and thus, a high possible application resolution. Classical ion implantation used in the semiconductor industry (instrument type 2 in section V.C.1) reaches dopant atom distribution homogeneity challenges on the scale of future devices. This is because device sizes approach average distances between impurity atoms. Single ion implantation employing FIB and secondary electron detection [275] can improve this by tailoring the number of dopant atoms, thus the dopant concentration and their exact position.

The dopant atom position can be defined very accurately employing dedicated LMAIS instrumentation (a modified type 6 in section V.C.1). Shinada et al. showed pattern placement capabilities of the technique by

implanting individual Si^{++} ions (60 keV, LMAIS, modified tool type 2 in section V.C.1 has been employed) into Polyallyldiglycolcarbonat (PADC or CR-39), within a diameter of 100 nm [176], the results are shown in FIG. 23. The same group placed phosphorous atoms –in a different experiment- into a transistor channel region (30 kV) [177] and analyzed the electrical devices afterwards. FIG. 23 shows the larger transistor threshold voltage (V_{th}) shift compared to the undoped case (ΔV_{th}) and a statistical distribution (tighter confined bell curve) of ΔV_{th} than conventionally fabricated ones [177].

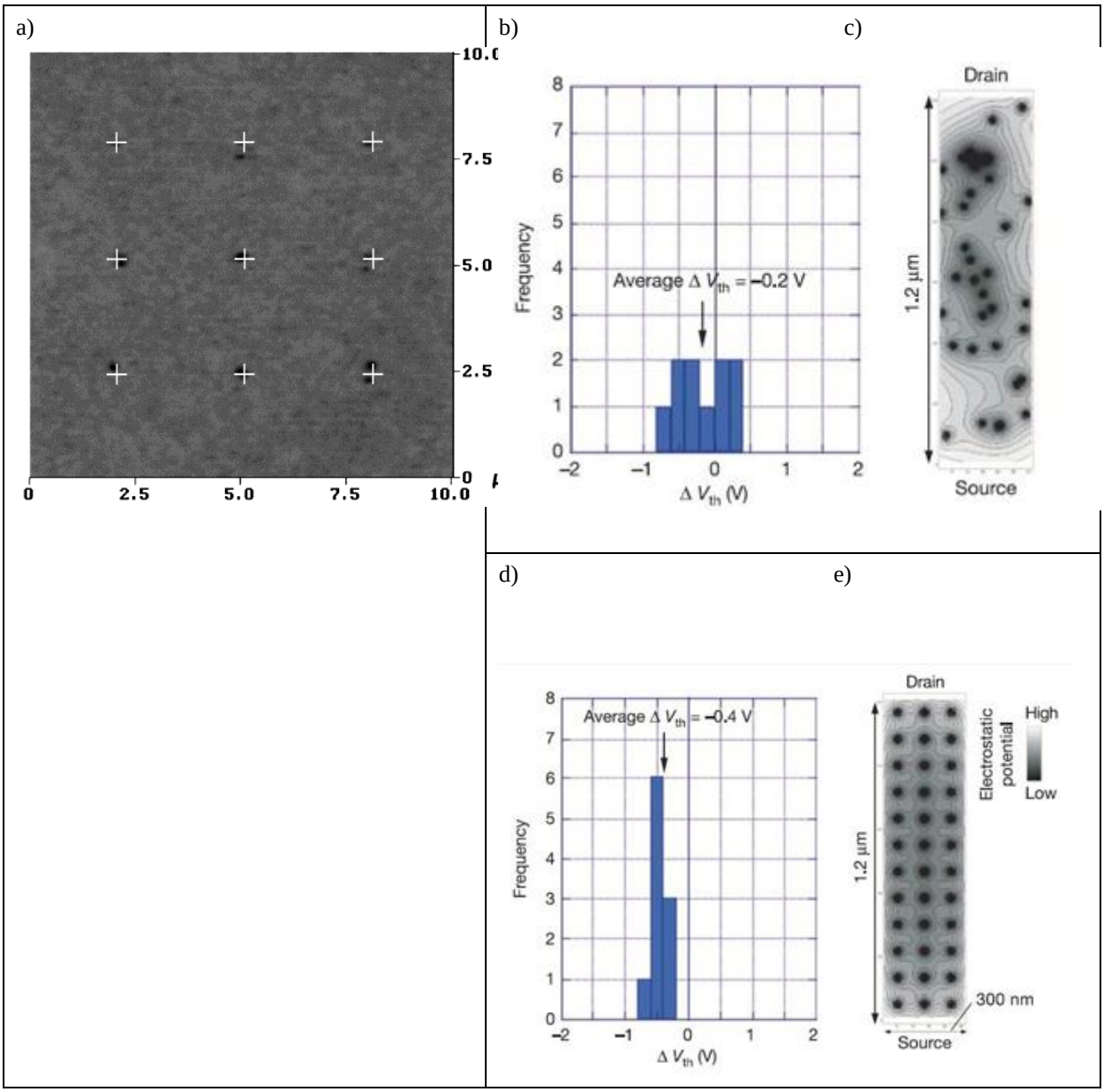

FIG. 23. (a) AFM image of etch pits created in CR39 by single-ion incidence. Histograms of V_{th} shift (ΔVth) before and after single-ion implantation from 10 resistors and calculated contour maps of the Coulomb potential in the channel.
Fig. 4a in [176] reused with permission from APEX/JJAP
(b), (c) Conventional random dopant distribution
(d), (e) Ordered dopant distributions
The Gaussian fitting curves of the V_{th} shifts in the ordered dopant distribution shows a standard deviation of only 0.1V, which is three times smaller than the random dopant distribution.
Fig. 4 in [177], Reprinted by permission from Macmillan Publishers Ltd: Nature **437**, 1128-1131 (2005), copyright 2005

These remarkable results prove the successful application of single ion event LMAIS FIB for semiconductor doping altering the electrical properties of FETs.

V.D.2. Si and Au implantation II (surface functionalization / graphene nano ribbon growth)

Another nano fabrication challenge is the reproducible fabrication of graphene at specific sample locations in the desired material quality to integrate it into devices.

As described in [178], [179]:

Graphene can have exceptional optical, chemical, mechanical and electrical properties like, e.g. very high carrier mobilities. In addition it is compatible with planar processing technologies developed for silicon and it is a candidate for metal oxide semiconductor (CMOS) devices. It can be grown onto different substrates by different techniques such as mechanical exfoliation, chemical vapor deposition (CVD), and thermal decomposition. The mechanical exfoliated one is described as the purest graphene possessing a high electron mobility. However, because of the current size limitations of the flakes, they are not used in commercial devices. Employing CVD or thermal decomposition wafer scale graphene sheets can be synthesized. Trying to transfer CVD graphene onto a dedicated substrate can degrade its electrical properties. Graphene can be formed on insulating or semiconducting of silicon carbide (SiC) by thermal decomposition, and thus be integrated into devices. A low-dose LMAIS FIB process with a high potential application resolution is achievable by combining ion implantation or multi-ion beam lithography and thermal or pulsed laser annealing (PLA) to selectively synthesize graphene only where ions have been implanted [178], [179]. Regions where Au, Cu, Ge, or Si ions have been implanted show a lower processing temperature than crystalline SiC (c-SiC), so thermal annealing can be used to initiate local graphene growth [178]. There is also evidence that the implanted species affect the needed PLA fluence for the formation of graphene [179]. A multispecies LMAIS instrument has been used for the implantation (type 7 in section V.C.1) [178], [179]. Direct patterning with nanometer resolution can be achieved without using conventional lithography techniques, see FIG. 24. By controlling the ion beam lithography and annealing conditions single or a few layers of graphene can be synthesized.

a)

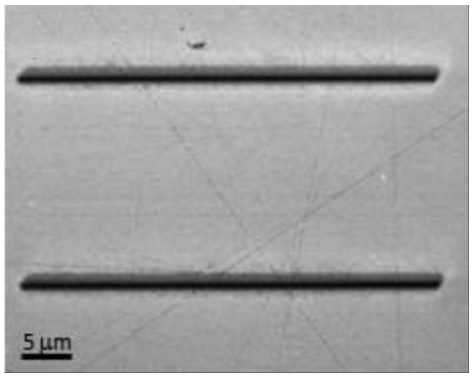

b)

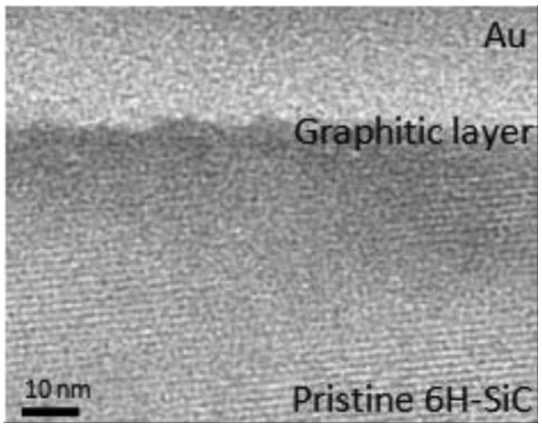

FIG. 24. a) "…SEM images taken on … graphene nanoribbon surfaces, …where the width of the two parallel nanoribbons (dark lines) is on the order of 200 nm …"
Figure 3 c) in [178] ("c" removed), Reproduced with permission from Appl. Phys. Lett. **100**, 73501 (2012). Copyright 2012 American Institute of Physics
b) "…TEM images taken across the Au / graphene / 6H-SiC…", „…shows the underlying 6HSiC's structural perfection…"
Figure 3 d) in [178] ("d" removed), Reproduced with permission from Appl. Phys. Lett. **100**, 73501 (2012). Copyright 2012 American Institute of Physics

In addition Raman spectra have revealed that graphitization is stronger for incident ions Au and Cu (CVD catalytic species, than Ge and Si (isoelectronic), compare the intensity of the relevant bands D, G and 2D in FIG. 25).

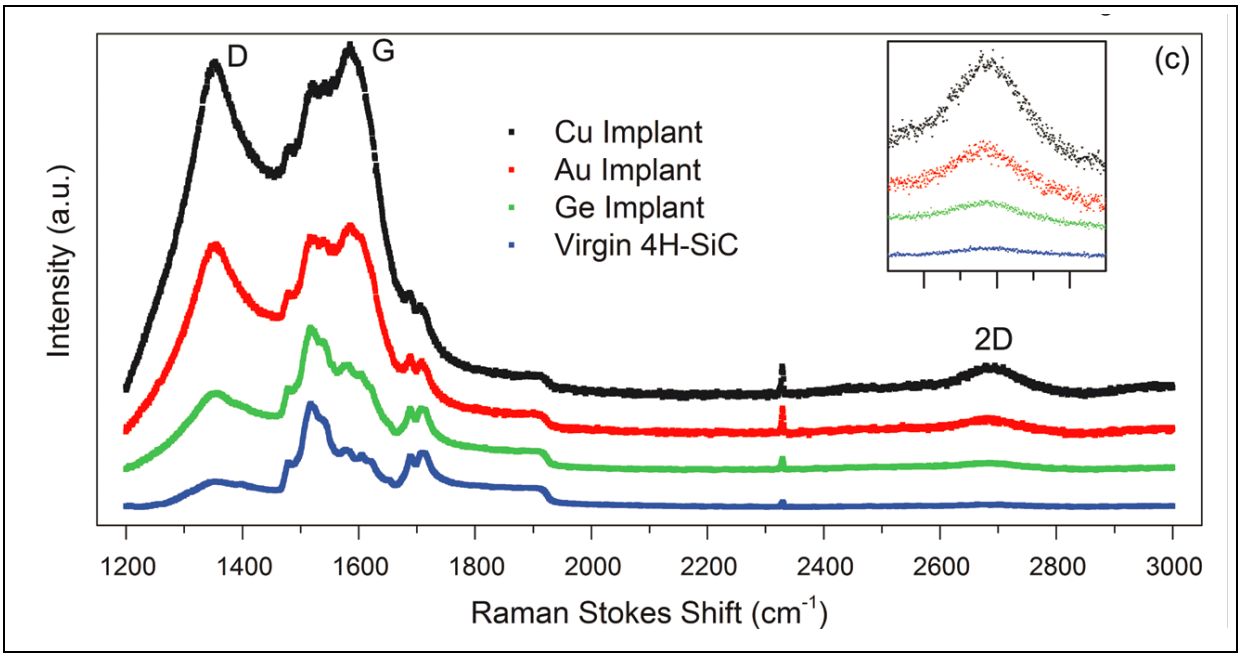

FIG. 25. "Raman spectra for each implant condition annealed at 1 J / cm^2 and 50 pulses. The spectra are normalized by the shoulder at 1920 cm^{-2} to avoid interference with the large convoluting G-band. Inset: Magnified plot of the 2D-bands."
Fig. 2 c in [179]. Reproduced with permission from Appl. Phys. Lett. **100**, 73501 (2012). Copyright 2012 American Institute of Physics

A combination of LMAIS FIB ("35 keV Au ions … fluence 5 x 10^{16} ions / cm^2") and pulsed laser annealing (PLA) in air are shown in FIG. 26. Here "a periodic micro-ribbon array composed of five lines, each 2 µm wide and 10 µm long, separated by 2 µm was patterned". FIG. 26 shows "the Raman map of the 2D-band intensity … of this area" which "shows graphitization only where the SiC was implanted". Thus, LMAIS FIB implantation into c-Si locally lowers the temperature or fluence in PLA needed for graphitization, so graphene nano ribbon growth can be locally initiated.

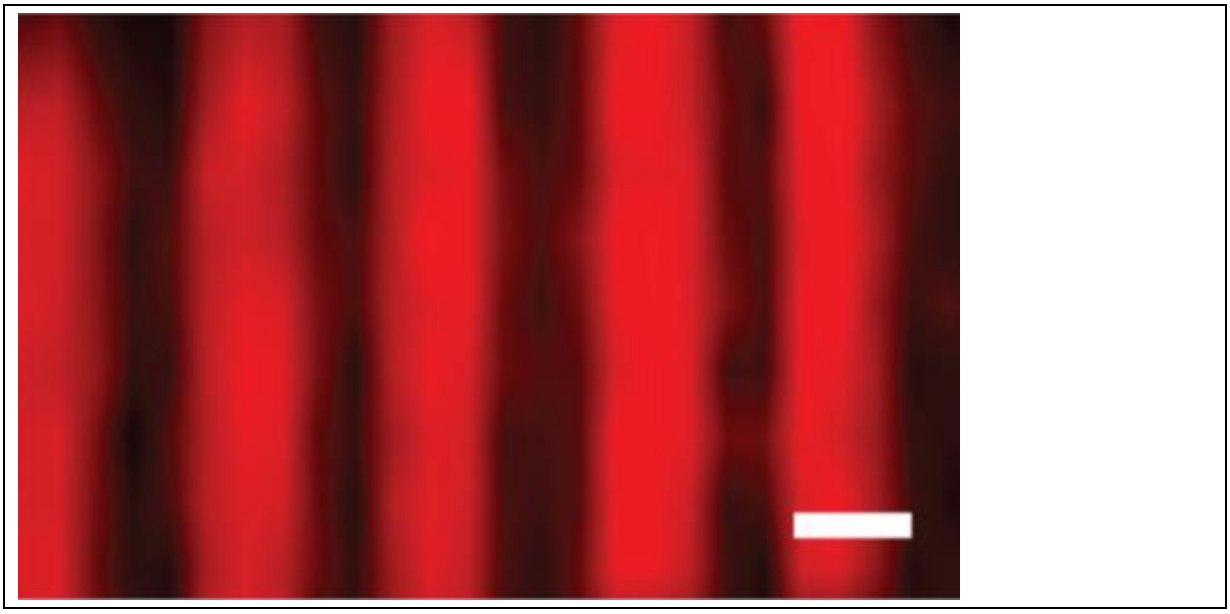

FIG. 26. "Growth of FLG with nanoscale features by Au-ion beam lithography and PLA….
(c) Raman 2D-band map of the metamaterial array." Scale bar is 2 μm
Part of Fig 3c in [179], Reproduced with permission from Appl. Phys. Lett. **100**, 193105 (2012).
Copyright 2012 American Institute of Physics

V.D.3. Nanopores I (DNA manipulation - milling / local surface atoms removal – SiC membranes)

DNA manipulation employing holes, channels, apertures or nanopores with diameters < 10 nm is a promising technique. A single molecule detector can be created by electrically monitoring the current variation flowing through an orifice. If nanoparticles, colloids or DNA is added to the solution current variations are observed resulting from the passage of the nano-objects through the orifice. This is done by applying a voltage between two electrodes in a conductive solution and measuring the resulting current (as illustrated by FIG. 28a). If a molecule passes the nanopore the current decreases, this effect is called "current blockade". Current changes indicate molecule compositions for in vivo virus analysis or DNA manipulation [276], [277], [278].

The current nano patterning challenge is to reproducibly create nanopores in a range from 5 to 30 nm diameter. Such nanopores can be fabricated by various techniques like EBL (electron beam lithography) and subsequent reactive ion etching (RIE) [279]. The current leading technique aims at directly drilling nanopores in a membrane using a highly focused and dense electron beam in a TEM, before it was also found very convenient for fine-tuning pore sizes to smaller sizes [280]. These methods allow ultra small pore fabrication, but require one-by-one nanopore processing. A FIB sculpturing processes [281] on the other side allows batch patterning of multiple devices since specimen size limitations are not an issue for FIB machines. Advantages of EBL (section II) are: it is an established, wide spread and well understood process technology. However challenges exist for reproducible sub 5 nm holes creation: the resist resolution limit in combination with the required aspect ratio for the RIE process step [282]. A sculpturing technology can reproducibly create sub 5 nm holes [281], however it is a rather slow and manual process (first mill larger holes and close them again in a second process step).

Simple direct milling of nanopores is not possible, as ion solid interaction regimes and lateral scattering of the primary beam limit the resolution [276], [282]. However high dose milling ion matter interaction regime combined with clever processing can result in a high application resolution, even below the instrument resolution. A refined process is required and a Ga LMIS FIB has been used (NanoFIB, type 7 in section V.C.1): Biance et al. [276] took a SiC membrane (30 or 10 nm thick) instead of bulk material (thickness in the range of the projected range of the impinging ions). This results in direct pattering of sub 5 nm holes ("application resolution") on the rear side of a membrane. The process exploits the lateral extension of the interaction volume (described in section V.C.2 and V.C.4) at the membrane rear side, when patterned from the top [249]. As a result some of the displaced atoms are directly ejected at the rear side of the membrane. This "forward scatterin" almost eliminates redeposition effects [249]. In addition the membrane is patterned from one side and stopped as soon as a small diameter opening is created on the rear side [249] (as shown in FIG. 27a) and the result in FIG. 27b).

a) b)

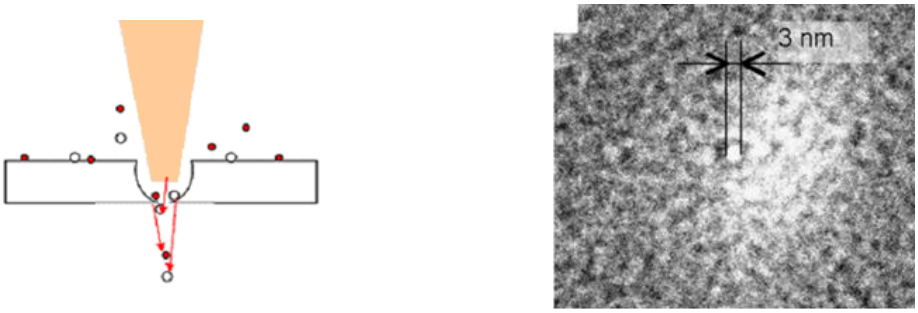

FIG. 27. Patterning process and result
Schematic of the membrane engraving processes.
(a) Entry side milling, milled until the nanopore is opened at the rear side, Fig. 3 c in [245], Reproduced with permission from Ultramicroscopy **109**, 457 (2009) / Elsevier, Copyright 2009 Elsevier
(b) TEM micrograph of a resulting nanopore drilled by a Ga beam into a 20 nm thick SiC membrane with around $2.5 \cdot 10^7$ ions / point, "d" removed, Fig. 5 (left) in [245], Reproduced with permission from Ultramicroscopy **109**, 457 (2009) / Elsevier, Copyright 2009 Elsevier

FIG. 28 a) shows a molecule measurement set-up [283] and b) an ionic current variation measurements induced by λ DNA molecules passing through or inserted in a Si_3N_4 nanopore [277].

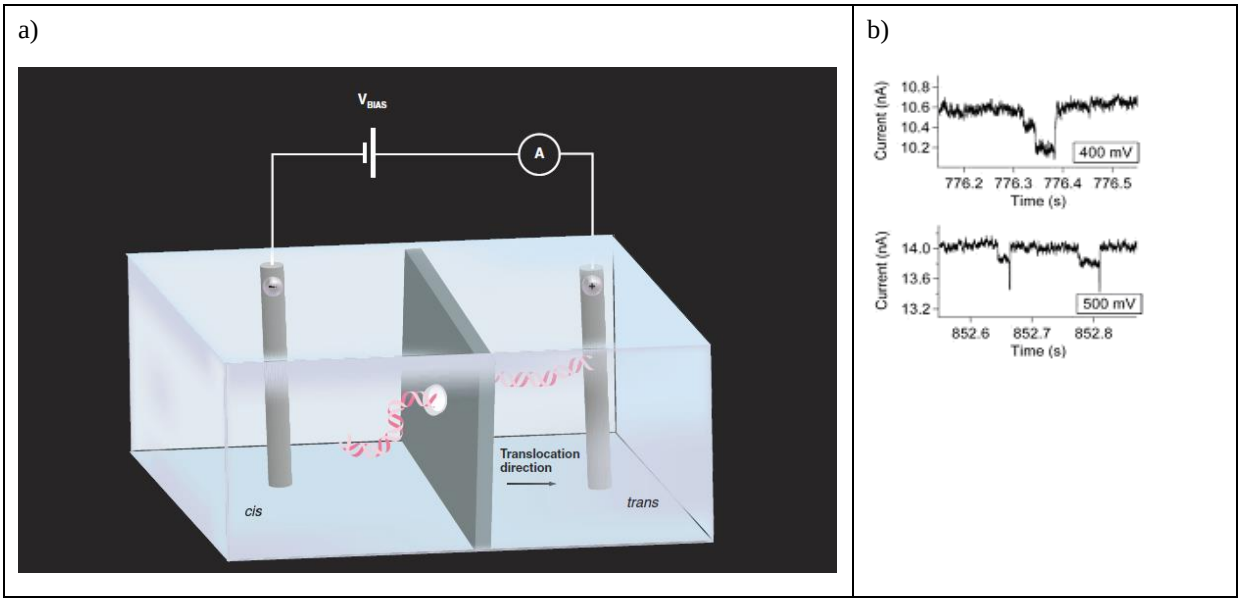

FIG. 28. (a) molecule measurement concept employing nanopores
Fig. 1 in [283], Reproduced with permission from Nanomedicine Vol. **2**, No. 6, Pages 875-897, Copyright 2007, Future Medicine
b) Ionic current variation measurements induced by λ DNA molecules passing through or inserted in a Si_3N_4 nanopore Fig. 3b in [277], Reproduced with permission from Microelec. Eng. **87**, 1300 (2010) / Elsevier, Copyright 2010 Elsevier

The results achieved so far are competitive to those reached by other patterning techniques. The advantage is that it is a one process step technique. Each hole is patterned in a few tens of ms (typically 20), because of its size and the thin sample (membrane), thus only a tiny material volume has to be removed for each hole allowing precise dose calibration and a high reproducibility. However the process (milling) belongs in the large dose regime ($2.5 \cdot 10^6$ ions / point equaling $1 \cdot 10^{19}$ ions / cm^2 calculating with the 5 nm spot size as given in [249]), thus the resulting lower application resolution can be overcome by clever processing. FIG. 28 shows exemplary ionic current variations, caused by the insertion of DNA molecules passing through a nanopore used as a dividing wall, which has been detected at different voltages 400 and 500 mV [277].

V.D.4. Magnetics I (small single magnetic domains)

Small single magnetic domain regions are created to study their thermal stability and their coupling effects between dots organized in matrixes. Thus, nano patterning processes are required to fabricate small single magnetic domain areas which allow to overcome [284] the so-called superparamagnetic limit as 2D discrete media with perpendicular anisotropy [285]. This can be done by conventional lateral nano patterning techniques like EBL (section II) followed by a pattern transfer [286] or self-organized 3D epitaxy [287] process. An advantage for EBL is the freedom in feature shapes and position on the sample, whereas a disadvantage is the process complexity (pattern transfer). For self-organized 3D epitaxy (section III) the advantages are the reported feature sizes down to 3 nm and the potential patterning speed for volume production purposes. Ion irradiation can locally alter magnetic properties of ultra-thin magnetic films, down to the nm scale [288]. Depending on the ion dose the surface properties can be tailored from ferromagnetic with reduced coercitivity to paramagnetic

[288], [284]. In the presented results, the ion beam has been employed to create domain walls (displayed in FIG. 29b), using a Ga LMIS FIB (NanoFIB, type 7 in section V.C.1). The ion-matter interaction regime responsible for this is called atom intermixing resulting in a magnetic "smoothing" effect.

The fabrication challenge of magnetic layer smoothing here is to reduce reproducibly the size of the fabricated magnetic cells. This can be done by the low to medium dose combination of the ion implantation and atom intermixing ion matter interaction regime. The employed dose for this application ($6.3 \cdot 10^4$ ions / point or $2 \cdot 10^{16}$ ions / cm^2, assuming 20 nm effective beam size) is in the medium dose regime resulting in a medium potential application resolution.

During the ion irradiation atoms from the substrate and a few incident Ga^+ ions are mixed into the thin magnetic film. This alters locally the magnetic properties. The material composition has been: Pt(3.4 nm) / Co(1.4 nm) / Pt(4.5 nm) grown on a transparent Al_2O_3(0001) substrate.

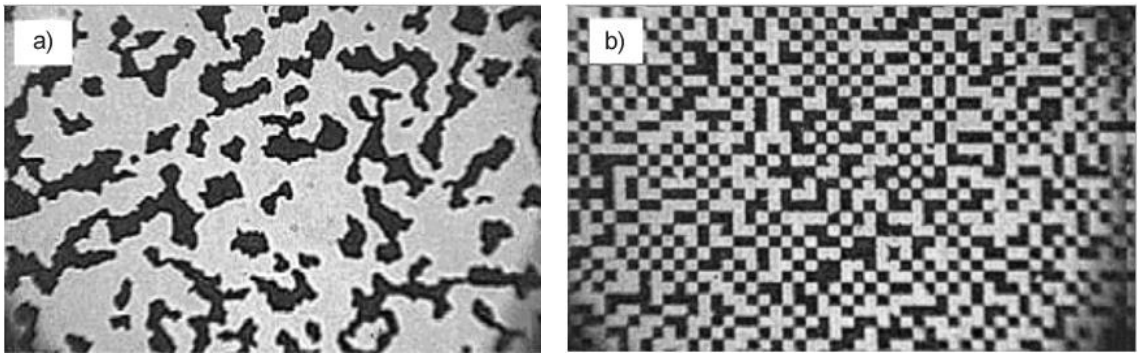

FIG. 29. Magneto optical image of a thin line array patterned by Ga:
a) $2 \cdot 10^{13}$ ions / cm^2 not sufficient for the formation of domain walls and
b) with $2 \cdot 10^{16}$ ions / cm^2
Fig. 2 a and d (enumeration modified) in [288], Reproduced with permission from J. Magnetism Magnetic Materials **240**, 34 (2002) / Elsevier, Copyright 2002 Elsevier

Advantages of this technique are the process simplicity (only one process step), the freedom in feature shape as well as position, and the extreme sensitivity (only a few Ga ions per pixel are necessary for feature creation). For volume production requirements the overall process is slower than for example self-organized 3D epitaxy (section III), however these remarkable direct patterning results open fascinating opportunities for magnetic nano device prototyping.

V.D.5. A x-ray zone plate

The scope is to reproducibly fabricate zone lens plates for X-rays. Here the challenge is to combine high resolution in the outer rings with pattern placement accuracy requirements, so operating devices can be manufactured. Alternative techniques are electron beam lithography in combination with a suitable pattern transfer technique.

If Ga LMIS FIB milling is applied, the patterning sequence can take many hours (over 15 hours with the tool type described under No. 7 in section V.C.1)). Thus, automatic (unattended) drift compensation after partial patterning of the design has been carried out at a mark outside the active area. This has been done in the following sequence: a periodic stop of the patterning process, blank the beam, stage movement away from the device, an automated mark recognition process with a position adjust, driving back to the device and continue patterning at the corrected position. In our example an operating device (X-ray zone lens), with the desired x-ray focusing capabilities has been manufactured in one process step [72]. It is a milling process, into a 500 nm Au layer on a silicon nitride membrane. Milling is a high dose, thus potentially lower reachable application resolution ion matter interaction regime. The zone plate diameter is 100 µm and the outer rings are 100 nm wide. FIG. 31 shows the device performance of the x-ray zone lens, published under [31].

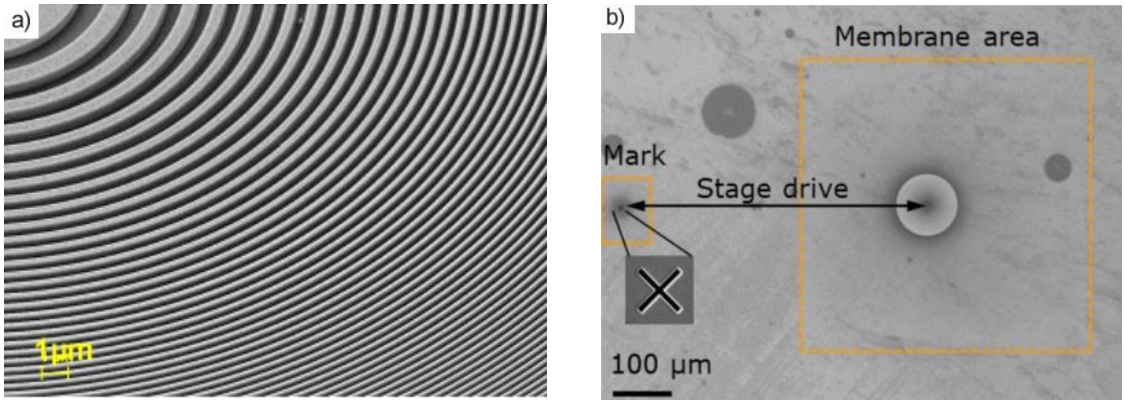

FIG. 30. SEM micrographs a) showing a 45° tilted view of the zone plate: inner zones
Fig. 3a in [72], Reproduced with permission from Microelec. Eng. **98**, 198 (2012) / Elsevier, Copyright 2012 Elsevier
b) showing the silicon nitride membrane with active area including gold zone plate and position of reference mark for automatic positioning correction on bulk sample Fig. 1 in [72], Reproduced with permission from Microelec. Eng. **98**, 198 (2012) / Elsevier, Copyright 2012 Elsevier

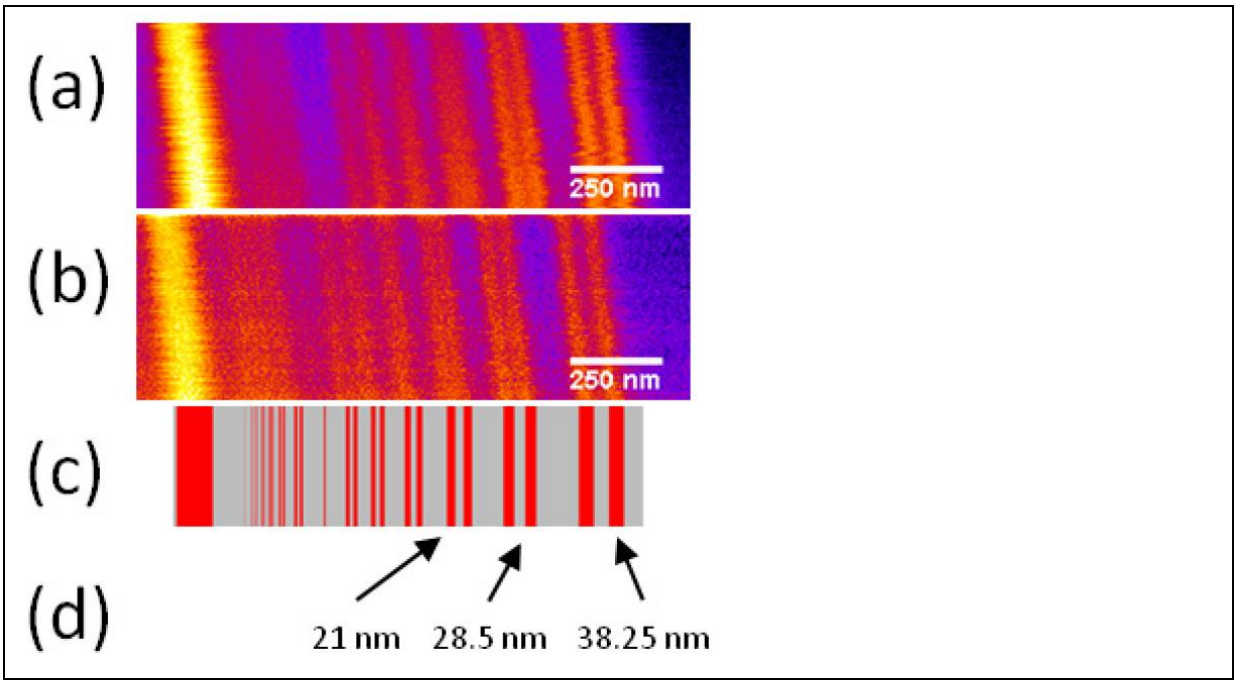

FIG. 31. „Scanning X-ray microscopy image of a certified commercial test sample (BAM L200) recorded at 1200 eV
(a) image acquired in the 2nd order focus of the FZP with a pixel size of 5 nm and a dwell time of 10 ms
(b) image acquired in the 3rd order focus of the FZP with a pixel size of 5 nm and a dwell time of 15 ms
(c) schematic representation of the certified test object
(d) width of the features (half pitch)"
Fig. 5 in [31], Reproduced with permission from Optical Express **21**, 11747 (2013), Copyright 2013 OSA publishing

V.E. Further exemplary applications

Now, an overview about further application fields and other approaches for the already described ones, will be given: microfluidics, photonics, nanopores, magnetics, large area milling, classical organic resist exposure, unconventional resists or treatments, feature refinement, local doping, surface functionalization, gas assisted processes and a form of regular feature self-organization under ion beam bombardment. The application results have been created utilizing 6 out of the 7 mentioned ion source and tool concepts in section V.C.1.

We take a look at the application results with respect to:

- ion matter interaction regimes exploitable for nano pattering
- precision
- process times / (instrument) stability
- resolution
- periodicity

V.E.1. Fluidics

Nano and micro fluidics have many potential applications in separation science [289], energy conversion [289], chemistry and biology taking place on small length scales, e.g. for medical applications [290]. The shown results demonstrate the technologies's feature shape and 3D capabilities as well as versatility. Exemplary devices created partially by milling can be seen in FIG. 32, which is a high dose and thus lower potential application resolution process technology employing Ga LMIS technology.

A first example (displayed in FIG. 32 a) has been carried out on a Si wafer as a combination of EBL and –Ga LMIS FIB (type 6 in section V.C.1) micromachining. A second (shown in FIG. 32 b) has been patterned on Cr on quarz sample by optical lithography and Ga LMIS FIB (type 7 in section V.C.1).

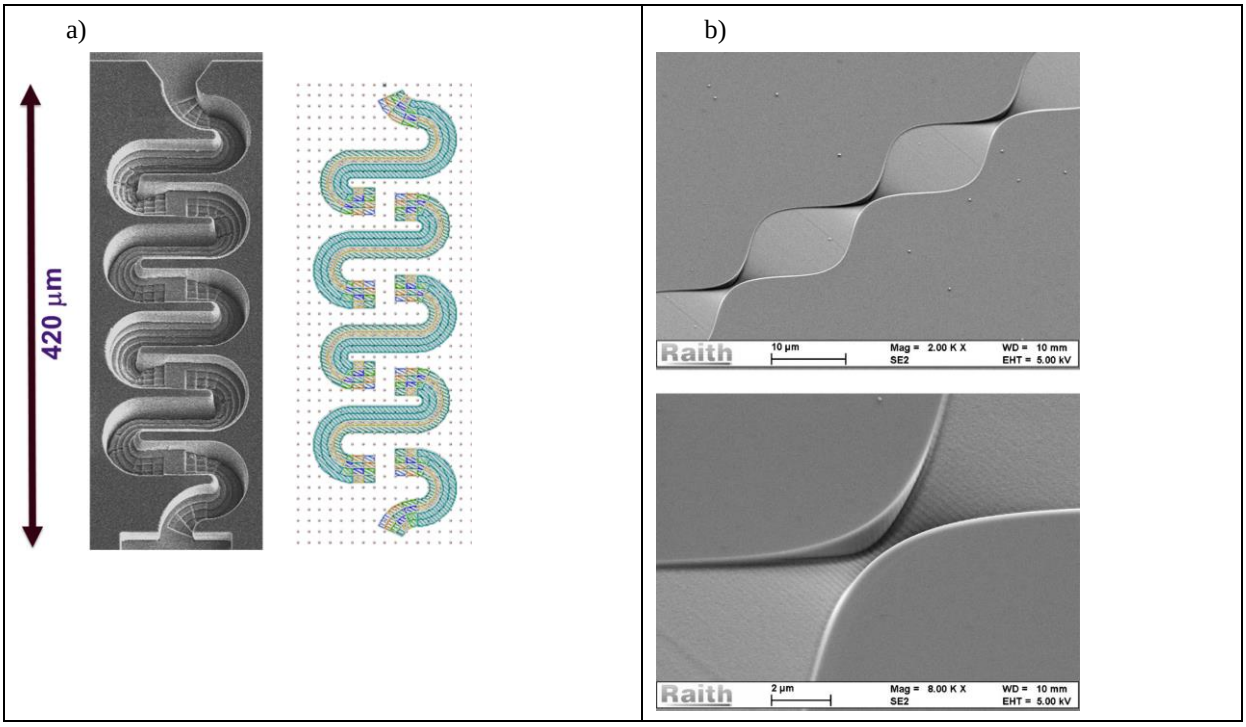

FIG. 32. SEM micrographs of exemplary microfluidic devices created by focused ion beam microfluidic devices
a) "View of CAD data used for making the 3D serpentine mixer. Data consist of curved polygons that have no cuts through the entire length of the device."
FIG. 8. in [290], Reproduced with permission from J. Vac. Sci Technol. B **31**, 06F401-1 (2013). Copyright 2013 American Vacuum Society
b) with complex 3D microfluidic geometry
FIG. 10. in [291] ("a" and "b" removed), Reproduced with permission from J. Vac. Sci Technol. B **28**, C6I1 (2010), Copyright 2010 American Vacuum Society

FIG. 33 shows the result of a combinatory technique using FIB, nano-manipulation and electron beam induced deposition. A single transmembrane boron nitride nanotube (BNNT) was realized [292]. The displayed hierarchical nanofluidic device (BNNT) interfuses an ultrathin membrane and links two fluid reservoirs, so fluidic transport can be analyzed through a single nanotube initiated by different forces like: electric fields, pressure drops and chemical gradients [292].

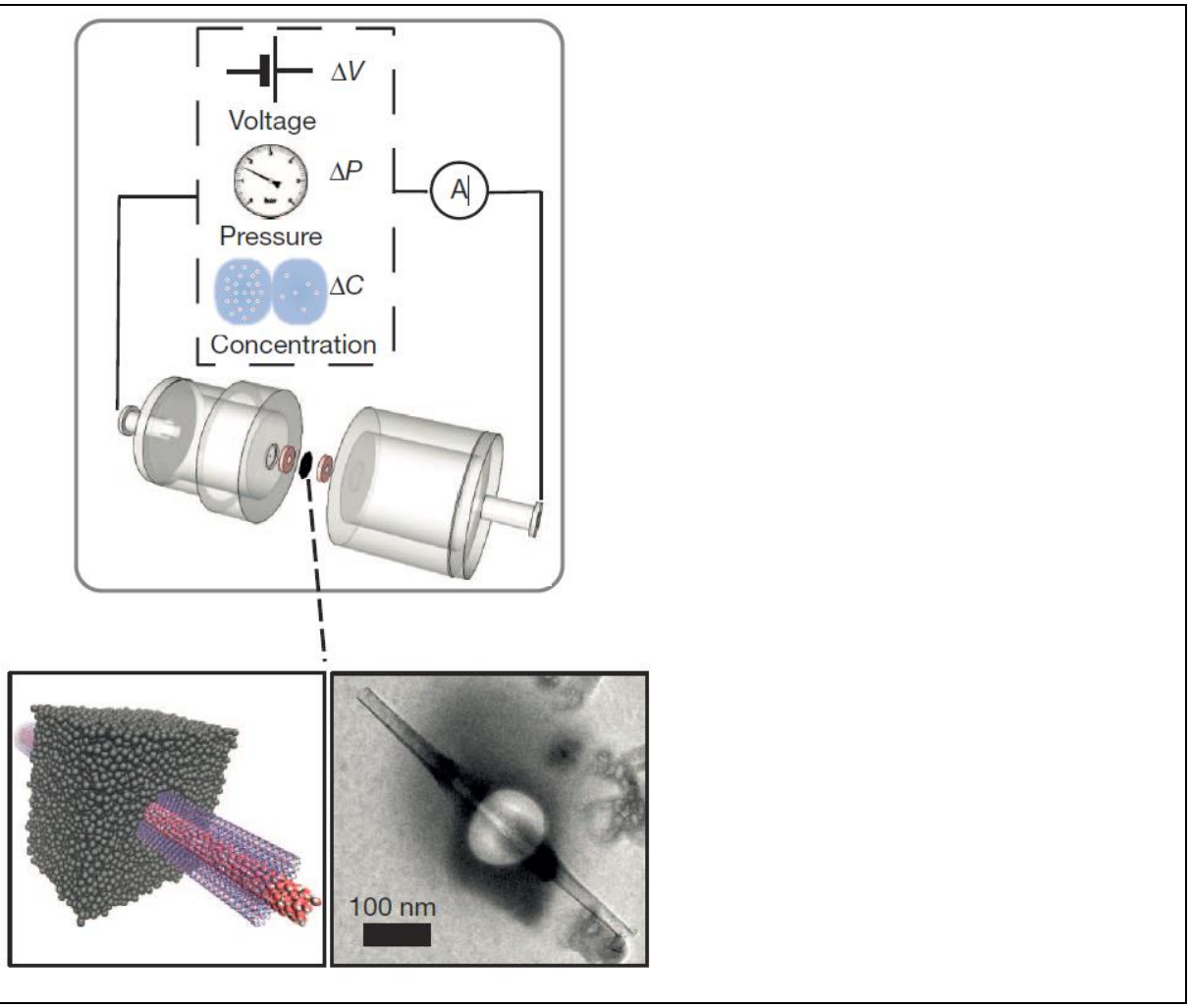

FIG. 33.Top: Measurement set-up schematic for a single transmembrane BNNT, lower left: concept, lower right: TEM micrograph of a result
Fig. 1 b) in [292], Reprinted by permission from Macmillan Publishers Ltd: Nature **494**, 455-458 (2013), copyright 2013

V.E.2. Plasmonics (surface plasmons)

Many different optical devices patterned in Au films for plasmonic applications are nano devices prototyped by ion beam nanopatterning, employing the ion matter interaction regime called milling. The devices can be used to guide light, reflect it or filter frequencies. Here reproducible periodicities can be a challenge as well as surface quality and pattern placement accuracy. To achieve the latter automatic drift correction away from the active device area can be used (as described in section V.D.5). Further on the size of a device is sometimes larger than a field of view, so special patterning techniques or instrument architectures might be required. FIG. 34 a) and b), FIG. 35 and plasmonic tapered coaxial holes (PTCH) FIG. 36 as well as FIG. 37 show exemplary small features repeated in a special way forming an optical device. The results have been realized utilizing a Ga LMIS FIB (type 7 in section V.C.1).

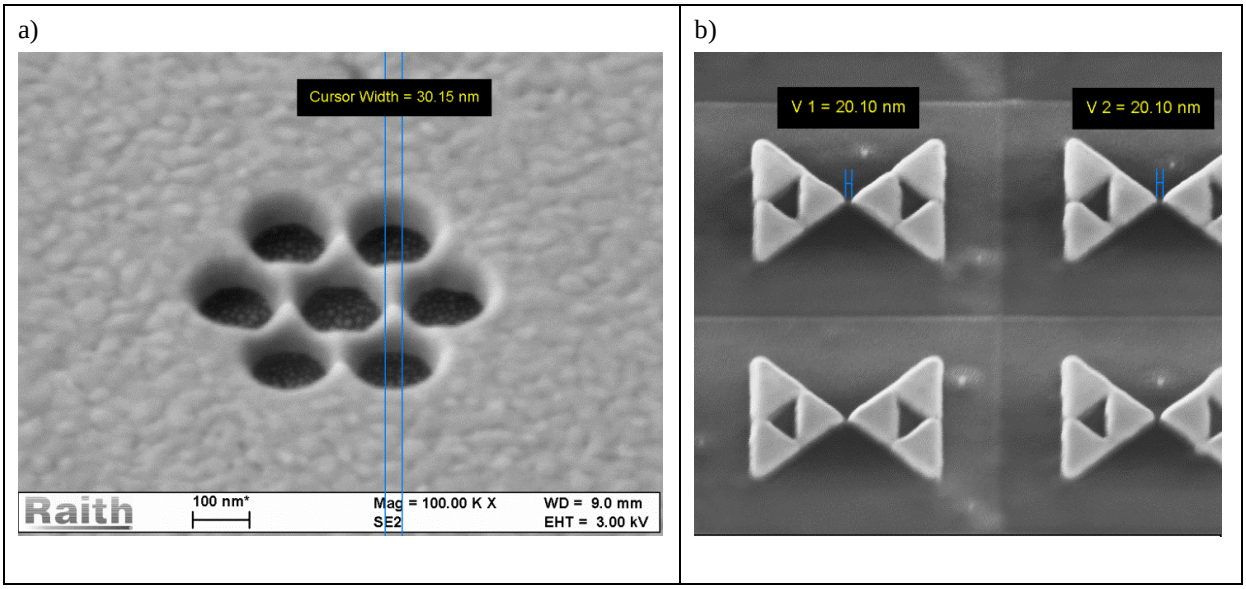

FIG. 34. SEM micrographs of exemplary optical devices created by Ga LMIS focused ion beam milling
a) a single base feature consisting of 6 circles (“oligomere”), where 12000 of them have been created within a 100 µm · 100 µm area (35 kV Ga LMIS FIB milled into 80 nm Au on a SiO_2 substrate) – courtesy and copyright H. Giessen University of Stuttgart and Application lab Raith GmbH
b) other base features are triangles (“fractal bow tie”, 35 kV Ga LMIS milled into Cr (5nm) Au (35 nm) on a SiO_2 substrate, probe current 5.3 pA, process time 25 hours to pattern 144x144 bow ties over about 100 µm) – courtesy and copyright of A. Elezzabi Univerity of Alberta and Application lab Raith GmbH

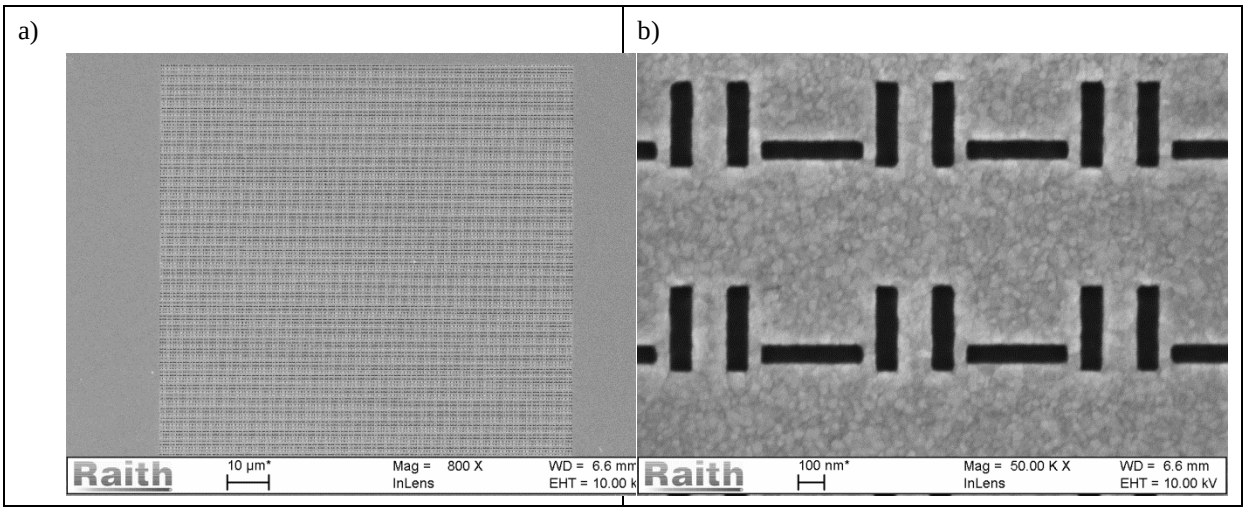

FIG. 35. SEM micrographs of Si and Ga milled feature in Au on SiO_2 (35 kV, LM(A)IS)
a) overview at an instrument magnification of 800
b) a few elements at an instrument magnification of 50000,
both courtesy and copyright of Prof. Giessen University of Stuttgart and Application Lab Raith GmbH

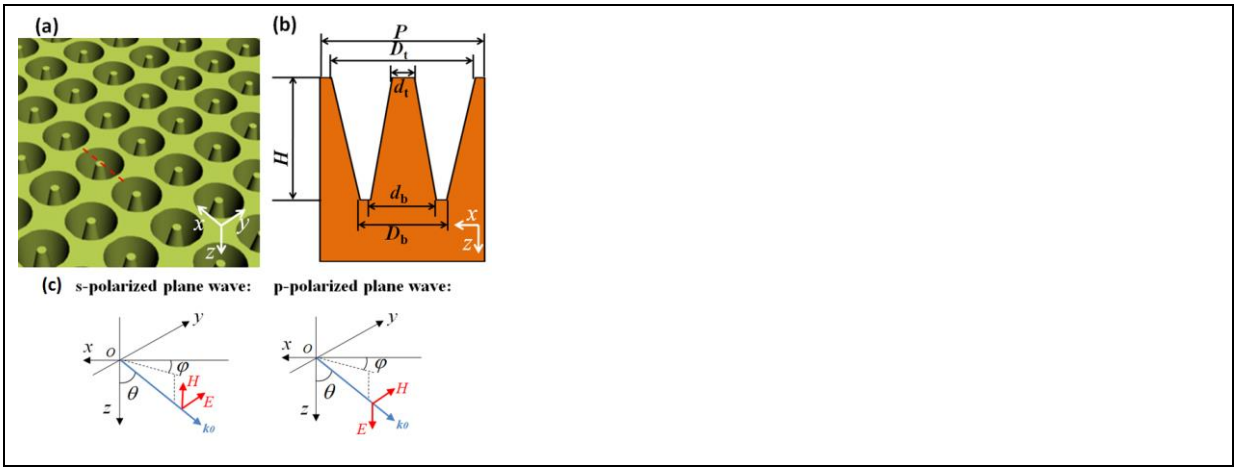

FIG. 36. (a) "Three-dimensional schematic diagram of PTCH-based absorber… with all the structural parameters illustrated."
b) "Cross section of one unit cell in the xz plane along the red dashed line in (a)"
(c) "s- and p-polarized plane waves are considered as the light source incident from the top."
Fig. 1 in [293], Reproduced with permission from Optics Express **22**, 32233 (2014), Copyright 2014 OSA publishing

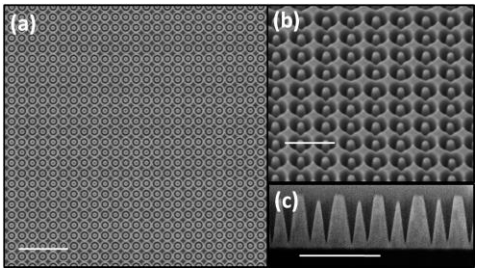

FIG. 37. "SEM images of the combined absorber based on PTCHs … milled in Au"
(a) "topview (scale bar: 2 μm)"
(b) "tilted-view (scale bar: 800 nm)"
(c) "cross-section (scale bar: 800 nm)"
Fig. 7 in [293], Reproduced with permission from Optics Express **22**, 32233 (2014), Copyright 2014 OSA publishing

Plasmonic nanoantennas have also sucessfully patterned by He GFIS milling into a 30 nm thick polycrystalline gold film (instrument type 3 in section V.C.1), an exemplary result is displayed in FIG. 38 [294].

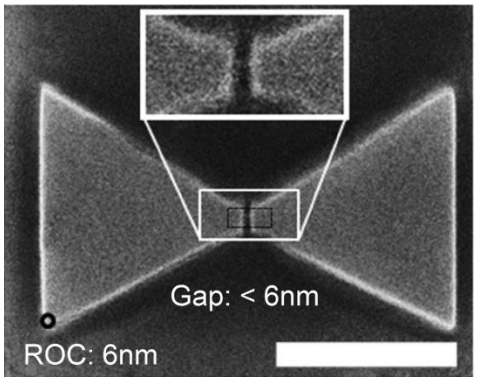

FIG. 38. "Scanning helium ion microscopy image of bowtie nanoantennas fabricated by He^+-ion beam milling. … milled into a 30 nm thick polycrystalline gold film evaporated onto a glass substrate… Bowtie antenna fabricated by He^+ milling…" [294]
Fig. 1d in [294] ("d" removed), Reproduced with permission from Nano Lett. **14**, 4778 (2014). Copyright 2014 American Chemical Society

V.E.3. Photonics devices, larger than one field of view

An exemplary device (FIG. 39), which is significantly larger than one field of view: is an about 2 mm long light guiding one (35 kV, Ga beam, over all patterning time about 4h). Here repetitive stitching with dose control at the stitching border has been carried out to create it, utilizing a Ga LMIS FIB instrument (type 7 in section V.C.1).

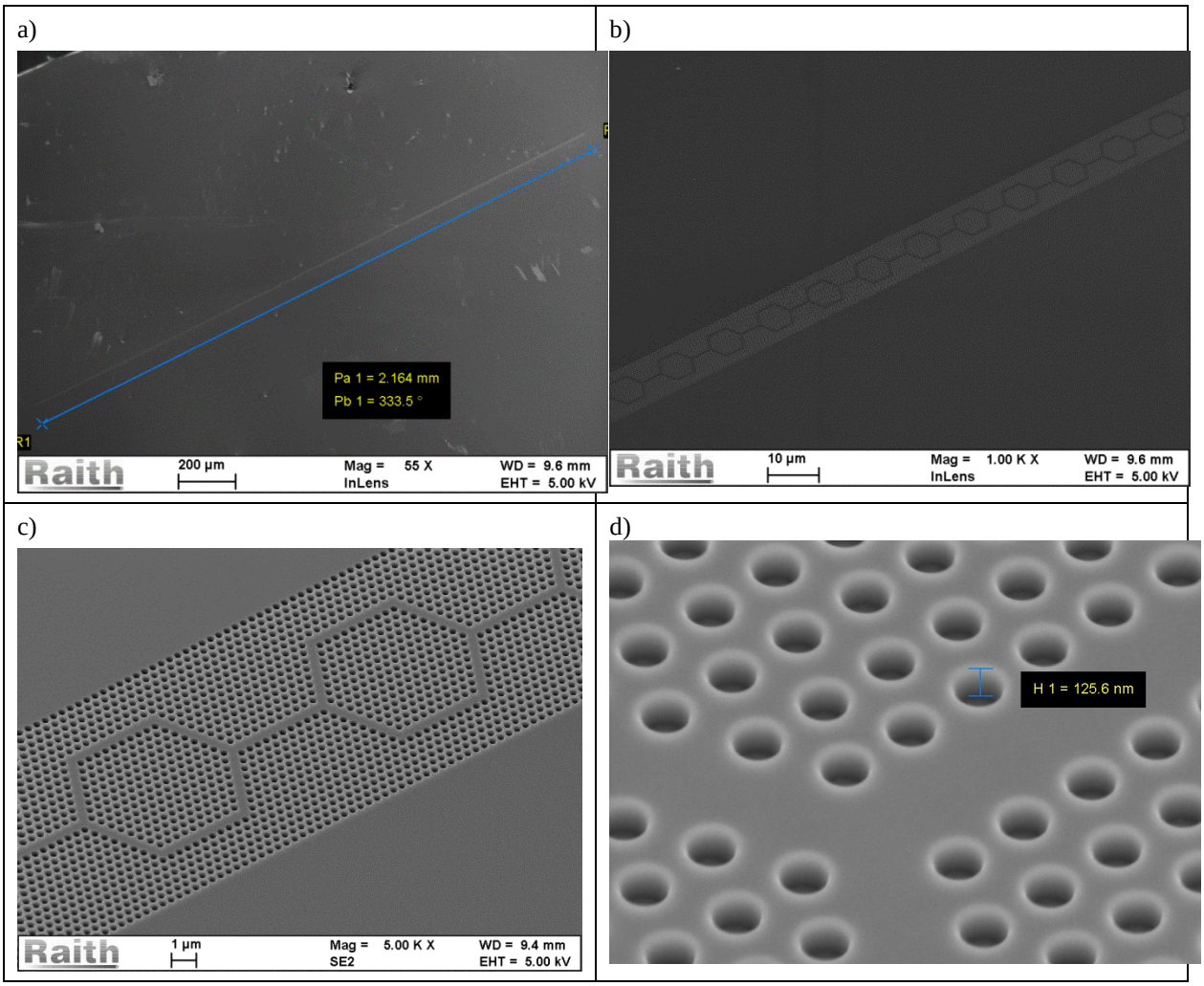

FIG. 39. SEM micrographs of a photonic crystal light guiding devices fabricated by Ga LMIS FIB (35 kV) milled into a Si sample
a) about 2 mm long (blue measurement line) wave guide at an instrument magnification of 55
b) an instrument magnification of 1000
c) an instrument magnification of 13000
d) tilted view cut from an instrument magnification of 20000 to estimate the milling depth
all micrographs courtesy and copyright of L.-M. Peng of Peking University and Application lab Raith GmbH

Another example (FIG. 40) of optical devices extending one field of view is a wave guide with optical resonators. This has been realized by field stitching with with the same instrument as described above (35 kV).

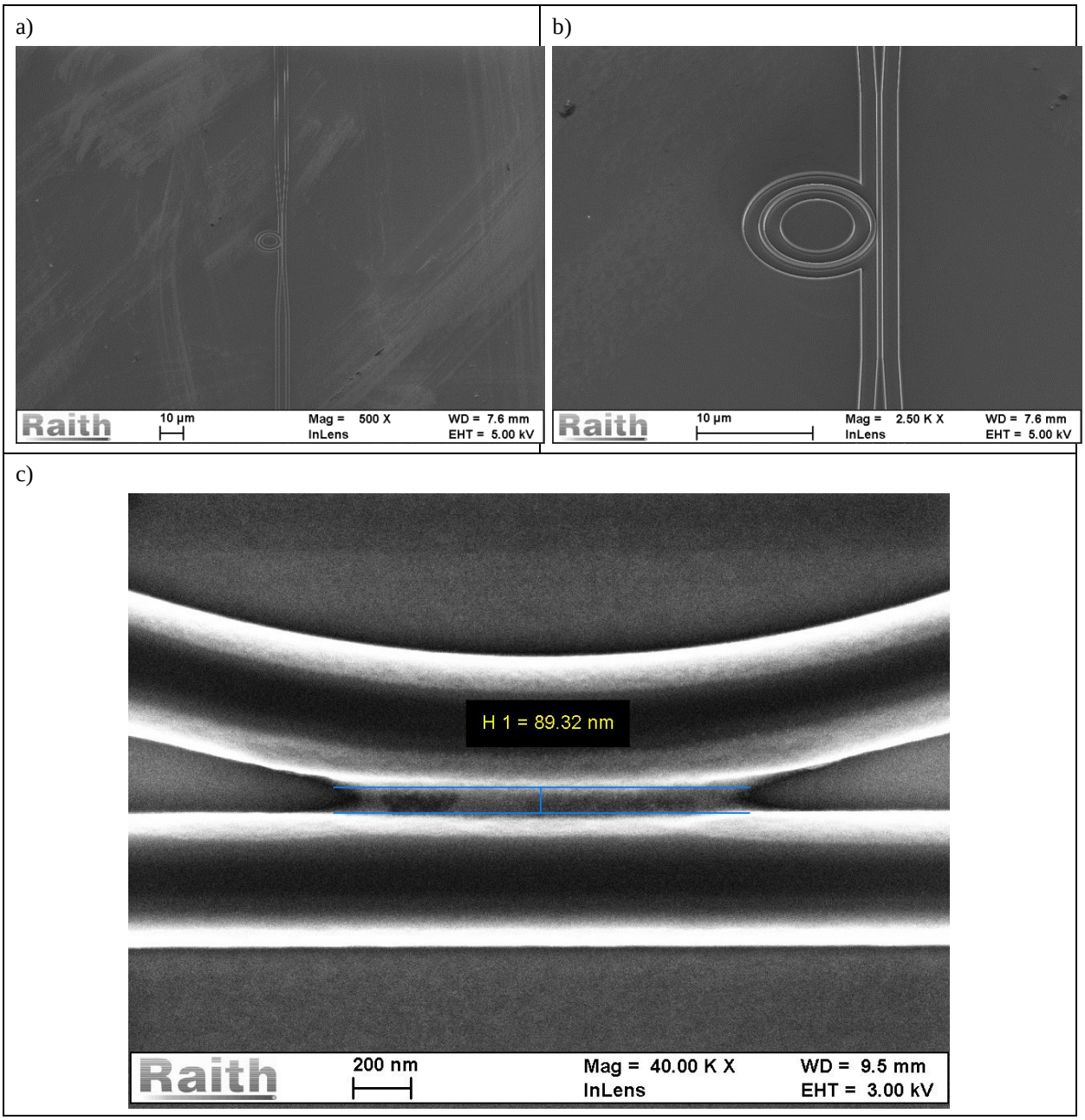

FIG. 40. SEM micrographs of further photonic waveguiding devices milled by Ga LIMS FIB (35 kV) into a
a) Si sample taken at an instrument magnification of 500
b) Si sample taken at an instrument magnification of 2500
c) Si on insulator sample taken at an instrument magnification of 40000
all micrographs courtesy and copyright of L.-M. Peng of Peking University and Application lab Raith GmbH

V.E.4. Nanopores II

A further nanopore fabrication example (to the one described in section V.D.3) has been produced by He ion milling (HIM, by an instrument of type 3 in V.C.1) [240], exemplary results are displayed in FIG. 41. Feature sizes below 3 nm have been achieved applying this technology.

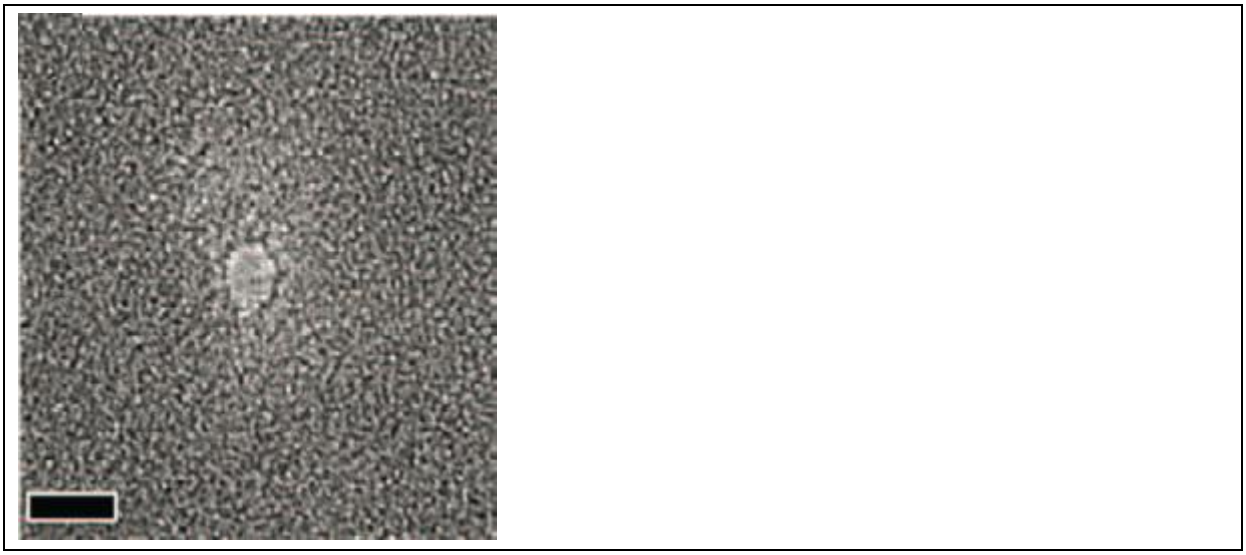

FIG. 41. "Transmission electron micrograph of a 2.5 nm diameter HIM nanopore (scale bar is 5 nm)" [240] ("c" removed from image)
Fig. 2 c in [240], Reproduced with permission from Microscopy Today **20**, 24 (2012). Copyright 2013 Cambridge University Press

V.E.5. Magnetics II

Alternatively, to the above described application example employing ion matter interaction regime of atom intermixing and magnetic smoothing (described in section V.C.2), another ion matter interaction regime – milling- has been successfully used to create small single magnetic domain areas (6 nm deep into a 20 nm thin film of $Co_{70}Cr_{18}Pt_{12}$) using a Ga LMIS FIB (tye 6 in section V.C.1) [285], the exemplary results are displayed in FIG. 42.

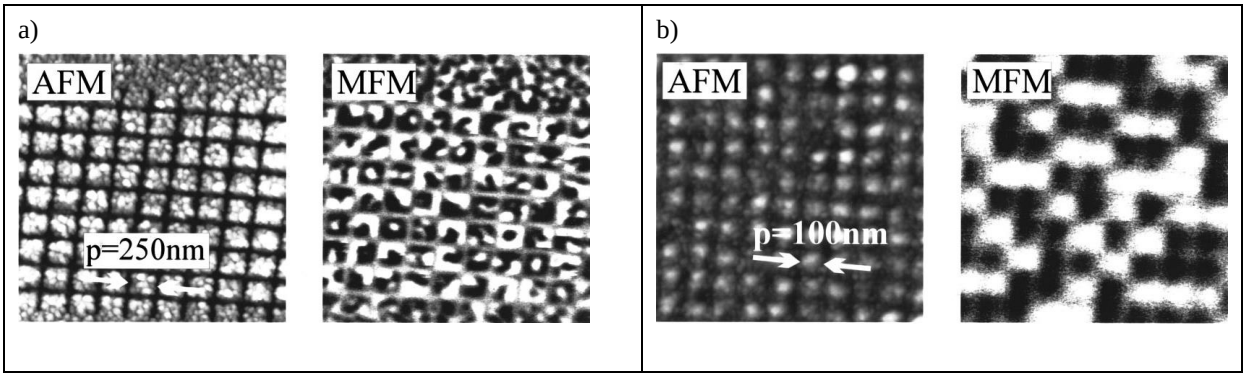

FIG. 42. AFM and MFM images of small single magnetic domain areas, "… of granular perpendicular CoPtCr recording " media, patterned at a period
a) of 250 nm and
b) of 100 nm
FIG. 1 in [295], Reproduced with permission from Appl. Phys. Lett. **78**, 990 (2001). Copyright 2001 American Institute of Physics

V.E.6. FIB removal of larger amounts of material

If larger volumes than μm^3 shall be milled away, Xe ions -from plasma sources- (type 4 in section V.C.1) are a better choice than Ga LMIS. These Xe ions can mill up to 50 times faster, because of the significantly larger accessible beam currents (for example 1 µA for Xe compared to about 20 nA for Ga LMIS, comp. section V.C.1) and the higher mass of Xe about 131 u compared to Ga with about 70 u . Exemplary milling results of different size apertures in an aperture stripe (molybdenum) are displayed in FIG. 43 (aperture diameters of about 10 µm and above).

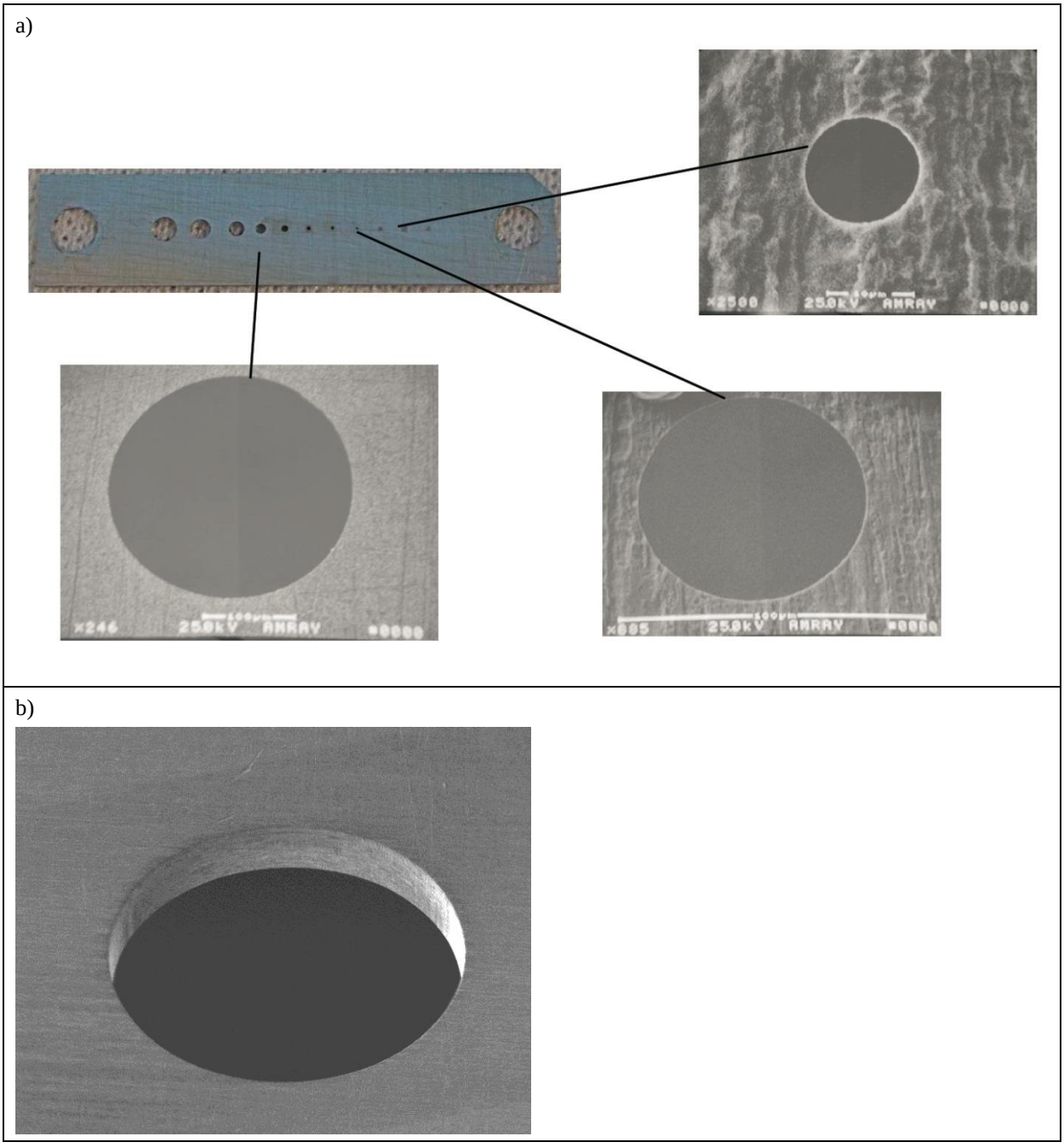

FIG. 43. SEM micrographs of Micromachined holes in FIB aperture strip (molybdenum). Holes machined with Xenon beam currents of 150nA to 1500nA beam current. [175], a) from top b) an exemplary one tilted, courtesy and copyright Oregon Physics

V.E.7. Organic resist lithography (EBL resists)

A low-dose, thus high application resolution technique is organic resist exposure. Experiments have been carried out since the historical ion beam patterning start (see section V.B), together with the long tradition of electron beam lithography employing the same resists (compare section II) the process know-how is wide spread inside the nanotechnology community. Here impressive example results are shown in FIG. 44., patterned by a He microscope (type 3 in section V.C.1, GFIS, scanning helium ion beam lithography, SHIBL) [239], [238] and a Ga LMIS FIB [208] instrument (type 7 in section V.C.1), using the negative tone resist called hydrogen silsesquioxane (HSQ). The resist process details can be found in [78].

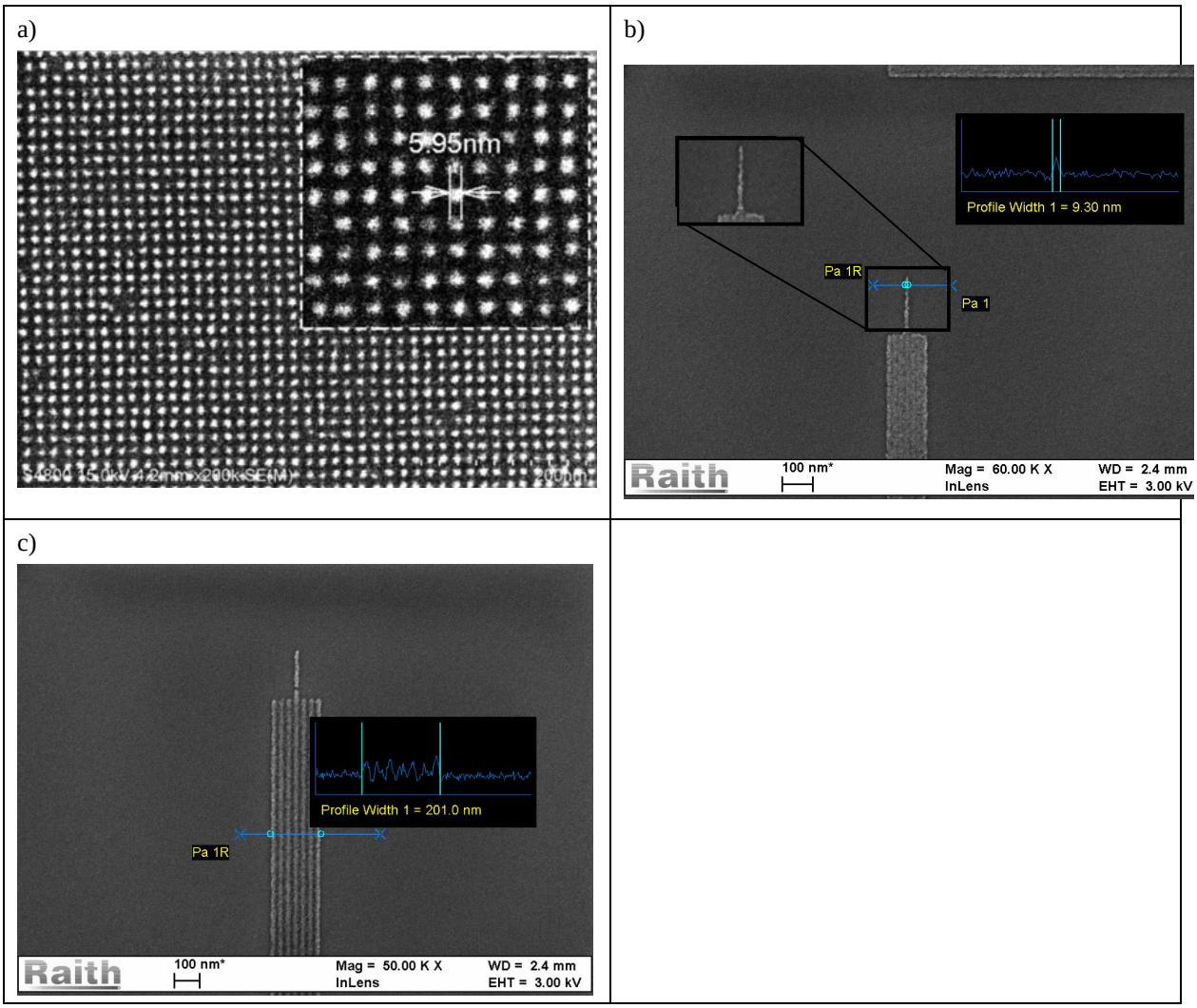

FIG. 44. micrographs of high resolution and small periodicity experiments in HSQ employing a
a) He GFIS instrument "… arrays of dots written in a 5 nm thick HSQ layer using SHIBL at pitches of … 14 nm, .. The insets are SEM images at a higher magnification. The average dot size for all pitches is 6.1 nm."
Fig. 1 in [238], ("c" removed), Reproduced with permission from J. Vac. Sci. Technol. B **27**, L18 (2009). Copyright 2009 American Vacuum Society
b) Ga LMIS instrument "…, feature size <10 nm (6 nm HSQ on Si, exposed by 40 kV Ga, dose 19.4 pAs/cm"
Fig. 1 in [208], Reproduced with permission from Microelec. Eng. **97**, 48 (2012) / Elsevier, Copyright 2012 Elsevier
c) same as b) but now taking a look at the minimum periodicity of 30 nm (6 nm HSQ on Si, exposed by 40 kV Ga, dose 23.6 pAs/cm
Figure 2 in [208], Reproduced with permission from Microelec. Eng. **97**, 48 (2012) / Elsevier, Copyright 2012 Elsevier

V.E.8. Sample surface swelling

FIG. 45 shows even smaller features and periods (3.5 nm half pitch), which have been created by a He GFIS instrument (type 3 in section V.C.1). A Si sample surface has been irradiated by the He ions, then swelling – often unwanted- has been used for pattern definition [297].

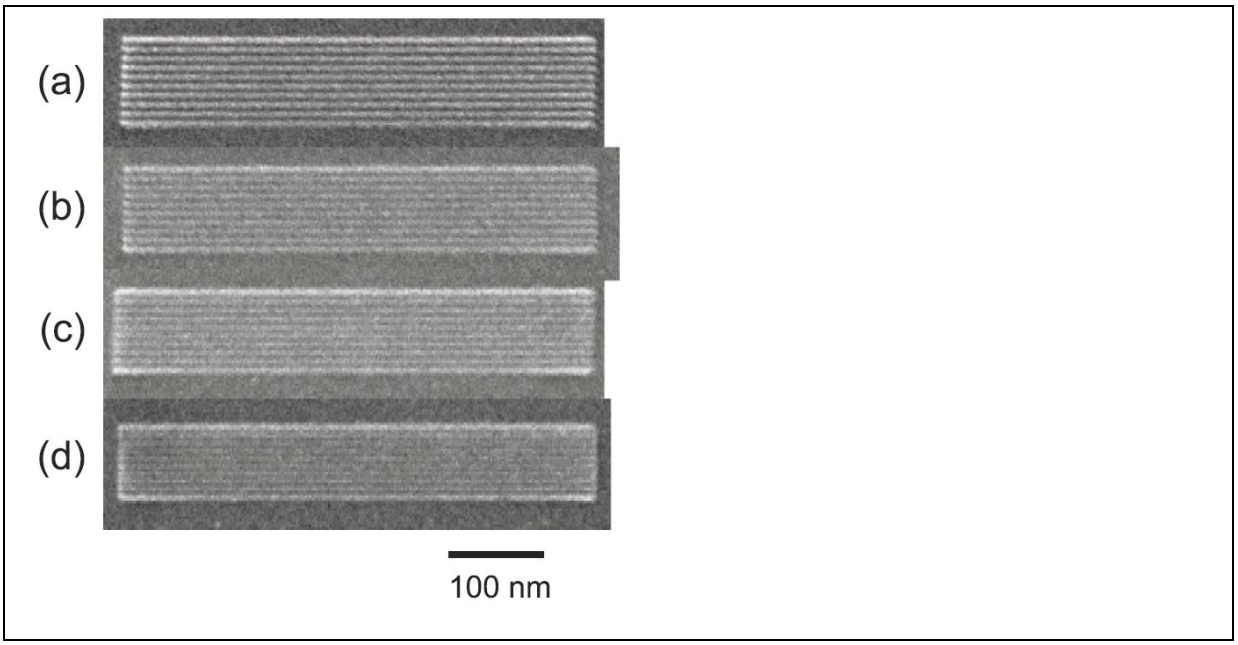

FIG. 45. HIM images of sets of ten parallel lines (with a dose of 6×10^{10} ions cm^{-1} for each line) of 500 nm long with half pitch of (a) 5 nm, (b) 4 nm, (c) 3.5 nm and (d) 3 nm, all patterned with a HIM using swelling for pattern definition
Fig. 1 in [297]

V.E.9. Alternatives organic resist exposure and development

As classical organic electron beam resist exposure revealed challenges employing ions (described in the history section V.B), alternative routes have been tried, altering locally the reactive ion etching resistance of the ion bombardment patterned organic resist areas, "surface imaged resist" [209], [298], example results are illustrated in FIG. 46. This is a kind of surface functionalization, a low to mid dose regime, thus a potential high application resolution ion matter interaction regime. In two examples ion irradiation has been carried out on an organic resist directly followed by reactive ion etching (RIE) process. An example result from a process called "Silylation" (ions are implanted into SAL 601 resist, oxygen RIE) [299], is shown in FIG. 46 a) and another one called NERIME (SPR505A resist), in FIG. 46 b) [298]. Both result in a higher reactive ion etch resistance to subsequent physical etching at the irradiated locations, The combination of silylation or NERIME and FIB lithography decouples the resist film thickness (exposure depth) from the ion penetration depth in the RIE etching process [183]. Experiments have been carried out using Ga LMIS FIB instruments (FIG. 46 b) type 6 in section V.C.1).

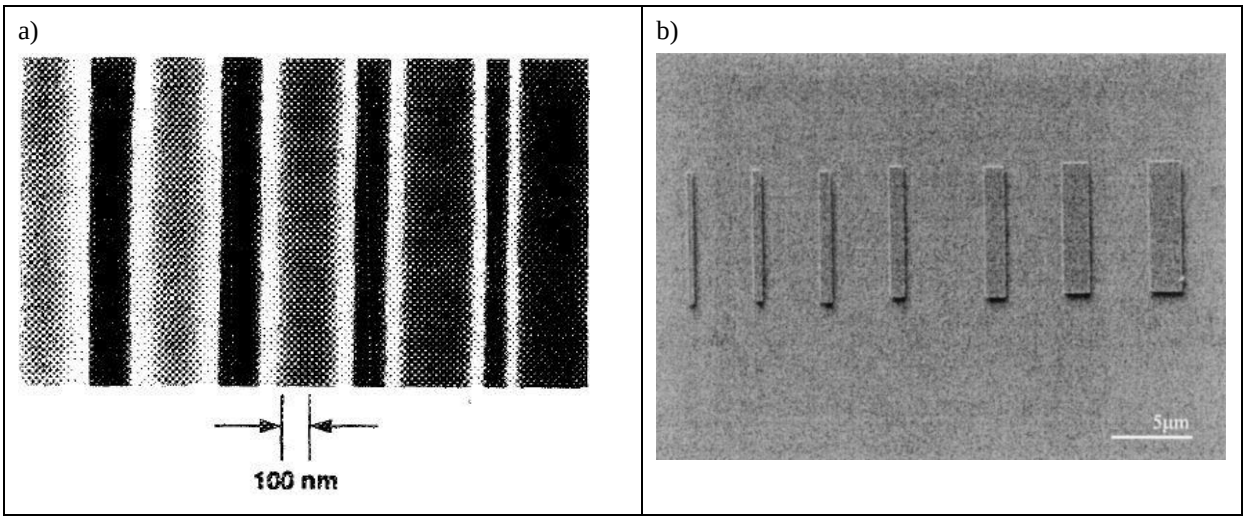

FIG. 46. SEM micrographs of lines where in both LMIS technology has been employed to
a) implant Be, Si, Ga, and Au ions, "Lines ranging in width from 120 to 80 nm patterened with 30-keV Ga^+ at a dose of $9x10^{22}$ ions/cm^{2}" in SAL 601 resist
Fig. 2 in [299], Reproduced with permission from J. Vac. Sci. Technol. B **9**, 3432 (1991), Copyright 1991 American Vacuum Society
b) Top-down FIB image of NERIME processed patterns of (right to left) 2, 1.5, 1, 0.75, 0.5, 0.25, and 0.1 µm in a SPR505A resist with thickness of 1.5 µm; (Ga^+ beam dose 4700 µC/cm^2, 1100 s RIE at 16 mTorr
Fig. 7 in [298], Reproduced with permission from J. Vac. Sci. Technol. B **22**, 189 (2004), Copyright 2004 American Vacuum Society

V.E.10. Ligand stabilized Au clusters as unconventional resist

In FIG. 47 non classical resist results are shown, containing a metal (50 nm $Au_{55}(PPh_3)_{12}Cl_6$ film on SiO_2 / Si samples) [300], [301], [41]. The results have been patterned using a Ga LMIS nano patterning instrument (NanoFIB as well as the commercialized one, type 7 in section V.C.1). The exposure cuts the link between the metal and the ligand. The ligand gets dissolved during development (broken bonds).3 D capabilities can be tailored by the point ion dose and pixel to pixel spacing, allowing the matal clusters to reorganize on nucleation sites. The impressive 3D capabilities can be seen in FIG. 47 d), where the height of the gate has been purposely reduced. Details about the resist process can be found in [300]. This is a relatively low-dose resist exposure process with potential high application resolution capabilities.

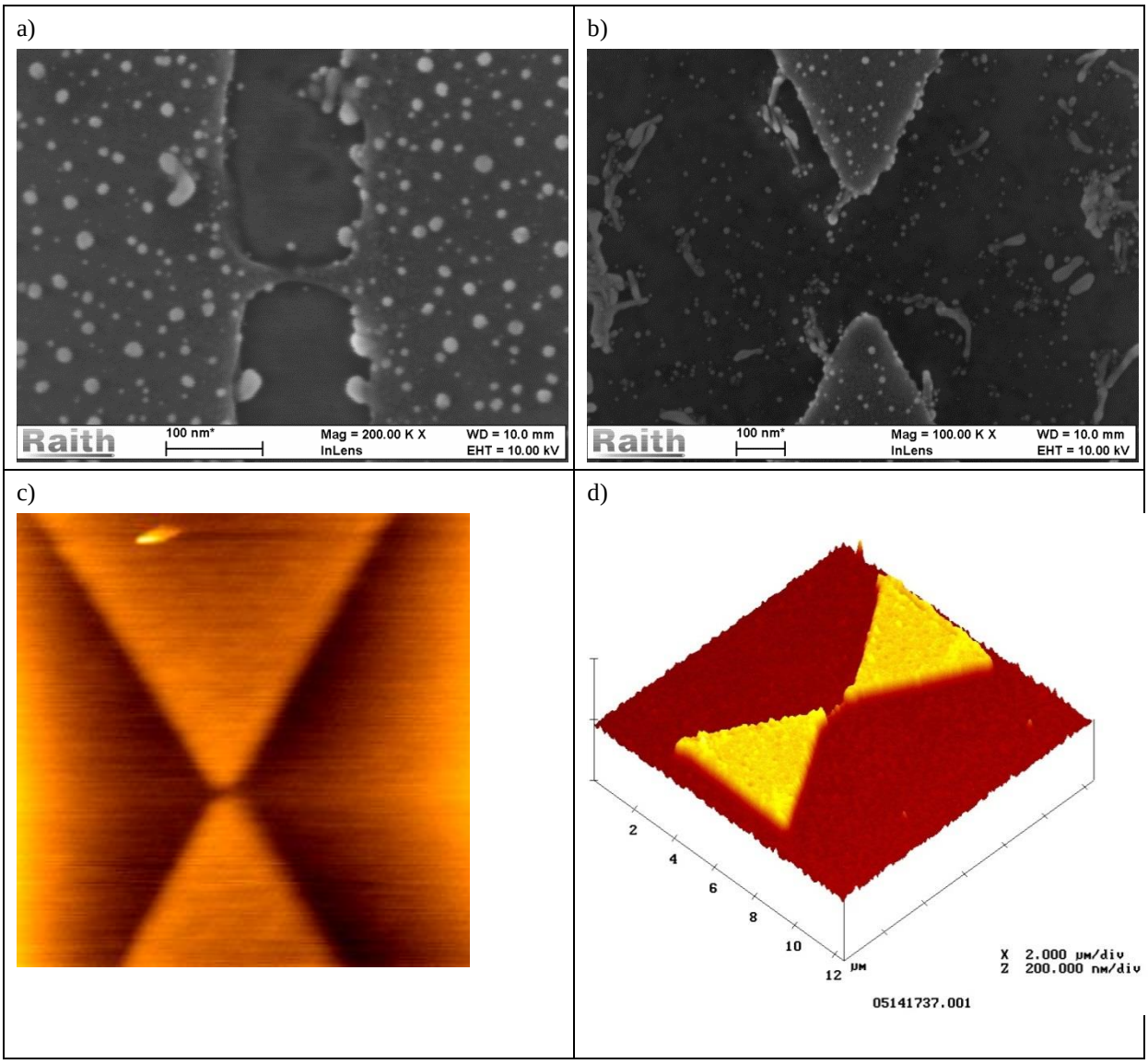

FIG. 47. non conventional resist (50 nm $Au_{55}(PPh_3)_{12}Cl_6$ film) patterned by Ga LMIS, on SiO_2 / Si samples (240 nm oxide thickness),
SEM micrographs of high resolution results after development
a) thin interconnection (<20 nm) with 100 nm contact pad distance < 6 pAs/cm
Figure 52 d) in [41]
b) the inner part of a device
Figure 54 a) in [41]
AFM images
c) of a nanogap realized by FIB irradiation of a single solid $Au_{55}(PPh_3)_{12}Cl_6$ resist layer (field of view 3µm · 3 µm, gap about 35 nm, feature thickness about 1 nm)
d) of a butterfly structure of a single solid $Au_{55}(PPh_3)_{12}Cl_6$ resist layer
Fig. 6 in [300], Reproduced with permission from J. Vac. Sci. Technol. B **17**, 3132 (1999), Copyright 1990 American Vacuum Society

V.E.11. Nano scale modifications of existing features

A combined technology to create quickly small features, is the FIB modification of existing (resist) objects on the sample surface. The initial nano pattern can be realized by any technique. The examples shown in FIG. 48 show Au nano particles, which have been cut by a Ga ion beam final process step, so for example an optical

prototype device can be quickly (slightly) modified to examine possible improvements of its collection efficiency. Experiments have been carried out employing a Ga LMIS FIB (type 7 in section V.C.1).

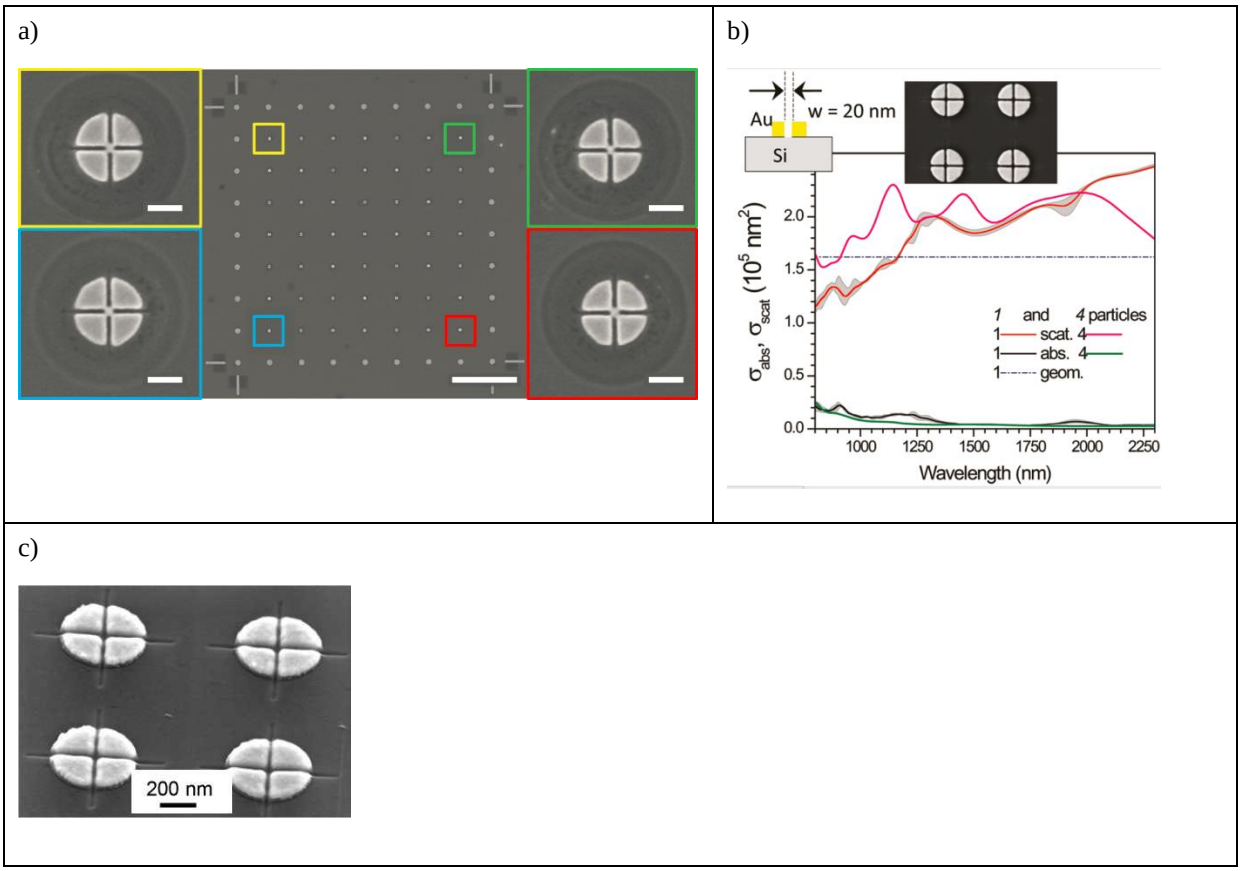

FIG. 48. a) "SEM image of an array of gold nano-disks manufactured using EBL standard lift-off method and overlay of nanopatterns using our proposed method, colored insets show single nanoparticles in the corresponding corners of pattern. Scale bars are 10 μ m for main figure and 250 nm for insets."
Fig 2. in [303] G. Gervinskas , G. Seniutinas , L. Rosa , and S. Juodkazis: Arrays of Arbitrarily Shaped Nanoparticles: Overlay-Errorless Direct Ion Write. Adv. Optical Mater. 2013. **1**. 456-459. http://dx.doi.org/10.1002/adom.201300027. Copyright Wiley-VCH Verlag GmbH & Co. KGaA. Reproduced with permission.
b) "The absorption, σ_{abs}, and scattering, σ_{cat}, cross sections plotted as average of four single nanoparticles (Figure 2(b)) and the entire assemble of four particles. Calculations were carried out by importing SEM images and extruding them to a height of 40 nm. Gray regions depict error range. Numerical simulations of the ideal structures with cuts."
Fig. 3a in [302], Reproduced with permission from J. Phys. Chem. **115**, 5251 (2011), Copyright 2011 American Chemical Society
c) "SEM images of the through-cuts of Au-nano-particles by lines about 17 nm wide with IBL: "a slanted view" 17 +/- 3 nm lines cut (about 10 nm deep) into Au cylinders"
Fig. 2 a in [302], Reproduced with permission from J. Phys. Chem. **115**, 5251 (2011), Copyright 2011 American Chemical Society

V.E.12. Implantation III

Focused ion beam instruments can also be used for implantation (described in the application examples in section V.D.2 and V.D.3). Implantation can range from low-dose (single ion implantation) to high doses ion matter interaction regimes, depending on the application. In addition, implantation gives the opportunity to

introduce a well defined concentration of dopants for other nano-structure fabrication processes. Specifically, mass-separated FIB systems have the advantage of applying a broad spectrum of ion species [304] and being capable to do so at dedicated and intended locations on the sample surface and with almost arbitrary shapes. This potential is shown by the following examples.

FIG. 49 shows a set of nanowires (NWs) over a gap on top of a SOI wafer. The samples have been pre-patterned by optical lithography (contact pads (400 · 400 μm^2) aligned to the <1 1 0>-orientation) and conventional implantation, then the NWs have been defined by FIB irradiation (Ga^+, E = 30 keV, Dose = $3 \cdot 10^{16}$ cm^{-2}) [305]. FIG. 49b represents the temperature dependence of the voltage through the NW (w = 90nm) at a constant current of 50 nA which can be used for local temperature control.

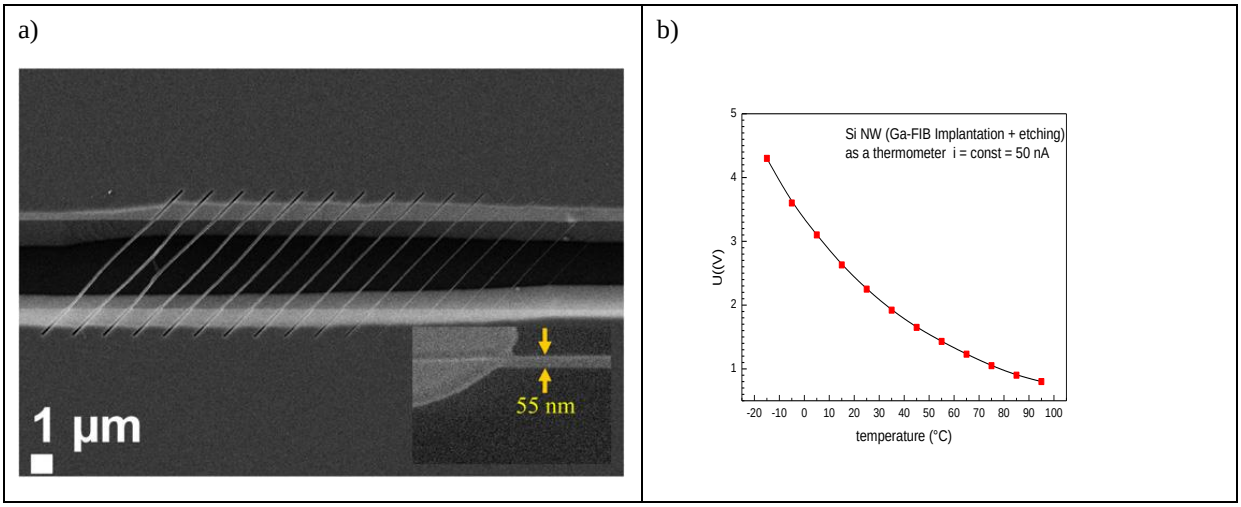

FIG. 49. a) SEM micrograph of a set of nanowires (NWs) over a gap on top of a SOI wafer. The reduction of the line fluence from $4 \cdot 10^{12}$ to $10^{11} \cdot cm^{-1}$ (from left to right) leads to a final wire width of 20 nm. The etching was performed in a 30% KOH/H_2O solution at 80 °C for 3 min. The inset shows the thickness of the NW corresponding to $R_P + 3\Delta R_P$ for 30 keV Ga in Si (SRIM 54 nm, SEM 55 nm) Fig. 1 in [305] © IOP Publishing. Reproduced with permission. All rights reserved
b) plot of the temperature dependence versus the voltage through the NW (w = 90nm) at a constant current of 50 nA which can be used for a local temperature control.

Further examples of FIB implantation are the creation of local pn-junctions by Ga into n-Si resulting in low-capacitance point diodes [306] or –a higher dose example- of a well defined concentration of dopants by implanting Co ions into Si at elevated temperatures to form $CoSi_2$ nanostructures, after a post-annealing process. They act as ohmic contacts or Schottky-junctions depending on the Si-doping [307].

As^{++} ions were implanted at an energy of 220 keV, 25 pA, defocused due to the low-dose of $1.5 \cdot 10^{11} \cdot cm^{-2}$ to increase the clocking frequency of long channel charged coupling devices (CCDs) [299]. A 16-fold increase in the maximum clocking frequency of a 26-µm-long-channel CCD has been demonstrated by the focused ion beam implantation of a lateral doping gradient [299]. Since the required doses in the gradient implant are low and high resolution is not needed, the focused-ion-beam implantation time is projected to be short, thus it possesses the potential to be used for volume production [299]. In addition FIG. 50 shows resistivity changes due to surface functionalization of insulating diamond like carbon (DLC, ion irradiation-induced sp3–sp2 rehybridization) have been observed by Philipp et al. [308].

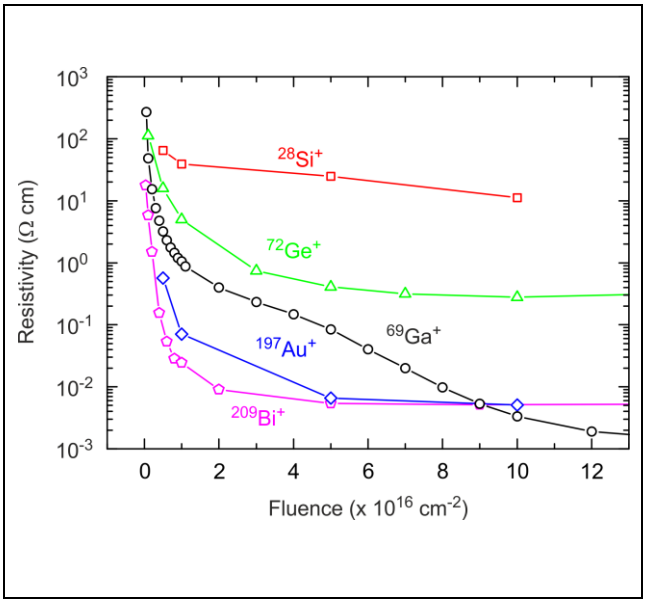

FIG. 50. Resistivity of DLC irradiated with different fluences and ion species (Ion energy = 30 keV; DLC layer thickness = 113 nm).
Fig. 3 in [308], Reproduced with permission from Carbon **80**, 677 (2014) / Elsevier, Copyright 2014 Elsevier

Ion implantation or local amorphization for surface functionalization is also a low-dose ion matter interaction regime with the potential for a high application resolution. This technique allows, in a second process step, such as, etching (oxidation) or epitaxy, the creation of vacancies which can serve as nucleation sites for material growth. In addition otherwise unreachable dose profiles can be created.

V.E.13. Surface functionalization

The first example is a dot surface functionalization of HOPG (highly oriented pyrolytic graphite) by Ga ions from a Ga LMIS FIB (type 7 in section V.C.1), followed by an oxidation process [309], [310].

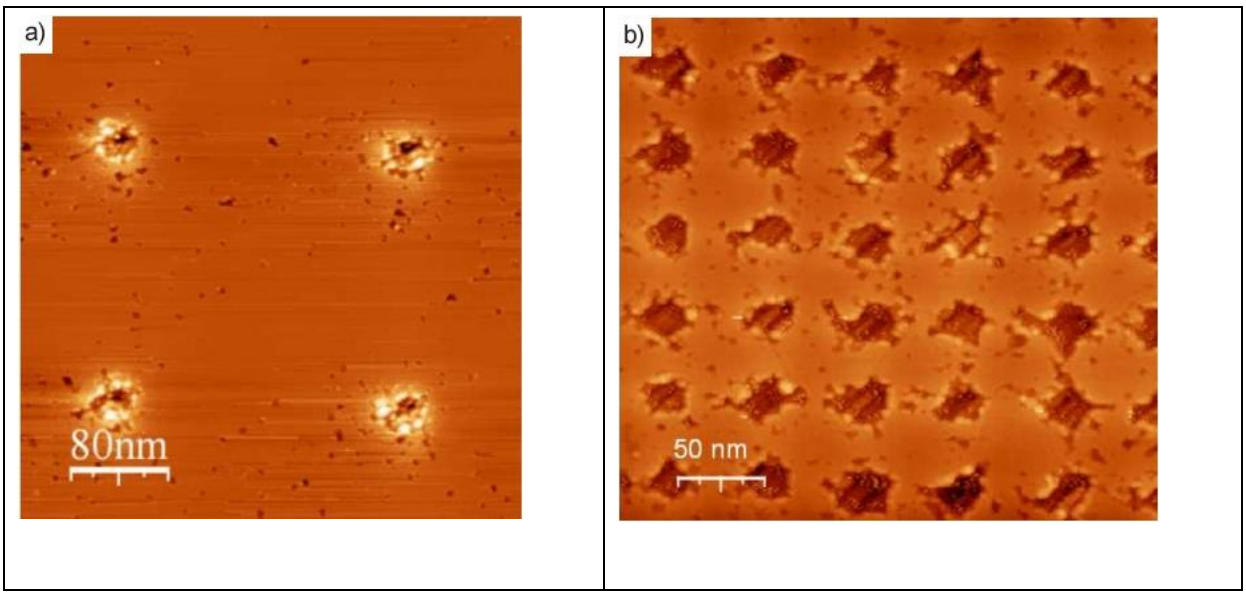

FIG. 51. Surface functionalization of HOPG by Ga LMIS FIB
UHV STM micrographs of HOPG patterned by a Ga ion beam, after oxidation, resulting in
a) sub 30 nm resolution (ion dose 1870 ions/point)
Fig. 5-34 c in [310]
b) 50 nm period (ion dose 1963 ions/point)
Fig. 5-32 d in [310] and Fig. 4 d in J. Appl. Phys. **101**, 044301 (2007), Copyright 2007 American Institue of Physics

Two further Ga surface functionalization examples are shown in FIG. 52. The first is a cluster (Au cluster 2.8 nm diameter) deposition using a laser vaporization technique [184], on artificial defects created by FIB employing a HOPG substrate FIG. 52 a). The second is a GaN epitaxy process, on AlN/6H–SiC (1 and 2 µm openings made on SiN_4) FIG. 52 b). Both FIB local surface functionalizations have been carried out employing a Ga LMIS FIB (NanoFIB, type 7 in section V.C.1).

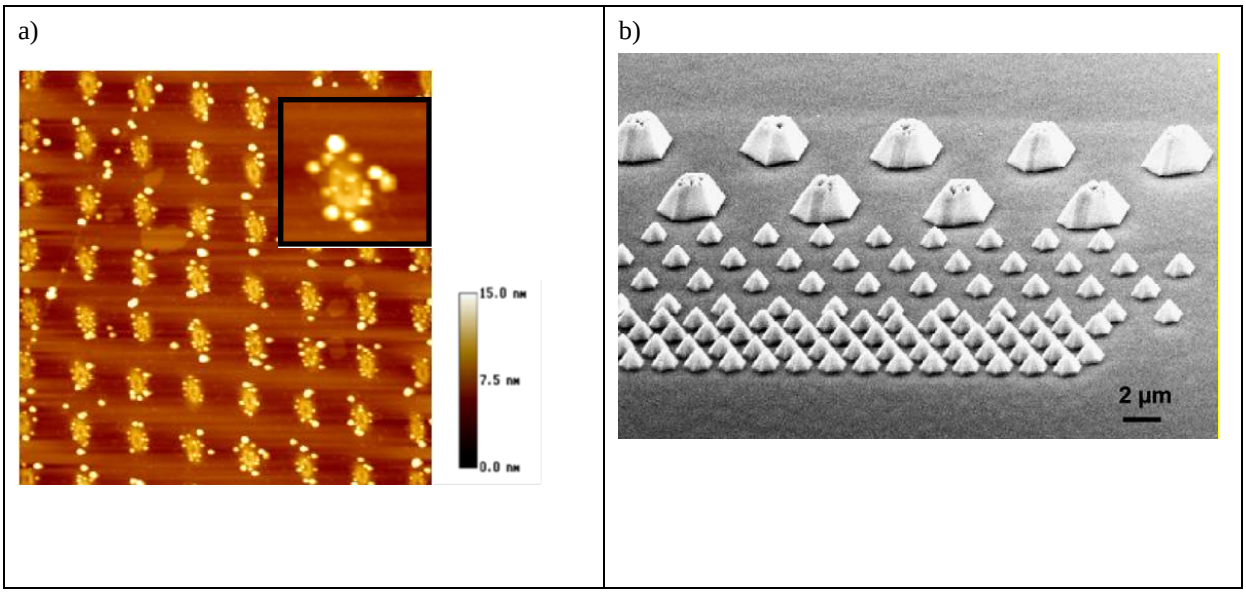

FIG. 52. a) AFM micrograph Surface functionalization of HOPG by Ga LMIS FIB patterned by a Ga ion beam, "(2 µm × 2 µm) … of the morphologies of a 10^{-2} ML gold film…" (deposited 2.8 nm gold clusters) on HOPG "surfaces patterned with a 30 keV Ga^+, 8 nm (FWHM) probe size and different ion fluences I_f and periodicities L_{def}. Gold clusters aggregated around etched nano-craters L_{def} = 300 nm, N = 37500 ions/pt, insert (300 nm × 300 nm)"
FIGURE 4b in [184], Reproduced with permission from Appl. Phys. A **80**, 187 (2005), Copyright 2005 Springer
b) SEM micrograph "of selectively epitaxially grown GaN on AlN/6H–SiC on 1 and 2 µm openings made on SiN_4 by FIB with a dose of 2.7 x 10^{16} ions/cm^2 (Ga^+ 30 keV). Note that for the largest opening, the selective epitaxy is not fully terminated"
Fig. 3 in [311]; Reproduced with permission from Microelectr. Eng. **73-74**, 610 (2004) / Elsevier, Copyright 2004 Elsevier

In the following example nucleation of Ge clusters at regions where Ga has been implanted by focused-ion beam micropatterning is shown [108]. A clean Si (001) surface has been irradiated with a Ga^+ focused ion beam, using a beam energy of 25 keV and a beam current of 10 pA ($6.2 \cdot 10^7$ ions / s). After irradiation, the Si (001) was annealed (600 to 750°C) to recover its crystal orientation, followed by a Ge deposition process. An example is shown in FIG. 53 a). The impact of an annealing process after FIB irradiation can be seen in FIG. 53 b) and c) [108]. The Ga FIB has been type 6 in section V.C.1.

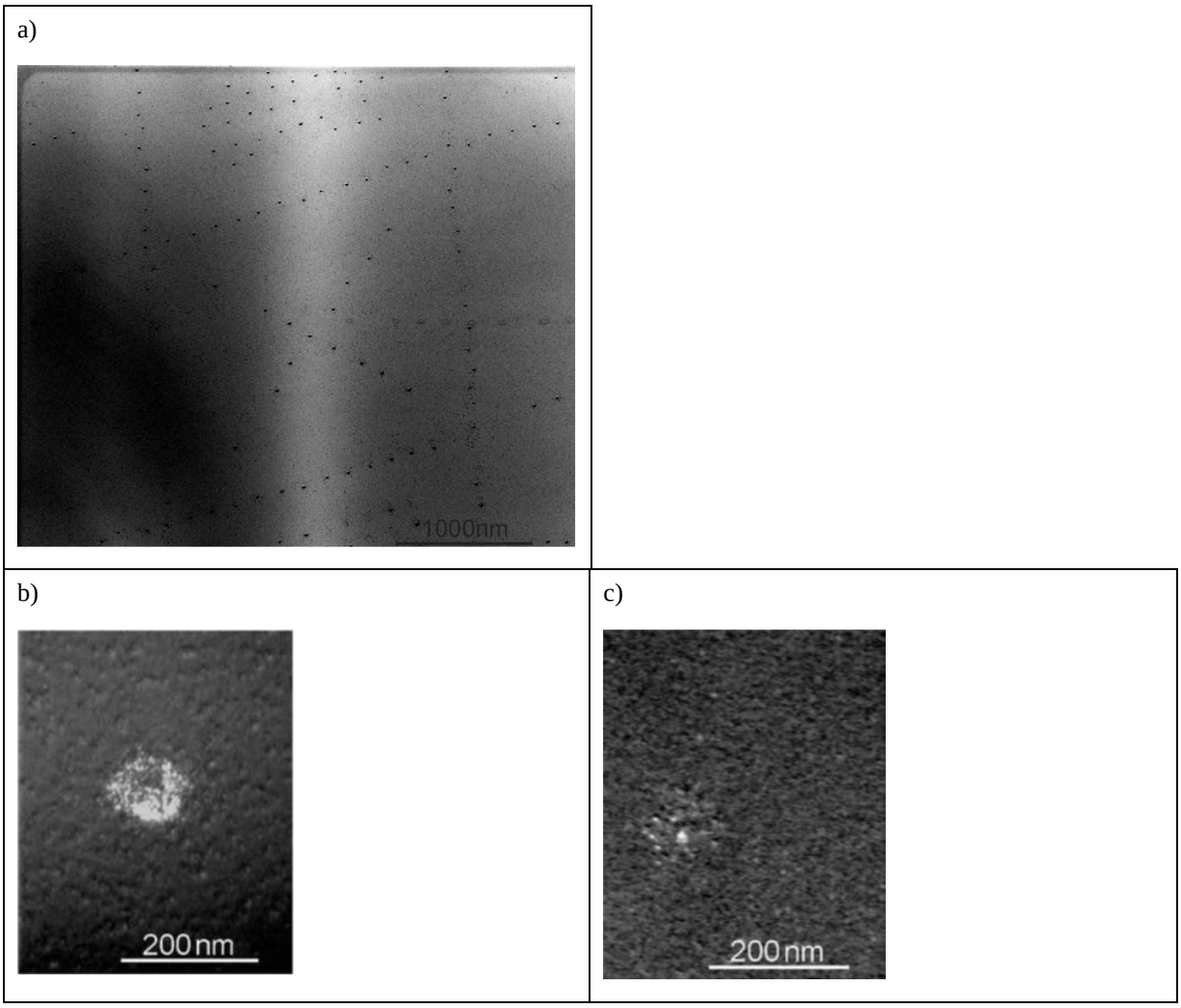

FIG. 53: TEM micrographs of features
a) after Ge cluster growth (precursor digermane, temperature of 650°C and a digermane partial pressure of $5 \cdot 10^{-8}$ Torr)
Fig. 3 in [108], Reproduced with permission from Mat. Sci. Eng. B **101**, 1 (2003) / Elsevier, Copyright 2003 Elsevier
b) and c) a feature as shown in a)
(b) "As implanted and"
(c) after "annealing at 750 °C for 15 min"
(c) and (d) Fig. 2 in [108], Reproduced with permission from Mat. Sci. Eng. B **101**, 1 (2003) / Elsevier, Copyright 2003 Elsevier

V.E.14. Gas assisted growth

In this section a selection of published gas assisted patterning results are shown, employing FIB instruments. Although not in all dimensions "nanotechnology" (definition in preface, section I), however giving access to the 3rd dimension, examples are shown in FIG. 54 and FIG. 55. Here the applied dose and patterning parameters may vary depending on the employed gas, target height and lateral dimensions of the features, which can influence the potential application resolution.

First FIG. 54 a) shows, Ga LMIS deposited carbon pillars from a phenanthrene precursor, second FIG. 54 b) etching into TiN using Br_2 gas and third FIG. 54 c) diamond like carbon (DLC) field emitters which have been deposited on a glass fiber with a FIB-CVD instrument [312]. For all three Ga LMIS FIB instruments (type 6 in section V.C.1) have been employed.

a)

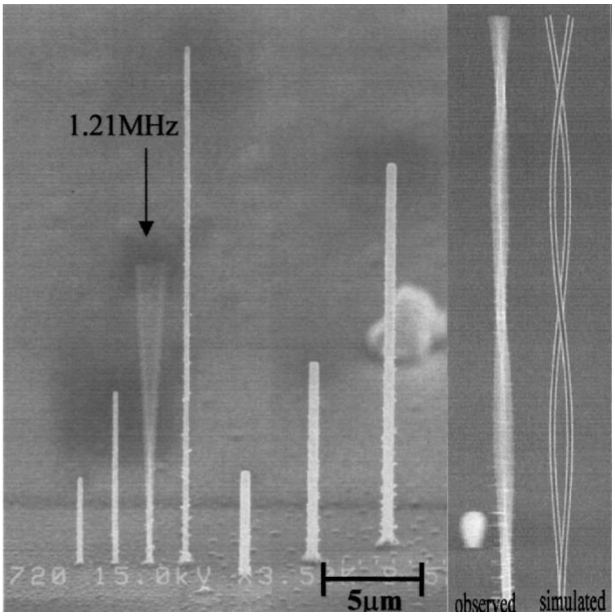

b)

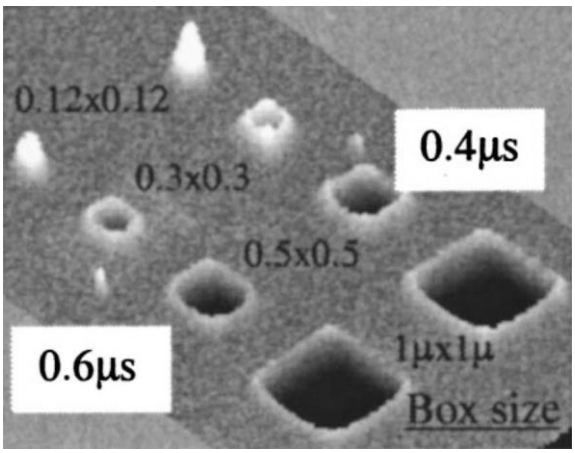

c)

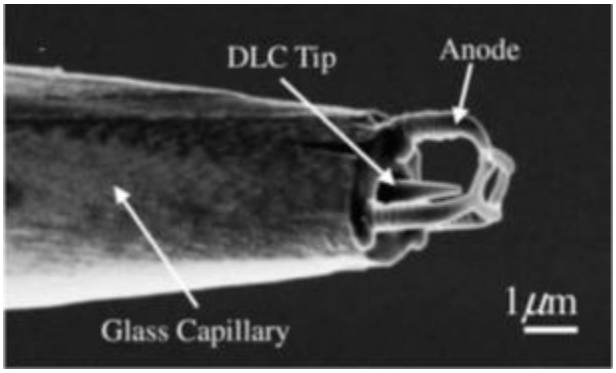

FIG. 54. SEM mircrographs

a) "Tilt view of FIB deposited carbon pillars from phenanthrene precursor. Excitation of the fundamental resonance mode left and the second order resonance mode right from Fig. 2 and 5 (merged) in [313], Reproduced with permission from J. Vac. Sci. Technol. B **19**, 2834 (2001), Copyright 2001 American Vacuum Society

b) High resolution FIB photomask repair. AFM image of gas assisted FIB etching. Boxes were etched into TiN using Br_2 gas and Ga^+ ions (20 keV, 22 pA) Fig. 3 right side in [314], Reproduced with permission from J. Vac. Sci. Technol. B **18**, 3216 (2000), Copyright 2000 American Vacuum Society

c) FIB deposited emitter-anode arrangement on glass fiber ("d" removed) Fig. 3 in [312], reused with permission from APEX/JJAP

Fourth FIG. 55 a) displays an electrostatic gripper, which has been created with a FIB CVD instrument using a phenanthrene ($C_{14}H_{10}$) precursor [315].

Fifth, diamond like carbon (DLC) 3D rotors have been fabricated by nano-sheets, using a Ga LMIS FIB beam and a phenanthrene ($C_{14}H_{10}$) precursor GIS growth process. In addition rotation of the rotor (shown in FIG. 55 b) is possible by electrostatic forces or nitrogen gas flow (aerodynamic force) [316].

Sixth Ga LMIS milling and a mixture of tetraethylorthosilicate (TEOS) gas and H_2O precursor has been used to locally deposit SiO_2 and form nanopores of the desired size and biocompatible material composition, an example is displayed in FIG. 55 c).

Seventh growth of diamond like carbon (DLC) has been carried out, to study the biocompatibility and connection possibilities of the human nervous system with external devices, to transfer information between them [318]. A prototype of an electrode's segment as microtubes has been fabricated using FIB-CVD FIG. 55d), employing a 30 keV Ga^+ ion beam and a phenanthrene precursor ($C_{14}H_{10}$) [318].

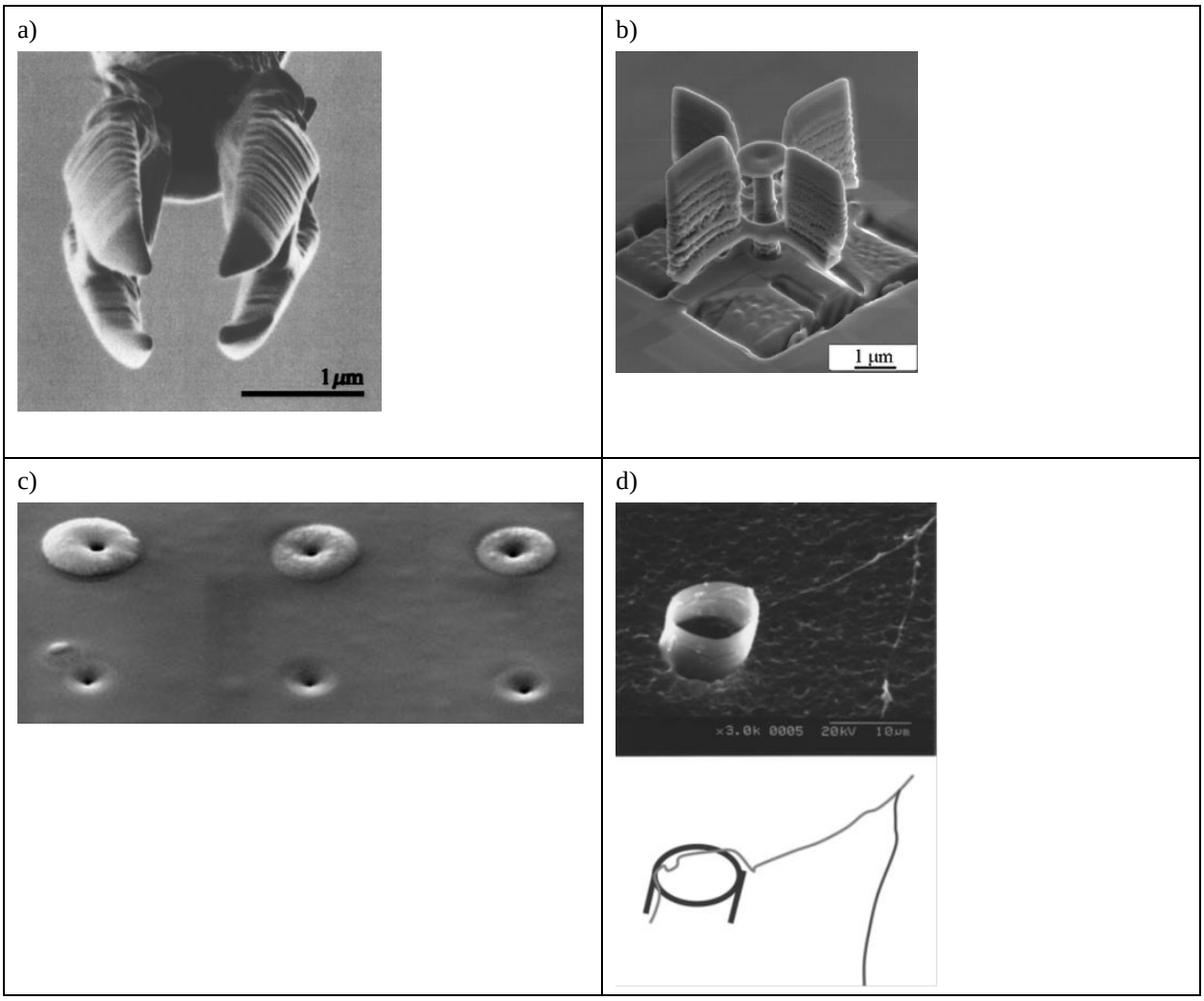

FIG. 55. SEM micrographs

a) FIB deposited electrostatically actuated gripper
Fig 6 in [315], Reproduced with permission from J. Vac. Sci. Technol. B **23**, 298 (2005), Copyright 2005 American Vacuum Society
b) SEM micrograph of a FIB deposited four wing rotor ("The rotor diameter, wing-height, wing-width and axis length were 6 µm, 3 µm, 500 nm and 2.6 µm, respectively.")
Fig. 7 in [316], Reproduced with permission from Microelec. Eng. **83**, 1221 (2006) / Elsevier Copyright 2006 Elsevier
c) "FIB fabricated biological structures. Nanopore diameter tuning with FIB deposition from tetraethoxysilane(TEOS). Nanopores were FIB milled into membrane"
Fig. 2c in [317], J. Nilsson, J. R. I. Lee, T. V. Ratto, and S. E. Létant: Localized Functionalization of Single Nanopores. Adv. Mat. 2006. **18.** 427-431. http://dx.doi.org/10.1002/adma.200501991. Copyright Wiley-VCH Verlag GmbH & Co. KGaA. Reproduced with permission.
d) "Biocompatible FIB deposited diamondlike carbon microtube with an in vitro grown nerve. "Axon extension on a microtube attached to a polycarbonate membrane."
top – "SEM image of the microtube and the axon… The axon grew from the upper right …" "… to the microtube, extended along the inner surface of the microtube, and then exited from it…"
Process parameters for the DLC growth: 30 keV Ga^+ ion beam employing a phenanthrene precursor ($C_{14}H_{10}$).
bottom – Schematic for the device concept in the SEM image above
(Rem: a) and b) removed from original)
Fig. 8 in [318], Reproduced with permission from J. Vac. Sci. Technol. B **24**, 2538 (2006), Copyright 2006 American Vacuum Society

V.E.15. Self-organization under ion irradiation

So far results from 4 kinds of ion source / instrument technologies (described in section V.C.1) have been reported, operating in the linear cascade regime (5-50 kV, explained in section V.C.2).:

- GFIS (low beam current, currently highest resolution, type 3 in section V.C.1)
- Xe ICP (resolution optimized plasma ion sources, high probe currents, type 4 in section V.C.1)
- versatile LMIS (type 6 in V.C.1)
- as well as nano patterning dedicated LM(A)IS instruments (mid beam current, high resolution, maturity, large selection of incident ions, type 7 in V.C.1)

Finally, fascinating self-organized regular structures like dots and ripples can evolve under ion irradiation, employing mainly "…collimated beams of low energy ions…" [319]. Atoms are removed from the face of the sputter plate and some accumulate at the nearby target sample surface [112] or "…roughening induced by ion milling and smoothing due to surface diffusion…" [125] can be seen in FIG. 56, FIG. 57 and FIG. 58.

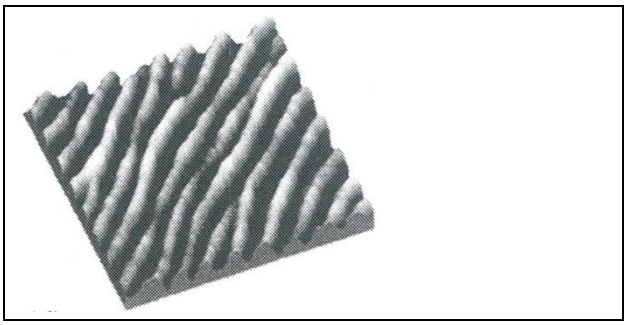

FIG. 56. "Three- dimensional view of the surface morphology resulting after 20 min Ne^+ bombardment of Ag(110) at an ion dose rate of $\Phi = 5$ µA / cm^2. Images are taken after grazing incidence milling $\theta_i = 70°$ at T = 180 K (erosive regime)"
5 d in [90], Reproduced with permission from Mat. Sci. Eng. C **23**, 201 (2003) / Elsevier, Copyright 2003 Elsevier

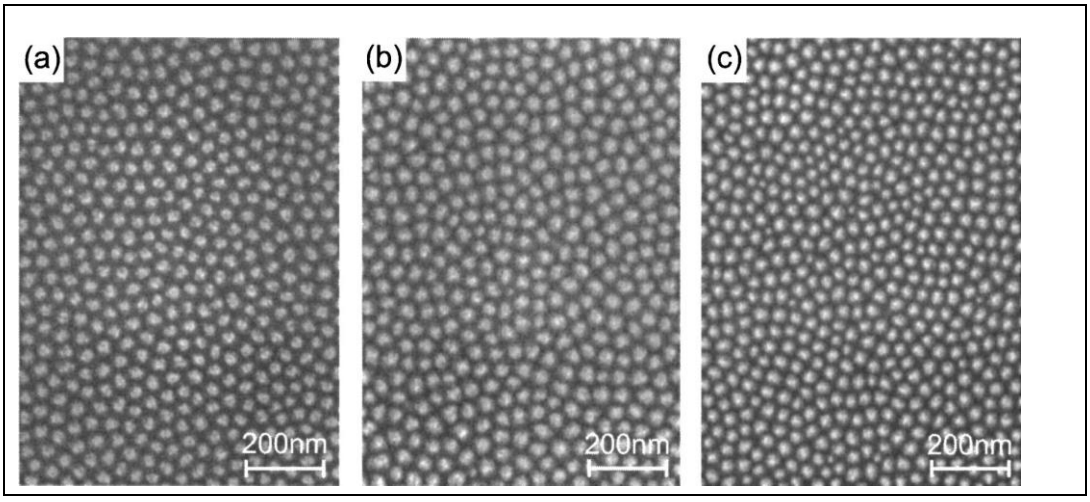

FIG. 57. "Scanning electron micrographs of dot patterns on GaSb films:
a) the initial layer is c-GaSb (100),
b) the initial layer is c-GaSb (111),
c) the initial layer is amorphous GaSb deposited on Si(111). The patterns are created at an Ar^+-ion energy of 500 eV, an ion flux of 1 X 10^{16} cm^2 s^{-1}, and an erosion time of 200 s"
Fig. 1 in [261], Reproduced with permission from Applied Physics Letters **80**, 130 (2002), Copyright 2002 American Institute of Physics

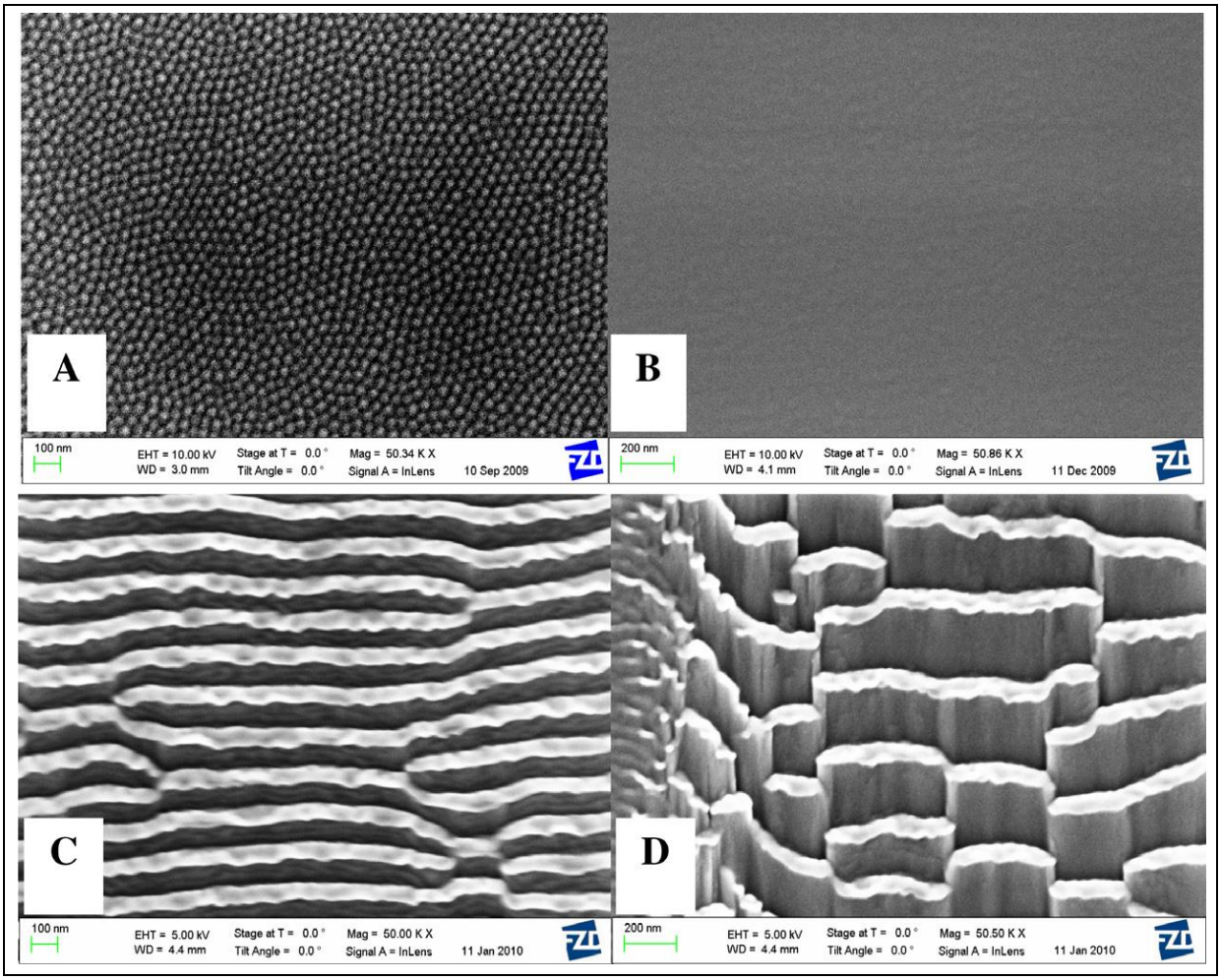

FIG. 58. SEM micrograph "Pattern evolution as a function of angle of incidence: dot pattern at normal incidence (A), smoothing at 45° (B), ripple structures at 75° (C) and shingles at 85° (D)"
Fig. 3 in [320], Reproduced with permission from Nucl. Instrum. Meth. i. Phys. Res. B **272**, 198 (2012) / Elsevier, Copyright 2012 Elsevier

FIG. 59 shows exemplary results employing a different instrument type: a focused ion beam (FIB, type 6 in section V.C.1) [321], [322], which allows these regular self-organizing patterns to be positioned at specific locations on the sample and the tailoring of the outer geometries of these regions.

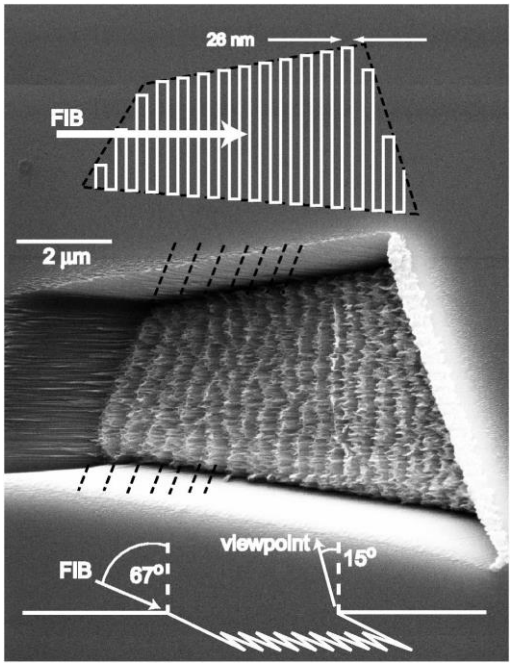

FIG. 59. SEM micrograph example of self-organized regular features with well-defined boundary shape at a dedicated sample location by an FIB instrument.
"Ripple alignment with boundary of FIB-milled irregular quadrilateral.SEM image taken at 15° from normal. Ion irradiation 67° from normal, projected ion beam direction shown by arrow: ion dose of $0.4 \cdot 10^{18}$ / cm^2. A schematic cross section is shown at the bottom. Schematic of raster pattern in plan view is shown at the top. Raster path is the white line: left boundary of the raster pattern is inclined by 10°. Note that the actual line pitch of the raster is much smaller than drawn, 10 nm / cos(67°), or 26 nm. Ripple alignment with boundary near left edge decays over several periods until ripples align normal to the projected ion beam in the center of the milled region. Diagonal lines drawn along the ripples are guides to the eye."
Fig. 2 in [321], Reproduced with permission from J. Vac. Sci. Technol. B **23**. 1068 (2005), Copyright 2005 American Vacuum Society

V.F. Capabilities for nano device prototyping

The examples above prove that feature sizes below 5 nm and periodicities down to 7 nm are accessible for point ion source nano patterning. For some of the examples given for ion matter interaction regimes used for nano patterning (milling and gas-assisted processing) the process know-how is wide spread, however other examples given (surface functionalization, atom intermixing, …) are only used by a small number of researchers.

Technology costs for FIB vary similarly as for EBL. Depending on FIB equipment availible and patterning requirements, the integrated patterning capabilities of the FIB instrument can be used, or upgraded at moderate cost by patterning attachments. However for some applications, dedicated equipment might be necessary to facilitate the work, and these are similar in expense to an EBL writer.

Computer controlled FIB nano patterning is a similar serial fabrication process as electron beam lithography and therefore rather slow in volume production respects, compared to parallel techniques like optical projection lithography, nano imprint or self-organized 3D epitaxy (compare section III); however for R&D type rapid nano device prototyping, the overall process time from an idea to an actual working device can be very short.

Some application examples show that a dedicated patterning instrument architecture -similar to dedicated EBL writers- can handle large samples and successfully pattern large areas. In addition, a high pattern placement accuracy and reproducibility can be achieved. Further, focused ion beam techniques give easy access to 3D patterning, especially as the application resolution can be tailored to sub ten nm in the 3 dimensions. In addition unique material properties can be locally created at almost arbitrary shapes, "… not obtainable by other techniques …" [166].

Point ion beam nano patterning is a top-down lithography technique employing SW designs, which can be easily and quickly modified. Device design, shape and position fine tuning is easy and quick as in the SPM and EBL writer techniques.

As the ion beam is a charged beam, the charge has to be removed from the sample surface, thus charge removal is necessary either by a sufficiently conducting sample/ resist surface (adequate to the selected probe current) or by other means. Most applications and material systems can be addressed neglecting this, as many substrates are (semi) conducting and for high resolution small beam currents are required.

The large variety of accessible ions allow unique tailoring of many material (systems) and interfacing to the surface (for details see section III.C), where sometimes a subsequent annealing process step is necessary.

The technologies versatility is unique, due to the large variety of exploitable ion matter interaction regimes and incident ions. If the desired ion species is not (yet) available as a source, a thin layer material system might be composed to get the desired atoms into the surface layer by means of atom intermixing (the fundamentals have been described in section V.C.2 and an application example has been given in V.D.4), where the layer below a thin active layer consists of the desired atoms.

Vector scan "Gaussian" beam nano pattering is well suited for R&D type rapid prototyping, especially with the potential beauty to create operating nano devices in a single process step.

The techniques' capabilities for nano device prototyping will be summarized and compared with the others -covered in this article- in Table II.

V.G. Conclusion

We have presented many successful nano device prototypes created by a variety of ion-matter interaction regimes. They include: intended surface modification, atom intermixing, refining classical milling, gas assisted and combined processes with other technologies. They can create operating devices in many application fields, for example: microfluidics, photonics, small holes, local doping or magnetics. This large variety of leading edge application results (examples have been illustrated in section V.D and V.E), representing only a fraction of all published and tested ones, show that (almost) all challenges or drawbacks reported for ion beam nano patterning in the literature (listed at the.end of section V.B) have been sucessfully resolved by recent process and technical developments.

Finally, the dedicated focused ion beam nanopatterning instrument (developed by us, type 7 in section V.C.1); has been realized on an EBL instrument architecture, thus with long term instrument stability, correction mechanisms and unattended batch process capabilities known from EBL writers. This refutes the previously reported statement: "But, and perhaps most telling, the available tooling for electron beam lithography is much

more sophisticated, which is perhaps the single-most reason it is much more widely used." [83], explained in section V.B.

In addition for some cases, alternative processes have been developed where the drawbacks have no relevance especially as some ion beam technologies possess the versatility to quickly select incident ions, clusters, charge states, acceleration voltage, and dose to easily match the application requirements.

As a result, point ion source vector beam nano patterning is well suited for R&D type rapid nano device prototyping and small scale production. This is because of its high resolution capabilities, software design based pattering and the availability of point ion beam technology in most R&D nanopatterning labs. Thus, they offer a uniquely fast (process time) device creation capability for many applications, some devices can even be created within a single process step or as an all-in-one instrument fabrication. In addition, unique patterning capabilities exist with regard to process simplicity, 3D patterning and interface quality.

Depending on the instrumentation the results can be seen immediately, either with an electron beam or the same ion beam employing a lower dose or a different ion species.

Finally, complementary capabilities for ion beam techniques are expected from improvements for the other ion source technologies descibed above, such as GFIS, ICP or ECR plasma sources (type 3 and 4 in section V.C.1). Additional progress can be expected from promising ion source concepts like: atomic-size metal ion sources [323], a “super-tip” concept for LMIS [233], liquid ionic sources [324], [224], and [195], heavily charged ions [325] or cold solid state sources [326].

VI. Summary and outlook

As shown by this collection of nano device prototyped application results from different techniques, there exist many ways to create nano features. We have reviewed processes by four technology families suitable for nano device prototyping: (organic resist) electron beam lithography (EBL), self-organized 3D epitaxy, atomic probe microscopy (STM/AFM) patterning derivatives and in particular focused ion beam (FIB) technologies, especially those from liquid metal (alloy) ions sources (LM(A)IS).

On one hand, there exist matured and established technologies with the related process know-how for many applications. On the other hand new challenges and requirements have evolved beyond well understood processing, and in these instances, clever ways have been found to meet these needs (exemplary application results have been given in section V.D and V.E).

We took a look at these techniques with respect to the following criteria for nano device prototyping (NDP): application resolution; minimum periodicities; interfacing to the surface (in a manner realizable like in homoepitaxy, for details see section III.C); freedom for arbitrary geometry and shape; the ability to produce features at dedicated sample positions / locations, with a high accuracy; 3 dimensional objects; large area patterning exceeding a write-field (see section II.C.1 and II.C.2); time required to develop a new process; the process know-how accessibility to the community ("standardization"); process and instrumentation maturity; over all time and efforts necessary to create devices which can be tested and measured ("time to device"); time required for design changes; versatility of the technology for all kind of applications and material systems; costs from idea to device ready for testing, and finally the reproducibility for structuring more than a few devices up to the feasibility to run small scale production lines. Among these criteria, every technique possesses favorable ones. Some of them are uniquely favorable or advanced " ★ ", others very good "++", good "+", some are "variable" depending on the processes as well as the actual pattern definition effect, or their performance to fulfill this criterion is not so developed (yet) "–", which are summarized in Table II. For details, compare the corresponding capabilities for nano device prototyping sections of each technology family above II.E, III.E, IV.E and V.F.

Table II: R & D type nano device prototyping techniques, detailed definition criteria see text and the detailed explanations inside each techniques' "capabilities for nano device prototyping" sections above: II.E, III.E, IV.E and V.F.

Criteria	EBL	STM / AFM	Self-organized 3D epitaxy	FIB LM(A)IS
Resolution	++	★	++	++
Periodicity	++	★	++	++
Interfacing to surface	variable	++	★	++
Free Shapes	++	++	-	++
Placement accuracy	++	++	-	++

3D	variable	variable	+	++
Large area	++	-	★	+
Overall process complexity	++	++	variable	★
Process standardization	★	-	-	variable
Process and instrumentation maturity	★	variable	variable	++
Duration ("time to device")	variable	variable	variable	★
Little Modifications ("design changes / adjustments")	++	variable	variable	++
Versatility	++	++	+	★
Costs	variable	variable	★	variable
Reproducibility suitable for small scale production	++	-	★	++

Electron beam lithography patterning of organic resist possesses more than 50 years of history [84], thus the process know-how and instrumentation are wide spread, and have reached an incredible level of stability, maturity, precision and automation. As a result, it is also well suited and regularly used for small scale production jobs.

Self-organized 3D epitaxy is well suited for the creation of regular 3D features with perfect interfaces to the substrate (as described in section III.C). It can be applied at extremely low costs, can cover large areas and possess simple single process step capabilities for nano devices creation, so small times to device are possible.

Atomic probe microscopy (APM) patterning has leading edge single atom placement capabilities, so gives access to very small scale device concepts down to the few atoms level and can give access to good interfaces to the substrate.

EBL, APM and FIB based technologies all share the beauty of software designs (no need for expensive masks and their sometimes time consuming production period), allowing fast design modifications. In addition arbitrary shapes (limited only by the application resolution) at dedicated sample locations can be created.

Ion beam technologies, especially FIB, possess outstanding capabilities like: good interfacing to the surface (sometimes requiring a subsequent annealing process), 3D patterning, only one process step, thus (for some applications) the quickest time from idea to device and the largest versatility. The large variety of successful application results (section V.D and V.E summarized in V.G) prove that solutions for almost all reported challenges (end of section V.B) have been found -especially the tooling one, because commercial solutions have become available [184], [41], [220] and [221]. In comparison to EBL, the instrument stability, control and feedback mechanisms, as well as dose control and patterning field calibration are available now on the level necessary for many applications, also in dedicated ion beam instruments. As a result, large area patterning (few hundreds of microns) of small features is possible with point ion beams ("FIB instruments").

In addition the promising new ion source technologies mentioned in section V.C.1 and V.G can bring additional unique capabilities for ion beam technologies.

A combination of the techniques discussed can provide further nano patterning process alternatives. For example ions can locally functionalize sample surface areas (also possible by an electron beam [109]) and then another processes step like nano patterning or self-organized 3D epitaxy could follow. This can widen the application space, thus increase the number of successful results of nano device prototyping by more unique or different combinations of the criteria described in Table II above.

In addition there exist further technologies, which can be combined for similar reasons: Block copolymers [327], [328], [329], [330]; lithography and microcontact printing [12]; assisted assembly of nanoparticles using gold nanoparticles stabilized with ligands and self-assembled on irradiation with ultraviolet light [10]; “on wire lithography” a template-directed synthesis of nanowires [331], electrochemical deposition and wet-chemical etching [331], prepatterning by holographic lithography followed by a MBE Ge deposition [117], [14].

In this article, we have reviewed many powerful nano device prototyping fabrication alternatives. If an application is limited by conventional processing technologies, exploring one of the described or other non-conventional alternatives with unique capabilities may be an option.

VII. Acknowledgments

The authors thank especially:

Bill R. Appleton (University of Florida, USA and Co-Editor of APR) for the invitation and advice; J. Fridmann (Raith America, Troy, NY, USA) for proof reading and together with S. Bauerdick (Raith GmbH, Dortmund, Germany) and A. Nadzeyka (Raith GmbH, Dortmund, Germany) for the tremendous application work; J. E. Sanabia (Raith America, Islandia, NY, USA) and R. Jede (Raith GmbH, Dortmund, Germany) for proof reading, discussions, scientific guidance and suggestions; K. E. Burcham, J. Fridmann and J. Klingfus (all Raith America, Islandia, NY, USA) for native speaker proof reading; H. Romijn and M. Butler (Raith BV, Netherlands) for assisting the EBL history section; R. Schott (Ruhr-Universität Bochum, Germany), as well as M. Olmstead (University of Washington) advice on the self-organized 3D epitaxy chapter; J. Orloff for assisting the CPO section, our application cooperation partners for providing ideas, samples, final testing of the devices and much more; the European Commission (EC, Contract No. G5RD-CT2000-0034) and BMWI (contract No. (ZIM) KF2712302DF1) for funding the initial research project and the multispecies option. respectively; all colleagues at Raith for jointly realizing the instrument technology.

VIII. References

[1] Nanotechnology definition (NSET, February 2000)
http://www.nsf.gov/crssprgm/nano/reports/omb_nifty50.jsp, (10.07.2008)

[2] A. A. Tseng, A. Notargiacomo, and T. P. Chen, J. Vac. Sci. Technol. B **23**, 877 (2005),
(http://dx.doi.org/10.1116/1.1926293)

[3] https://de.wikipedia.org/wiki/Giraffe (28.10.2015)

[4] http://county.wsu.edu/king/gardening/mg/factsheets/Fact%20Sheets/Ants%20-%20Household.pdf
(28.10.2015)

[5] "Asian"hair from http://www.optics.rochester.edu/workgroups/cml/opt307/spr06/xue/project.htm,
(28.10.2015)

[6] https://en.wikipedia.org/wiki/Lasius, (28.10.2015)

[7] http://science.energy.gov/bes/community-resources/scale-of-things-chart/ (18.05.2016)

[8] A. T. S. Wee, in *Selected Topics in Nanoscience and Nanotechnology*, World Scientific Publishing Co. Pte. Ltd., Singapore, ISBN 978-981-283-955-8 (2009), Preface
(http://www.worldscientific.com/doi/pdf/10.1142/9789812839565_fmatter)

[9] S. Srivastava, and N. A. Kotov, Soft Mat. **5**, 1146 (2009), (http://dx.doi.org/10.1039/b812115j)

[10] Z. Nie, A. Petukhova, and E. Kumacheva, Nature Nanotechnology **5** (1), 15 (2010),
(http://dx.doi.org/10.1038/nnano.2009.453)

[11] A. Böker, J. He, T. Emrick, and T. P. Russell, Soft Mat. **3**, 1231 (2007),
(http://dx.doi.org/10.1039/B706609K)

[12] S. Kinge, M. Credo-Calama, and D. N. Reinhoudt, ChemPhysChem **9**, 20 (2008),
(http://dx.doi.org/10.1002/cphc.200700475)

[13] A. Singh and K. M. Ryan, Part. Part. Syst. Charact. **30**, 624 (2013),
(http://dx.doi.org/10.1002/ppsc.201300008)

[14] J. Stangl, V. Holý, and G. Bauer, Rev. Mod. Phys. **76**, 725 (2004),
(http://dx.doi.org/10.1103/RevModPhys.76.725)

[15] Y. Min, M. Akbulut, K. Kristiansen, Y. Golan, and J. Israelachvili, Nature Mat. **7**, 527 (2008),
(http://dx.doi.org/10.1038/nmat2206)

[16] Abteilung 5 Schlüsseltechnologien https://www.bmbf.de/de/die-organisation-des-hauses-192.html
(14.12.2015)

[17] G. Shalev, S. W. Schmitt, H. Embrechts, G. Brönstrup, and S. Christiansen, Scientific reports 5, 8570 (2015), (http://dx.doi.org/10.1038/srep08570)

[18] M. C. Demirel, M. Cetinkaya, A. Pena-Francesch, and H. Jung, Recent Advances in Nanoscale Bioinspired Materials", Macromoelcular Bioscience **15**, 300 (2015),
(http://dx.doi.org/10.1002/mabi.201400324)

[19] R. Bappert, S. Benner, B. Häcker, U. Klein, and G. Zweckbronner, in *Biologie Technik Bionik: Zukunfts-Technik lernt von der Natur*, SiemensForum Munich/Berlin Germany, ISBN 3980493059, (1999)

[20] J. E. Ayers, in *Heteroepitaxy of Semiconductors: Theory, Growth, and Characterization*, Taylor & Francis Group, CRC Press, Boca Raton Fl USA, ISBN 0-8493-7195-3 (2007)

[21] E. V. Shevchenko,D. V. Talapi, N. A. Kotov, S. O'Brien, and C. B. Murray, Nature **439**, 55 (2006), (http://dx.doi.org/10.1038/nature04414)

[22] M. Gentili, and C. Giovannella (ed.), in *nanolithography: A borderland between STM, EB, IB, and X-Ray Lithographies*, Nato ASI Series, Series E: Applied Science - Vol 264, Kluwer Academic Publishers Dordrecht, ISBN 0-7923-2794-2 (1994)

[23] H. J. Levinson, and W. H. Arnold, in *Handbook of Microlithography, Micromachining and Microfabrication Volume 1: Microlithography*, edited by Rai-Choudhury , SPIE Optical Engineering Press, Bellingham, Washington, USA, ISBN 978-0852969069 (1997), Chapter 1, "optical lithography", pp. 11

[24] C. Wagner, and N. Harned, Nature Photonics **4**, 24 (2010), (http://dx.doi.org/10.1038/nphoton.2009.251) and further articles about optical lithography in the same issue

[25] S. Y. Chou, P. R. Kraus, P. J. Renstrom, Science **272**, 85 (1996), (http://dx.doi.org/10.1126/science.272.5258.85)

[26] R.F. Pease and S.Y. Chou, in *Proceedings of the IEEE* **96**, edited by R. J. Trew, 248 (2008)

[27] M. A. McCord, M. J. Rooks, in *Handbook of Microlithography, Micromachining and Microfabrication Volume 1: Microlithography*, Rai-Choudhury, P. (Ed), SPIE Optical Engineering Press, Bellingham, Washington, USA, ISBN 978-0852969069 (1997), Chapter 2, "electron beam lithography", pp. 139, http://www.cnf.cornell.edu/cnf_spietoc.html, 10.04.2015

[28] A. A. Tseng (ed,), in *Nanofabrication Fundamentals and Applications*, World Scientific Publishing Singapore 2008, ISBN 10-981-270-076-5, Preface, pp. vii (http://www.worldscientific.com/doi/pdf/10.1142/9789812790897_fmatter)

[29] K. Holmberg, in *Tribology of Mechanical Systems: A Guide to Present and Future Technologies*, edited by J. Vizintin, M. Kalin, K. Dohda, S. Jahanmir, ASME Press NY, USA ISBN 0791802094 (2004)

[30] R. Bennewitz, and N. Strobach, Physik Journal **14**, 37 (2015),

[31] K. Keskinbora, C. Grévent, M. Bechtel, M. Weigand, E. Goering, A. Nadzeyka, L. Peto, S. Rehbein, G. Schneider, R. Follath, J. Vila-Comamala, H. Yan, and G. Schütz, Optical Express **21**, 11747 (2013), (http://dx.doi.org/10.1364/OE.21.011747)

[32] F. K. Men, Feng Liu, P. J. Wang, C. H. Chen, D. L. Cheng, J. L. Lin, and F. J. Himpsel, Appl. Phys. Lett. **88**, 096105-1 (2002), (http://dx.doi.org/10.1103/PhysRevLett.88.096105)

[33] R.P. Feynman, Engineering and Science **23**, 22 (1960)
the actual talk has been given at Caltech at 29.12.1959,
http://calteches.library.caltech.edu/47/02/1960Bottom.pdf or.
http://www.zyvex.com/nanotech/feynman.html (14.12.2015)

[34] S.P. Newberry, in Proceedings of the Fourth SEBT, edited by R. A. Bakish, **81** (1962)

[35] SC Technol. 2008 - http://www.semiconductor-technology.com/features/feature226/ (14.12.2015)

[36] L. Veneklasen, in *Handbook of VLSI microlithography, principles, technology and applications*, edited by W. B. Glendinning, and J. N. Helbert, Noyes publications, Park Ridge New Yersey, USA, ISBN 0-8155-1281-3 (1991), chapter 5 electron beam lithography, pp. 365

[37] G. Owen, and J. R. Sheats, in *Microlithography*, edited by J. R. Sheats, and B.W. Smith, M. Dekker Inc., New York, USA, ISBN 0-8247-9953-4 (1998), Chap. 6, pp. 367-402

[38] R.K. Watts, in *VLSI Technology*, edited by S.M. Sze, 2nd ed., McGraw-Hill Book Company Singapore; ISBN 0-07-100347-9 (1988), chapter 4, pp.141

[39] Raith GmbH, Technical description Pioneer Two (document No. 15-2-1463-1.0, from 20.2.2015)

[40] Ellionix 2015 - http://www.elionix.co.jp/english/products/ELS/ELSF125.html, 10.04.2015

[41] L. Bruchhaus, PhD Thesis, TU Dortmund, Dortmund, Germany (2012), (http://dx.doi.org/10.17877/DE290R-14294)

[42] J.P. Beasley, International Conference on Electron and Ion Beam Science and Technology **4**, 515 (1970)

[43] http://www.computerhistory.org/semiconductor/timeline/1955-Photolithography.html (16.09.2008)

[44] E. Ruska, Rev. Mod. Phys. **59**, 627 (1987), (http://dx.doi.org/10.1103/RevModPhys.59.627)

[45] L. de Broglie, PhD thesis, Universtié de Paris, France (1924), published in Ann. Phys. Paris, **10**, 3, 22 (1925)

[46] B. Lencová, in *Handbook of Charged Particle Optics*, edited by J. Orloff, 2nd edition (CRC Press, Boca Raton, USA, ISBN 1-4200-4554-7 (2009), Chap. 5, pp. 161-208

[47] E. Ruska, Z. Phys. **87**, 580 (1934), (http://link.springer.com/article/10.1007%2FBF01333326?LI=true)

[48] W. Glaser, *Grundlagen der Elektronenoptik*, Springer Verlag, Wien, Austria, ISBN 978-3662236208 (1952)

[49] P. W. Hawkes and E. Kasper, *Principles of electron optics: Volume 1*, Academic press, London, GB, ISBN 0-12-333351-2 (1989)

[50] P. Hawkes, Annales de la Fondation Louis de Broglie, **29**, 837 (2004), (http://citeseerx.ist.psu.edu/viewdoc/download?doi=10.1.1.107.7275&rep=rep1&type=pdf)

[51] M. Knoll and E. Ruska, Z. Phys. **78**, 318 (1932), (http://link.springer.com/article/10.1007/BF01342199)

[52] M. Haider, S. Uhlemann, E. Schwan, H. Rose, B. Kabius, and K. Urban, Nature **392**, 768 (1998), (http://dx.doi.org/10.1038/33823)

[53] H.H. Rose, Sci. Technol. Adv. Mat. **9**, 014107 (2008), (http://dx.doi.org/10.1088/0031-8949/9/1/014107)

[54]Transmision electron microscope JEM-1000: http://www.jeol.co.jp/en/products/detail/JEM-1000.html (14.12.2015)

[55] 300 kV TEM Titan from FEI https://www.fei.com/products/tem/titan/ (29.04.2016)

[56] M. Schmallenberg, p.1-16 (2007), http://eipbn.org/wp-content/uploads/2015/01/EIPBN_history.pdf (12.12.2015)

[57] P. H. Carr, Rev. Sci. Instrum. AIP, NY, **1**, 711 (1930), (http://dx.doi.org/10.1063/1.1748661)

[58] D.A. Buck and K. Shoulders, in *Proceedings Eastern Joint Computer Conference*, Am. Inst. Elec. Engineers, Special Publication **t-114**, New York, ATEE (1958), p.55-59, (http://dx.doi.org/10.1145/1458043.1458057)

[59] R.F.M. Thornley, and M. Hatzakis, in *Record of the IEEE 9th Annual Symposium on electron, ion and laser beam Techn.*, 64 (1967)

[60] I. Haller, M. Hatzakis, S. Srinivasan, IBM J. Res. Dev. **12**, 251 (1968), (http://dx.doi.org/10.1147/rd.123.0251)

[61] A. N. Broers, W. W. Molzen, J. J. Cuomo, and N. D. Wittels, Applied Physics Letters **26**, 596 (1976), (http://dx.doi.org/10.1063/1.89155)

[62] I. Utke, P. Hoffmann, and J. Melngailis, J. Vac. Sci. Technol. B, **26**, 1197 (2008), (http://dx.doi.org/10.1116/1.2955728)

[63] I. Utke, S. Moshkalev, and P. Russell (ed.), in *Nanofabrication Using Focused Ion and Electron Beams*, Oxford University Press Inc., NY, NY, USA, ISBN 9-780-19-973421-4 (2012)

[64] R.M.F. Thornley, A.V. Brown, and A.J. Speth, IEEE Trans. Electron Components **EC-13**, 36 (1964), (http://dx.doi.org/10.1109/PGEC.1964.263833)

[65] Technical description of Raith 150-TWO. V TD_ RAITH150TWO _3.2, April 2010

[66] Ellionix ELS-F125
http://www.elionix.co.jp/english/products/ELS/ELSF125.html (05.10.2015)

[67] Jeol JBX-9500FS
http://www.jeol.de/electronoptics-en/products/semiconductor-equipment/electron-beam-lithography-systems/jbx-9500fs.php (05.10.2015)

[68] Crestec CABL-9000C
http://www.crestec8.co.jp/englishF/product/newfolder-1/ (5.10.2015)

[69] nanobeam nB4
http://www.nanobeam.co.uk/index.php?option=com_content&view=article&id=26&Itemid=48 (5.10.2015)

[70] L. Reimer, in *Scanning electron microscopy*, 2nd ed., Springer Verlag Berlin, Germany, ISBN 3-540-63976-4 (1998)

[71] EB Mask Repair 2010 - MeRiT HR 32 Zeiss SMT GmbH, http://www.zeiss.de/c1256c1500431210/Contents-Frame/6531cac4d5c10402c1256df7003f3cbc, (25.06.2010)

[72] A. Nadzeyka, L. Peto, S. Bauerdick, M. Mayer, K. Keskinbora, C. Grévent, M. Weigand b, M. Hirscher and G. Schütz, Microelec. Eng. **98**, 198 (2012), (http://dx.doi.org/10.1016/j.mee.2012.07.036)

[73] W.S. Mackie, PhD Thesis (7154); University of Glasgow, Glasgow, Great Britain; 2-3 (1984)

[74] L. Bruchhaus, Diplomarbeit BGUH Wuppertal, Wuppertal, Germany (1997)

[75] R. M. H. New, R. F. W Pease, and R. L. White, J. Vac. Sci. Technol. B. **12**, 3196 (1994), (http://dx.doi.org/10.1116/1.587499)

[76] S.R. Nassif, in International Conference on Simulation of Semiconductor Processes and Devices, SISPAD, 5 (2007)

[77] D. R. S. Cumming, S. Thoms, S. P. Beaumont, and J. M. R. Weaver, Applied Physics Letters **68**, 322 (1996), (http://dx.doi.org/10.1063/1.116073)

[78] J. K. W. Yang, B. Cord, H. Duan, K. K. Berggren, J. Klingfus, S.-W. Nam, K.-B. Kim, and M. J. Rooks, J. Vac. Sci. Technol. B **27**, 2622 (2009), (http://dx.doi.org/10.1116/1.3253652)

[79] W. F. van Dorp, C. W. Hagen, P. A. Crozier, and P Kruit, Nanotechnolgy **19**, 1 (2008), (http://dx.doi.org/10.1088/0957-4484/19/22/225305)

[80] Raith info No. 26, September 2005

[81] A. Fernández-Pacheco, L. Serrano-Ramón, J. M. Michalik, M. R. Ibarra, J. M. De Teresa, L. O'Brien, D. Petit, J. Lee, and & R. P. Cowburn, Scientific Reports **3**, 1492 (2013), (http://dx.doi.org/10.1038/srep01492)

[82] J. Kretz (private communication, 1998)

[83] C. R. K. Marrian, D. M. Tennant, J. Vac. Sci. Technol. **A 21**, S207 (2003), (http://dx.doi.org/10.1116/1.1600446)

[84] G. Moellenstedt and R. Speidel, Physik. Blaetter **16**, 192 (1960)

[85] http://www.amtc-dresden.com/content/index.php?xmlfile=overview.xml (15.12.2015)

[86] W. P. McCRAY, Nature Nanotechnology **2**, 259 (2007), (http://dx.doi.org/10.1038/nnano.2007.121)

[87] M. A. Herman, W. Richter, and H. Sitter, in *Epitaxy Physical Principles, and Technical Implementation* , Springer Series in Material Science, Springer Verlag Berlin, ISBN 3-540-67821-2

[88] C. W. Pearce, in *VLSI Technolgoy*, edited by S. M. Sze, 2nd edition, Mc- Graw-Hill book company - Elsevier Singapore, ISBN 0-07-100347-9 (1988), chapter 2 "epitaxy", 55

[89] D. Chrastina, S. Cecchi, J.P. hague, j. Frigerio, A. Samarelli, L. Ferre-Llin, D.J. Paul, E. Müller, T. Etzelstorfer, J. Stangl, and G. Isella, Thin Solid Films **543**, 153 (2013), (http://dx.doi.org/10.1016/j.tsf.2013.01.002)

[90] U. Valbusa, C. Boragno, and F. Buatier de Mongeot, Mat. Sci. Eng. C **23**, 201 (2003), (http://dx.doi.org/10.1016/S0928-4931(02)00268-0)

[91] D. Bimberg, M. Grundmann, N.N. Ledentsov, S.S. Ruvimov, P. Werner, U. Richter, J. Heydenreich, V.M. Ustinov , P.S. Kop'ev , and Zh. I. Alferov, Thin Solid Films **267**, 32 (1995), (http://dx.doi.org/10.1016/0040-6090(95)06597-0)

[92] D. Reuter, P. Kailuweit, A. D. Wieck, U. Zeitler, O. Wibbelhoff, C. Meier, A. Lorke, and J. C. Maan, Phys. Rev. Lett. **94**, 26808 (2005), (http://dx.doi.org/10.1103/PhysRevLett.94.026808)

[93] M. L. Frankenheim, Ann. Phys. **37**, 516 (1836), (http://dx.doi.org/10.1002/andp.18361130307)

[94] M. Ohirng, in *Materials Science of Thin Films: Deposition and Structure Account*, Academic Press San Diego, CA, USA, ISBN 978-0125249751 (2002), Chapter 3 "Thin-Film Evaporation Processes", 95

[95] I. N. Stranski, and L. Krastanow, Monatshefte für Chemie und verwandte Teile anderer Wissenschaften **71**, 351 (1937), (http://dx.doi.org/10.1007/BF01798103)

[96] H. Welker, Z. Naturforschg. **7a**, 744 (1952), (http://dx.doi.org/10.1515/zna-1952-1110)

[97] K. Brunner, Rep. Prog. Phys. **65**, 27 (2001), (http://dx.doi.org/10.1088/0034-4885/65/1/202)

[98] L. Esakit, and R. Tsu, IBM J. Res. Dev. **14**, 61 (1970), (http://dx.doi.org/10.1147/rd.141.0061)

[99] H. Kroemer, Proc. IEEE **51**, 1782 (1963)

[100] Zh. I. Alferov, CHEMPHYSCHEM **2**, 500 (2001), (http://dx.doi.org/10.1002/1439-7641(20010917)2:8/9%3c500::AID-CPHC500%3e3.0.CO;2-X)

[101] R. Dingle, H. L. Störmer, A. C. Gossard, and W. Wiegmann, Appl. Phys. Lett. **33**, 665 (1978), (http://dx.doi.org/10.1063/1.90457)

[102] A. D. Wieck, and D. Reuter, Comp. Semicond. **166**, 51 (2000)

[103] K. v. Klitzing, G. Dorda and M. Pepper, Phys. Rev. Lett. **45**, 494 (1980), (http://dx.doi.org/10.1103/PhysRevLett.45.494)

[104] D. C. Tsui, H. L. Stormer, and A. C. Gossard, Phys. Rev. Lett. **48**, 1559, (http://dx.doi.org/10.1103/PhysRevLett.48.1559)

[105] R. B. Laughlin, Phys. Rev. Lett. **50**, 1395 (1983). (http://dx.doi.org/10.1103/PhysRevLett.50.1395)

[106] L. Goldstein, F. Glas, J. Y. Marzin, M. N. Charasse, and G. Le Roux, Appl. Phys. Lett. **47**, 1099 (1985), (http://dx.doi.org/10.1063/1.96342)

[107] V. A. Shchukin, and D. Bimberg, Reviews of Modern Physics **71**, 1125 (1999), (http://dx.doi.org/10.1103/RevModPhys.71.1125)

[108] R. Hull, J.L. Gray, M. Kammler, T. Vandervelde , T. Kobayashi, P. Kumar, T. Pernell, J.C. Bean, J.A. Floro, and F.M. Ross, Mat. Sci. Eng. B 101, 1 (2003), (http://dx.doi.org/10.1016/S0921-5107(02)00680-3)

[109] G.B. Strinfellow, Rep. Prog. Phys. **45**, 469 (1982), (http://dx.doi.org/10.1088/0034-4885/45/5/001)

[110] Grzybowski 2009 – „Self-assembly: from crystals to cells", B. A. Grzybowski, C. E. Wilmer, J. Kim, K. P. Browne, and K. J. M. Bishop, Soft Mat. **5**, 1110 (2009), (http://dx.doi.org/10.1039/b819321p)

[111] R. Schott (private communication, 2013)

[112] K. Seshan (ed.), in *HANDBOOK OF THIN-FILM DEPOSITION PROCESSES AND TECHNIQUES Principles, Methods, Equipment and Applications*", 2nd edition, WILLIAM ANDREW PUBLISHING Norwich, USA, ISBN: 0-8155-1442-5 (2002)

[113] D. Reuter, A. D. Wieck, and A. Fischer, Rev. Sci. Instrum. **71**, 1125 (1999), (http://dx.doi.org/10.1103/RevModPhys.71.1125)

[114] U. Hillermann, in *Silizium Halbleitertechnologie*, Teubener, Wiesbaden, Germany, ISBN 3-519-30149-0 (2004), pp. 131

[115] M. Mühlberger, C. Schelling, G. Springholz, and F. Schäffler, Surface Science **532-535**, 721 (2003), (http://dx.doi.org/doi:10.1016/S0039-6028(03)00232-2)

[116] C. Schelling, M. Mühlberger, G. Springholz, and F. Schäffler, Physical Review B **64**, 041301 (R), (2001), (http://dx.doi.org/10.1103/PhysRevB.64.041301)

[117] N. Hrauda, J. J. Zhang, H. Groiss, T. Etzelstorfer, V. Holý, G. Bauer, C. Deiter, O. H. Seeck, and J. Stangl, Nanotechnology **24** (2013), 1, (http://dx.doi.org/10.1088/0957-4484/24/33/335707)

[118] T.O.Menteş, A.Locatelli, L.Aballe, M.A.Niño, E.Bauer, Ultramicroscopy **130**, 82 (2013), (http://dx.doi.org/10.1016/j.ultramic.2013.03.012)

[119] E. V. Shevchenko,D. V. Talapi, N. A. Kotov, S. O'Brien, and C. B. Murray, Nature **439**, 59 (2006), (http://dx.doi.org/10.1038/nature04414)

[120] P. Gambardella, and K. Kern, Surface Science Letters **475**, L229 (2001), (http://dx.doi.org/10.1016/S0039-6028(01)00696-3)

[121] S. Rohart, G. Baudot, V. Repain, Y. Girard, S. Rousset, H. Bulou, C. Goyhenex, and L. Proville, Surface Science **559**, 47 (2004), (http://dx.doi.org/10.1016/j.susc.2004.03.064)

[122] C. E. ViolBarbosa J. Fujii, G. Panaccione, and G. Rossi, New Journal of Physics **11**, 113046 (2009), (http://dx.doi.org/10.1088/1367-2630/11/11/113046)

[123] A. Greilich, D. R. Yakovlev, A. Shabaev, Al. L. Efros, I. A. Yugova, R. Oulton, V. Stavarache, D. Reuter, A. Wieck and M. Bayer, Science **313**, 341 (2006), (http://dx.doi.org/10.1126/science.1128215)

[124] W. Cheng, M. J. Campolongo, J. J. Cha, S. J. Tan, C. C. Umbach, D. A. Muller and D. Luo, Nature Mat. **8**, 519 (2009), (http://dx.doi.org/10.1038/NMAT2440)

[125] S. Facsko, T. Dekorsy, C. Koerdt, C. Trappe, H. Kurz, A. Vogt, and H. L. Hartnagel, Science **285**, 1551 (1999), (http://dx.doi.org/10.1126/science.285.5433.1551)

[126] J. Huang, F. Kim, A. R. Tao, S. Connor, and P. Yang, Nature Mat. **4**, 896 (2005), (http://dx.doi.org/10.1038/nmat1517)

[127] S. C. Glotzer, and M. J. Solomon, Nature Mat. **6**, 557 (2007), (http://dx.doi.org/10.1038/nmat1949)

[128] W.-Q. Wu, B.-X. Lei, H.-S. Rao, Y.-F. Xu, Y.-F. Wang, C.-Y. Su, and D.-B. Kuang, Sc. Rep. **3**, 1 (2013), (http://dx.doi.org/10.1038/srep01352)

[129] J. Kretz, PhD thesis, TU Dresden, Dresden, Germany (2001), GCA Verlag, Herdecke, Germany (2001), ISBN 3-89863-038-2

[130] U. Staufer, in *Scanning Tunneling Microscopy II*, 2nd edition, edited by R. Wiesendanger, and H.-G. Güntherodt, Springer Berlin Germany ISBN 978-3540585893 (1995), Chapter 8 Surface modifications with a Scanning Proximity Probe Microscope, 273

[131] X. N. Xie, and H. J. CHUNG, in *Selected Topics in Nanoscience and Nanotechnology*, edited by. A. T. S. Wee, World Scientific Publishing Co. Pte. Ltd., Singapore, ISBN 978-981-283-955-8 (2009), chapter 1 „ *Scanning Probe Microscopy Based Nanoscale Patterning and Fabrication* “,

[132] http://www.azom.com/article.aspx?ArticleID=3249 (15.12.2015)

[133] R. Young, J. Ward, and F. Scire, Rev. Sci. Instrum. **43**, 999 (1972), (http://dx.doi.org/10.1063/1.1685846)

[134] G. Binnig, H. Rohrer, C. Gerber, and E. Weibel, Phys. Rev. Lett. **49**, 57 (1982), (http://dx.doi.org/10.1103/PhysRevLett.49.57)

[135] G. Binnig and C. F. Quate, Phys. Rev. Lett. **56**, 930 (1986), (http://dx.doi.org/10.1103/PhysRevLett.56.930)

[136] K. Ivanova, Y. Sarov, T. Ivanov, A. Frank, J. Zöllner, C. Bitterlich, U. Wenzel, B. E. Volland, S. Klett, I. W. Rangelow, P. Zawierucha, M. Zielony, T. Gotszalk, D. Dontzov, W. Schott, N. Nikolov, M. Zier, B. Schmidt, W. Engl, T. Sulzbach, and I. Kostic, J. Vac. Sci. Technol. B **26**, 2367 (2008), (http://dx.doi.org/10.1116/1.2990789)

[137] A. Foster, and W. Hofer (ed.), in *Scanning Probe Microscopy Atomic Scale Engineering by Forces and Currents*, Springer NY, NY, USA, ISBN 0-387-40090-7 (2006)

[138] F. J. Giessibl, Science **267**, 68 (1995) (http://dx.doi.org/10.1126/science.267.5194.68)

[139] N. W. Ashcroft, and N. D. Mermin, in *Solid state physics*, New York, ISBN 0-03-083993-9 (1976), chapter 20 Cohesive Energy, pp. 395

[140] A.A. Tseng, S.D. Sartale, M.F. Luo, and C.C. Kuo, in *Nanofabrication*, edited by A. A. Tseng, World Scientific Publishing Co. Pte. Ltd., Singapore ISBN 981-270-076-5 (2008), Chapter 1, pp.1-32

[141] N. Kawasegi, D.W. Lee, N. Morita, and J.W. Park, in *Nanofabrication*, edited by A. A. Tseng, World Scientific Publishing Co. Pte. Ltd., Singapore ISBN 981-270-076-5 (2008), Chapter 2, pp.33-64

[142] C. Santschi, J. Polesel-Maris, J. Brugger, and H. Heinzelmann, in *Nanofabrication*, edited by A. A. Tseng, World Scientific Publishing Co. Pte. Ltd., Singapore ISBN 981-270-076-5 (2008), Chapter 3, pp.65-126

[143] E. E. Moon and H. I. Smith, J. Vac. Sci. Technol. B **24**, 3083 (2006), (http://dx.doi.org/10.1116/1.2393294)

[144] M. Kaestner, and I. W. Rangelow, J. Vac. Sci. Technol. B **29**, 06FD02-1 (2011), (http://dx.doi.org/10.1116/1.3662092)

[145] E. E. Moon, J. Kupec, M. K. Mondol, H. I. Smith, and K. K. Berggren, J. Vac. Sci. Technol. B **25**, 2284 (2007), (http://dx.doi.org/10.1116/1.2787794)

[146] K. Wilder, C. F. Quate, B. Singh, and D. F. Kyser, J. Vac. Sci. Technol. B 16, 3864 [1998], (http://dx.doi.org/10.1116/1.590425)

[147] M. Fuechsle, J. A. Miwa, S. Mahapatra, H. Ryu, S. Lee, O. Warschkow, L. C. L. Hollenberg, G. Klimeck, and M. Y. Simmons, Nature Nanotechnology **5**, 502 (2012), (http://dx.doi.org/10.1038/nnano.2012.21)

[148] J. W. Lyding, T.C. Shen, J. S. Hubacek, J. R. Tucker, and G. C. Abeln, Appl. Phys. Lett. **64**, 2010 (1994), (http://dx.doi.org/10.1063/1.111722)

[149] I.-W. Lyo, and P. Avouris, Science **253**, 173 (1991), (http://dx.doi.org/10.1126/science.253.5016.173)

[150] S. R. Schofield, N. J. Curson, M.Y. Simmons, F. J. Rueß, T. Hallam, L. Oberbeck, and R.G. Clark, Phys. Rev. Lett. **91**, 136104-1 (2003), (http://dx.doi.org/10.1103/PhysRevLett.91.136104)

[151] M. Fuechsle, S. Mahapatra, F. A. Zwanenburg, M. Friesen, M. A. Eriksson, and M. Y. Simmons, Nature nanotechlnolgy **5**, 502 (2010), (http://dx.doi.org/10.1038/nnano.2010.95

[152] D.M. Eigler and E.K. Schweizer, Nature **344**, 524 (1990), (http://dx.doi.org/10.1038/344524a0)

[153] S. W. Hla, K.-F. Braun and K.-H. Rieder, Phys. Rev. B 67, 201402(R) (2003), (http://dx.doi.org/10.1103/PhysRevB.67.201402)

[154] L. Bartels, G. Meyer, and K.-H. Rieder, Phys. Rev. Lett. **79**, 697 (1997), (http://dx.doi.org/10.1103/PhysRevLett.79.697)

[155] A.J. Heinrich, C.P. Lutz, J.A. Gupta, and D.M. Eigler, Science **298**, 1381 (2002), (http://dx.doi.org/10.1126/science.1101077)

[156] Z. Durrani, M. Kaestner, M. Hofer, T. Ivanov, and I. Rangelow, SPIE (2013), http://spie.org/x92224.xml

[157] I.-W. Lyo, and P. Avouris, Science **253**, 173 (1991) (http://dx.doi.org/10.1126/science.253.5016.173)

[158] T. A. Jung, R. R. Schlittler, J. K. Gimzewski, H. Tang, and C. Joachim, Science **271**, 181 (1996), (http://dx.doi.org/10.1126/science.271.5246.181)

[159] H. T. Soh, K. Wilder Guarini, C. F. Quate, in *Scanning Probe Lithography*, Kluwer Academic Publishers, Norwell Mass., USA, ISBN 0-7923-7361-8 (2001)

[160] S. Rusponi, G. Costantini, F. Buatier de Mongeot, C. Boragno, and U. Valbusa, Appl. Phys. Lett. **75**, 3318 (1999), (http://dx.doi.org/10.1063/1.125337)

[161] P. Vettiger, G. Cross, M. Despont, U. Drechsler, U. Dürig, B. Gotsmann, W. Häberle, M. A. Lantz, H. E. Rothuizen, R. Stutz, and G. K. Binnig, IEEE Transact. Nanotechnol. **1**, 39 (2002), (http://dx.doi.org/10.1109/TNANO.2002.1005425)

[162] Piner 1999 – „"Dip pen" Nanolithography", R. D. Piner, J. Zhu, F. Xu, S. Hong, and C. A. Mirkin, Science **283**, 661 (1999), (http://dx.doi.org/10.1126/science.283.5402.661)

[163] http://www.zyvexlabs.com/Products/STMLithoControlSystem.html (30.11.2015)

[164] http://www.swisslitho.com/index.php/en/company/references (30.11.2015)

[165] M. D. Giles, in *VLSI Technology*, edited by S.M. Sze, 2nd ed., McGraw-Hill Book Company Singapore ISBN 0-07-100347-9 (1988), pp. 327

[166] P.D. Townsend, J.C. Kelly, and N.E.W. Hartley, in *Ion Implantation, Sputtering and their applications*, Academic press, London, GB, ISBN 0-12-696950-7 (1976)

[167] F. A. Stevie, L.A. Giannuzzi, and B.I. Prenitzer, in *Introduction to Focused Ion Beams*, edited by L.A. Giannuzzi and F.A. Stevie, Springer, NY, USA, ISBN 0-387-23116-1 (2005), Chap. 1, pp. 1-12

[168] N. Yao, in *Introduction to Focused Ion Beams*, edited by L.A. Giannuzzi and F.A. Stevie, Springer, NY, USA, ISBN 0-387-23116-1 (2005), Chap. 1, pp. 1-30

[169] T. Fujii, T.Asahata, and T. Kaito, in *Introduction to Focused Ion Beams*, edited by L.A. Giannuzzi and F.A. Stevie, Springer, NY, USA, ISBN 0-387-23116-1 (2005), Chap. 14, pp. 355-390

[170] R. M. Langford, S. O'Reilly, and I. J. McEwen, Richard, MRS Proc. **739**, H7.2 (2003), (http://dx.doi.org/10.1557/PROC-739-H7.2)

[171] J. Mayer, L. A. Giannuzzi, T. Kamino, and J. Michael, "TEM Sample Preparation and FIB-Induced Damage", MRS bulletin **32**, 400 (2007), (http://dx.doi.org/10.1557/mrs2007.63)

[172] J.J. Van Es, J. Gierak, R.G. Forbes, V.G. Suvorov, T. Van den Berghe, Ph. Dubuisson, I. Monnet, A. Septier, Elsevier, Microelectronic Engineering **73-74**, 132 (2004), (http://dx.doi.org/10.1016/j.mee.2004.02.029)

[173] B. W. Ward, J. A. Notte, and N. P. Economou, J. Vac. Sci. Technol. B **24**, 2871 (2006), (http://dx.doi.org/10.1116/1.2357967)

[174] N. S. Smith, D. E. Kinion, P. P. Tesch, and R. W. Boswell, Microsc. Microanal. **13**, 180 (2007), (http://dx.doi.org/10.1017/S1431927607075605)

[175] „Nanoscale to Millimeter Scale Milling with a Focused Ion Beam Instrument", P. Tesch, N. Smith, N. Martin, and N. Kinion, EIPBN conference poster (2008), http://www.oregon-physics.com/pdf/EIPBN2008poster.pdf (05.01.2016)

[176] T. Shinada, H. Koyama, C. Hinoshita, K. Imamura, and I. Ohdomarj, Jpn. J. Appl. Phys **41** (3A), L287 (2002), (http://dx.doi.org/10.1143/JJAP.41.L287)

[177] T. Shinada, S. Okamoto, T. Kobayashi, and I. Ohdomari, Nature **437**, 1128 (2005), (http://dx.doi.org/10.1038/nature04086)

[178] S. Tongay, M. Lemaitre, J. Fridmann, A. F. Hebard, B. P. Gila, and B. R. Appleton, Applied Physics Letters **100**, 73501 (2012), (http://dx.doi.org/10.1063/1.3682479)

[179] M. G. Lemaitre, S. Tongay, X. Wang, D. K. Venkatachalam, J. Fridmann, B. P. Gila, A. F. Hebard , F. Ren, R. G. Elliman, and B. R. Appleton, Appl. Phys. Lett. **100**, 193105 (2012), (http://dx.doi.org/10.1063/1.4707383)

[180] T. Hiramoto, K. Hirakawa, and T. Ikoma, J. Vac. Sci. Technol. B **6**, 1014 (1988), (http://dx.doi.org/10.1116/1.584338)

[181] B. Schmidt, L. Bischoff, and J. Teichert, Sensors and Acturators A **61**, 369 (1997), (http://dx.doi.org/10.1016/S0924-4247(97)80291-9)

[182] H. Loeschner, G. Stengl, R. Kaesmaier, and A. Wolter, J. Vac. Sci. Technol. B **19**, 2520 (2001), (http://dx.doi.org/10.1116/1.1421562)

[183] M. A. Hartney, D.C. Shaver, M. I. Shepard, J. Melngailis, V. Medevdev, and W. P. Robinson, J. Vac. Sci. B **9**, 3432 (1991), (http://dx.doi.org/10.1116/1.585817)

[184] J. Gierak, D. Mailly, P. Hawkes, R. Jede, L. Bruchhaus, P. Mélinon, A. Perez, R. Hyndman, J.-P. Jamet, J. Ferre, A. Mougin, C. Chappert, V. Mathet, P. Warin, and J. Chapman, Appl. Phys. A **80**, 187 (2005), (http://dx.doi.org/10.1007/s00339-004-2551-z)

[185] E. W. Müller, Adv. Electron. Phys. **13**, 83 (1960)

[186] I.W. Drummond, J.V.P. Long, Nature **215**, 950 (1967), (http://dx.doi.org/10.1038/215950a0)

[187] R.L. Seliger, R.L. Kubena, R.D. Olney, J.W. Ward, V. Wang, J. Vac. Sci. Technol. **16**, 1610 (1979), (http://dx.doi.org/10.1116/1.570253)

[188] R.G. Wilson and G. R. Brewer, in *ION BEAMS With applications to Ion Implantantion*, Robert E. Krieger Publishing Compnay, Huntington, New York, USA, ISBN 0-88275-899-3 (1979)

[189] R. L. Seliger, J. W. Ward, V. Wang, and R. L. Kubena, Appl. Phys. Lett. **34**, 310 (1978)

[190] W.H. Escovitz, T.R. Fox, and R. Levi-Setti, Proc. Nat. Acad. Sci. **72**, 1826 (1975)

[191] K. Kanaya, H. Kawakatsu, S. Matsui, H,Yomazaki, I. Okazaki, and K. Tanaka, *in Proceedings of the ELBS*, edited by A.B. El-Kareh, 489 (1965)

[192] M. Gabby, R. Goute, C. Guilland, and C. Monllor, Comptes rendus de l'Académie des sciences **261**, 3325 (1965)

[193] R. Forbes, in *Handbook of Charged Particle Optics*, edited by. J. Orloff, 2nd edition, CRC Press, Boca Raton, USA, ISBN 1-4200-4554-7 (2009), Chap. 2 “LMIS”, pp. 29

[194] P.D. Prewett and G.L.R. Mair, in *Focused ion beams from liquid metal ion sources*, No.1 Electronic & electrical engineering research studies, Microengeneering series, Series, edited by P.S. Walsh, Research studies press Ltd. Taunton, Somerset GB, ISBN 978-0471930884 (1991)

[195] L. Bischoff, P. Mazarov, L. Bruchhaus, Appl. Phys. Rev. **3**, 021101 (2016), (http://dx.doi.org/10.1063/1.4947095)

[196] R. Clampitt, and D.K. Jeffries, Nucl. Instrum. Methods **149**, 739 (1978), (http://dx.doi.org/10.1016/0029-554X(78)90961-8)

[197] J. Melngailis, J. Vac. Sci. Technol. B **5**, 469 (1987), (http://dx.doi.org/10.1116/1.583937)

[198] Y. Ochiai, Y. Kojima, and S. Matsui, J. Vac. Sci. Technol. B **6**, 1055 (1988), (http://dx.doi.org/10.1116/1.584297)

[199] R. L. Kubena, and J. W. Ward, Appl. Phys. Lett. **51**, 1960 (1987), (http://dx.doi.org/10.1063/1.98313)

[200] P. H. LaMarche, R. Levi-Setti and Y. L. Wang, J. Vac. Sci. Technol. B **1**, 1056 (1983), (http://dx.doi.org/10.1116/1.582675)

[201] L. Bischoff, B. Schmidt, H. Lange, and D. Donzev, Nucl. Instr. Meth. B **267**, 1372 (2009), (http://dx.doi.org/10.1016/j.nimb.2009.01.047)

[202] R.L. Seliger and W.P. Flemming, J. Vac. Sci. Technol. **10**, 1127 (1973), (http://dx.doi.org/10.1116/1.1318486)

[203] R.L. Seliger and W.P. Fleming, J. Appl. Phys. **45**, 1416 (1974), (http://dx.doi.org/10.1063/1.1663422)

[204] J.H. Orloff and L.W. Swanson, J. Vac. Sci. Technol. **12**, 1209 (1975), (http://dx.doi.org/10.1116/1.568497)

[205] R.L. Kubena, J.W. Ward, F.P. Stratton, R.J. Joyce, G.M. Atkinson, J. Vac.Sci. Technol. B **9**, 3079 (1991), http://dx.doi.org/10.1116/1.585373)

[206] H. Ryssel, K. Haberger, and H. Kranz, J. Vac. Sci. Technol. **19**, 1358 (1981), (http://dx.doi.org/10.1116/1.571210)

[207] S. Matsui, K. Mori, K. Saigo, T. Shiokawa, K. Toyoda, and S. Namba, J. Vac. Sci. Technol. B, **4**, 845 (1986), (http://dx.doi.org/10.1116/1.583524)

[208] L. Bruchhaus, S. Bauerdick, L. Peto, U. Barth, A. Rudzinski, J. Mussmann, J. Gierak, and H. Hövel, Microelectronic Engineering 97 (2012), pp. 48,(http://dx.doi.org/10.1016/j.mee.2012.04.033)

[209] J. Melngailis, Nucl. Instrum. and Methods in Phys. Research B **80/81**, 1271 (1993), http://dx.doi.org/10.1016/0168-583X(93)90781-Z)

[210] S. Rejntjens, and R. Puers, Micromech. Microeng. **11**, 287 (2001), (http://dx.doi.org/10.1088/0960-1317/11/4/301)

[211] C. Lehrer, L. Frey, S. Petersen, H. Ryssel, M. Schäfer, and T. Sulzbach, J. Vac. Sci. Technol. B **22**, 1402 (2004), (http://dx.doi.org/10.1116/1.1689310)

[212] N.S. Smith, P.P. Tesch, N.P. Martin, and R.W. Boswell, Microscopy Today **17**, 18 (2009), (http://dx.doi.org/10.1017/S1551929509000315)

[213] W. J. MoberlyChan, D. P. Adams, M.J. Aziz, G. Hobler, and T. Schenkel, MRS bulletin **32**, 424 (2007), (http://dx.doi.org/10.1557/mrs2007.66)

[214] R. Forbes, in *Handbook of Charged Particle Optics*, edited by. J. Orloff, 2nd edition, CRC Press, Boca Raton, USA, ISBN 1-4200-4554-7 (2009), Chap. 3" GFIS", pp. 87-128

[215] N. S. Smith , J. A. Notte , and A. V. Steele , MRS bulletin **39**, 329 (2014), (http://dx.doi.org/10.1557/mrs.2014.53)

[216] G. Hlawacek, V. Veligura, R. v. Gastel, and B. Poelsema, J. Vac, Sci. Technol. B **32**, 020801 (2014), (http://dx.doi.org/10.1116/1.4863676)

[217] http://oregon-physics.com/products/high_brightness_specifications.html, 19.03.2015

[218] N. S. Smith, W. P. Skoczylas, S. M. Kellogg, D. E. Kinion, P. P. Tesch, O. Sutherland, A. Aanesland, and R. W. Boswell, J. Vac. Sci. Technol. B **24**, 2902 (2006), (http://dx.doi.org/10.1116/1.2366617)

[219] N.S. Smith, P.P. Tesch, N.P. Martin, and R.W. Boswell, Microscopy Today **15**, 18 (2009), (http://dx.doi.org/10.1017/S1551929509000315)

[220] J. Gierak, Nanofabrication **1**, 35 (2014), (http://dx.doi.org/10.2478/nanofab-2014-0004)

[221] A. Joshi-Imre, and S. Bauerdick, Journal of Nanotechnology, **Article ID 170415**, (2014) http://dx.doi.org/10.1155/2014/170415

[222] Raith ionLiNE 2015 - http://www.raith.de/products/ionline.html (22.05.2015)

[223] http://www.ruhr-uni-bochum.de/afp/downloads/ausstattung/ionen.pdf (22.05.2015)

[224] A. B. Tolstogouzov, S. F. Belykh, V. S. Gurov, A. A. Lozovan, A. I. Taganov, O. M. N. D. Teodoro, A. A. Trubitsyn, and S. P. Chenakin, Instruments and Experimental Techniques **58**, 1 (2015), (http://link.springer.com/article/10.1134/S002044121501011X)

[225] B. Knuffman, A. V. Steele, J. Orloff and J. J. McClelland, Nanoscale focused ion beam from laser-cooled lithium atoms, New Journal of Physics **13**, 103035 (2011), (http://dx.doi.org/10.1088/1367-2630/13/10/103035)

[226] A. Delobbe, O. Salord, P. Sudraud, The ECR–FIB, The European Focused Ion Beam Users Group (EFUG) annual meeting 2011, http://www.imec.be/efug/EFUG2011_08_Delobbe.pdf

[227] R. Kelley, K. Song, B. Van Leer, D. Wall, and L. Kwakman, Microsc. Microanal. **19**, 862 (2013), (http://dx.doi.org/10.1017/S1431927613006302)

[228] M. Nastasi, J.W. Mayer, and J.K. Hirvonen, in *Ion-solid interactions: Fundamentals and applications*, Cambridge University Press, GB, ISBN 0521 37376 X (1996)

[229] N. Imanishi, in *Focused ion beam systems*, edited by N. Yao, Cambridge University Press, ISBN 978-0521-83199-4 (2007), Chap. 2, pp. 31

[230] L.A. Giannuzzi, B.I. Prenitzer, and B.W. Kempshall, in *Introduction to Focused Ion Beams*, edited by L.A. Giannuzzi and F.A. Stevie, Springer, NY, USA, ISBN 0-387-23116-1 (2005), Chap. 2, pp. 13

[231] S. Tan, R. Livengood, and D. Shima, JVST B **28**, C6F15, (2010), (http://dx.doi.org/10.1116/1.3511509)

[232] S. Bauerdick, L. Bruchhaus, P. Mazarov, A. Nadzeyka, R. Jede, J. Fridmann, J. E. Sanabia, B. Gila and B. R. Appleton, J. Vac. Sci. Technol. **31**, 06F404-1 (2013), (http://dx.doi.org/10.1116/1.4824327)

[233] V.N. Tondare, J. Vac. Sci. Technol. A **23**, 1498 (2005), (http://dx.doi.org/10.1116/1.2101792)

[234] A. V. Steele, B. Knuffmann, J.J. McClelland, and J. Orloff, J. Vac. Sci. Technol. B **28**, C6F1 (2010), (http://dx.doi.org/10.1116/1.3502668)

[235] C. Perez-Martinez, S. Guilet, N. Gogneau, and Pascale Jegou, J. Gierak and P. Lozano, J. Vac. Sci. Technol. B **28**, L25 (2010), (http://dx.doi.org/10.1116/1.3432125)

[236] C. Perez-Martinez, S. Guilet, J. Gierak, P. Lozano, Microelec. Eng. **88**, 2088 (2011), (http://dx.doi.org/10.1016/j.mee.2010.11.042)

[237] S. Guilet, C. Perez-Martinez, P. Jegou, P. Lozano, J.Gierak, Microelec. Eng. **88**, 1968 (2011), (http://dx.doi.org/10.1016/j.mee.2010.12.037)

[238] V. Sidorkin, E. Veldhoven, E. Drift, P. Alkemade, H. Salemink, and D. Maas, J. Vac. Sci. Technol. B 27, L18 (2009), (http://dx.doi.org/10.1116/1.3182742)

[239] D. Winston, B.M. Cord, B. Ming, D.C. Bell, W.F. DiNatale, L.A. Stern, A.E. Vladar, M.T. Postek, M.K. Mondol, J.K.W. Yang, and K.K. Breggren. J. Vac. Sci. Technol. B **27**, 2702 (2009), (http://dx.doi.org/10.1116/1.3250204)

[240] A. R. Hall, Microscopy Today **20**, 24 (2012), (http://dx.doi.org/10.1017/S1551929512000703)

[241] http://applications.zeiss.com/C125792900358A3F/0/229D77787096B7BCC1257B91003F83C5/$FILE/DE_42_011_015_ORION_NanoFab.pdf (30.11.2015)

[242] A. Delobbe, O. Salord, P. Sudraud, The ECR–FIB, The European Focused Ion Beam Users Group (EFUG) annual meeting 2011, http://www.imec.be/efug/EFUG2011_08_Delobbe.pdf

[243] P. Kruit and. G. H. Jansen, in *Handbook of Charged Particle Optics*, edited by. J. Orloff, 2nd edition, CRC Press, Boca Raton, USA, ISBN 1-4200-4554-7 (2009), Chap. 7, 341

[244] G.L.R. Mair, D.C. Grindrod, M.S. Mousa, and R.V. Latham, J. Phys. D. **16**, L209 (1983), (http://dx.doi.org/10.1088/0022-3727/16/10/006)

[245] J. Gierak, E.Bourhis, G.Faini, G.Patriarche, A.Madouri, R.Jede, L.Bruchhaus, S.Bauerdick, B. Schiedt, A.L.Biance, and L.Auvray, Ultramicroscopy **109**, 457 (2009), (http://dx.doi.org/10.1016/j.ultramic.2008.09.007)

[246] R. Livengood, S. Tana, P. Hacka, M. Kanea, and Y. Greenzweig, Microscopy and Microanalysis **17**, 672 (2011), (http://dx.doi.org/10.1017/S1431927611004235)

[247] MRS bulletin **39**, (2014) (Focused Ion Beam Technology and Applications)

[248] EC growth project Contract No. G5RD-CT2000-0034

[249] J. Gierak, A. Madouri, A.L. Biance, E. Bourhis, G. Patriarche, C. Ulysse, D. Lucot, X. Lafosse, L. Auvray, L. Bruchhaus, and R. Jede, Microelec. Eng. **84**, 779 (2007), (http://dx.doi.org/10.1016/j.mee.2007.01.059)

[250] B. R. Appleton, S. Tongay, M. Lemaitre, B. Gila, J. Fridmann, P. Mazarov, J. E. Sanabia, S. Bauerdick, L. Bruchhaus, R. Mimura, R. Jede, Nucl. Instr. and Meth. B **272**, 153 (2012), (http://dx.doi.org/10.1016/j.nimb.2011.01.054)

[251] A.A. Tseng, in *Focused ion beam systems*, edited by N. Yao, Cambridge University Press, ISBN 978-0521-83199-4 (2007), Chap. 7, pp. 187

[252] G. Hakvoort and C.M. Hol, Journal of Thermal Analysis **52**, 195 (202)

[253] J.C. Beckman, T.H.P. Chang, A. Wagner, and R.F.W. Pease, J. Vac. Sci. Technol. B **15**, 2332 (1997), (http://dx.doi.org/10.1116/1.589640)

[254] J. Orloff, J.-L. Li, M. Sato, J. Vac. Sci. Technol. B **9**, 2609 (1991), (http://dx.doi.org/10.1116/1.585701)

[255] A. Benninghoven, R.D. Rüdenauer, and H.W. Werner, in *Secondary ion mass spectroscopy*, J. Wiley and Sons, New York, USA, ISBN 0-471-01056-1 (1987)

[256] J.F.Ziegler, J.P. Biersack, and M.D. Ziegler, SRIM, (12/15/2008 / v05, www.LuLu.com (on demand internet publisher), ISBN 0-9654207-1X (2008)

[257] SRIM 2008 - SRIM software, "The stopping and range of ions in matter", J.F. Ziegler, M.D. Ziegler, J.P. Biersack, Chester, MD, USA, http://www.srim.org.com

[258] F. Watt, A. A. Bettiol, J. A. van Kan, E.J. Teo, and M.B. Breese, Int. J. Nanoscience **4**, 269 (2005), (http://dx.doi.org/10.1142/S0219581X05003139)

[259] Ocola 2014 - L. E. Ocola, C. Rue, and D. Maas, MRS bulletin **39**, 336 (2014), (http://dx.doi.org/10.1557/mrs.2014.56)

[260] O. Bobes, K. Zhang, and H. Hofsäss, Phys. Rev. B **86**, 235414 (2012), (http://dx.doi.org/10.1103/PhysRevB.86.235414)

[261] S. Facsko, T. Bobek, H. Kurz, T. Dekorsy, S. Kyrsta, and R. Cremer, Applied Physics Letters **80**, 130 (2002), (http://dx.doi.org/10.1063/1.1429750)

[262] J. Orloff, M. Utlaut, and L. Swanson, in *High resolution focused ion beams*, Kluwer Academic Plenum Publishers, New York, USA, ISBN 0-306-47350-X (2003)

[263] M. Utlaut, in *Handbook of Charged Particle Optics*, edited by. J. Orloff, 2nd edition, CRC Press, Boca Raton, USA, ISBN 1-4200-4554-7 (2009), Chap. 11, pp. 523

[264] B. Basnar, A. Lugstein, H. Wanzenboeck, H. Langfischer, E. Bertagnolli, and E. Gornik, J. Vac. Sci. Technol. B **21**, 927 (2003), (http://dx.doi.org/10.1116/1.1565345)

[265] E. Abbe, „Beiträge zur Theorie des Mikroskops und der Mikroskopischen Wahrnehmung“, Archiv für mikroskopische Anatomie **9**, 456 (1873), article starts at p. 413, (http://dx.doi.org/10.1007/BF02956173)

[266] J.E. Barth, and P. Kruit, Optik **101**, 101 (1996)

[267] P. Grivet, P. W. Hawkes and A. Septier (ed.), in *Electron Optics: Part 1 Optics*, 2nd edition, English Edition, Pergamon Press, Oxford GB, (1972)

[268] P. W. Hawkes and E. Kasper, in *Principles of electron optics: Volume 2*, Academic press, London, GB, ISBN 0-12-333352-0 (1989)

[269] J. Großer, in *Einführung in die Teilchenoptik*, Teubener Studienbücher, B.G. Steubener, Stuttgart, Germany, ISBN 3-519-03050-0 (1983)

[270] J. Orloff, (private communication, via email 23.03.2016)

[271] J. Gierak , R. Jede and P. Hawkes, Nanofabrication Handbook, Edited by Stefano Cabrini and Satoshi Kawata, CRC Press 2012, pp 41–84

[272] http://www.ilp.physik.uni-essen.de/wucher/movies/movies.html (15.12.2015)

[273] Rudenauer 1981 - F.G. Rudenauer, and W. Steiger, Microchemika Akta **76**, 375 (1981), (http://dx.doi.org/10.1007/BF01196959)

[274] Z. Malamud, Y. Greenzweig, and A. Raveh, Microscopy and Microanalysis, **21**, 90 (2015) , (http://dx.doi.org/10.1017/S1431927615013197)

[275] Shinada 1998 - T. Shinada, Y. Kumura, J. Okabe, T. Matsukawa, and I. Ohdomari, J. Vac. Sci. Technol. B **16**, 2489 (1998), (http://dx.doi.org/10.1116/1.590196)

[276] A.-L. Biance, J. Gierak, E. Bourhis, A. Madouri, X. Lafosse, G. Patriarche, G. Oukhaled, C. Ulysse, J.-C.Galas, Y.Chen, L. Auvray, Microelec. Eng. **83**, 1474 (2006), (http://dx.doi.org/10.1016/j.mee.2006.01.133)

[277] B. Schiedt, L. Auvray, L. Bacri, G. Oukhaled, A. Madouri, E. Bourhis, G. Patriarche, J. Pelta, R. Jede, and J. Gierak, Microelec. Eng. **87**, 1300 (2010), (http://dx.doi.org/10.1016/j.mee.2009.12.073)

[278] G. Oukhaled, L. Bacri, E. Bourhis, B. Schiedt, A. Madouri, G. Patriarche, R. Jede, JM. Betton, P. Guegan, L. Auvray, J. Pelta, and J. Gierak, MRS Proceedings **1253**, (2010), (http://dx.doi.org/10.1557/PROC-1253-K10-33)

[279] A.N. Boers, A.C.F. Hoole, and J.M. Ryan, Microelectron. Eng. 32, 131 (1996), (http://dx.doi.org/10.1016/0167-9317(95)00368-1)

[280] C. Dekker, Nature Nanotechnolgy **2**, 209 (2007), (http://dx.doi.org/10.1038/nnano.2007.27)

[281] J. Li, D.Stein, C. McMullan, D. Branton, M. Aziz, and J.A. Golovchenko, Nature **412**, 166 (2001), (http://dx.doi.org/10.1038/35084037)

[282] T. Schenkel, V. Radmilovic, E.A. Stach, S.-J. Park, and A. Persaud, J. Vac. Sci. Technol. B **21**, 2720 (2003), (http://dx.doi.org/10.1116/1.1622935)

[283] K. Healy, B. Schiedt, and A. P. Morrison, Nanomedicine **2**, 875 (2007) , (http://dx.doi.org/10.2217/17435889.2.6.875)

[284] J-P. Adam, J-P. Jamet, J Ferré, A. Mougin, S. Rohart, R. Weil, E. Bourhis and J. Gierak, Nanotechnology **21**, 1 (2010), (http://dx.doi.org/10.1088/0957-4484/21/44/445302)

[285] Rettner 2001 - C. T. Rettner, M. E. Best, and B. D. Terris, IEEE Trans. Mg. **37**, 1649 (2001), (http://dx.doi.org/10.1109/20.950927)

[286] S. Y. Chou, M. S. Wei, P.R. Krauss, and P.B. Fischer, J. App. Phys. **76**, 6673 (1994), (http://dx.doi.org/10.1063/1.358164)

[287] S. Sun, C.B. Murray, D. Weller, L. Folks, A. Moser, Science **287**, 1989 (2000), (http://dx.doi.org/10.1126/science.287.5460.1989)

[288] R. Hyndman, A. Mougin, L.C. Sampaio, J. Ferre, J.P.Jamet, P. Meyer, V. Mathet, C. Chappert, D. Mailly, J. Gierak, J. Magnetism Magnetic Materials **240**, 34 (2002), (http://dx.doi.org/10.1016/S0304-8853(01)00721-1)

[289] W. Sparreboom, A. van den Ber, and J. C. T. Eijkel, Nature Nanotechnolgy **4**, 713 (2009), (http://dx.doi.org/10.1038/nnano.2009.332)

[290] L. E. Ocola, and E. Palacios, J. Vac. Sci. Technol. B **31**, 06F401 (2013), (http://dx.doi.org/10.1116/1.4819302)

[291] E. Palacios, L. E. Ocola, A. Joshi-Imre, S. Bauerdick, M. Berse, and L. Peto, J. Vac. Sci. Technol. B **28**, C6I1 (2010), (http://dx.doi.org/10.1116/1.3505128)

[292] A. Siria, P. Poncharal, A.-L. Biance, R. Fulcrand, and X. Blasé, Nature **494**, 455 (2013), (http://dx.doi.org/10.1038/nature11876)

[293] L. Mo, L. Yang ,A. Nadzeyka, S. Bauerdick, and S. He, Optics Express **22**, 32233 (2014), (http://dx.doi.org/10.1364/OE.22.032233)

[294] H. Kollmann, X. Piao, M. Esmann, S. F. Becker,D. Hou,C. Huynh, L.-O. Kautschor, G. Bösker, H. Vieker, A. Beyer, A. Gölzhäuser, N. Park, R. Vogelgesang, M. Silies, and C. Lienau, Nano Letters **14**, 4778 (2014), (http://dx.doi.org/10.1021/nl5019589)

[295] J. Lohau, A. Moser, C. T. Rettner, M. E. Best, and B. D. Terris, Appl. Phys. Lett. **78**, 990 (2001), (http://dx.doi.org/10.1063/1.1347390)

[296] http://www.zeiss.de/microscopy/de_de/produkte/fib-sem-instruments/crossbeam.html#highlights (14.03.2016)

[297] L. Zhang, N. F. Heinig, S. Bazargan, M. Abd-Ellah, N. Moghimi and K. T. Leung, Nanotechnology **26**, 1 (2015), (http://dx.doi.org/10.1088/0957-4484/26/25/255303)

[298] K. Arshak, M. Mihov, S. Nakahara, A. Arshak, D. McDonagh, J. Vac. Sci. Technol. B **22**, 189 (2004), (http://dx.doi.org/10.1116/1.1641058)

[299] M. A. Hartney, D.C. Shaver, M. I. Shepard, J. Melngailis, V. Medevdev, and W. P. Robinson, J. Vac. Sci. Technol. B **9**, 3432 (1991), (http://dx.doi.org/10.1116/1.585817)

[300] J. Gierak, E. Cambril, M. Schneider, C. David, D. Mailly, J. Flicstein, G. Schmid, J. Vac. Sci. Technol. B **17**, 3132 (1999), (http://dx.doi.org/10.1116/1.590967)

[301] P. Hoffmann, G. BenAssayag, J. Gierak, J. Flicstein, M. Maar-Stumm, H. van Bergh, J. Appl. Phys. **74** , 7588 (1993), (http://dx.doi.org/10.1063/1.354985)

[302] L. Rosa, K. Sun, V. Mizeikis, S. Bauerdick, L. Peto, and S. Juodkazis, J. Phys. Chem. **115**, 5251 (2011), (http://dx.doi.org/10.1021/jp109099m)

[303] G. Gervinskas , G. Seniutinas , L. Rosa , and S. Juodkazis, Adv. Optical Mater. **1**, 456 (2013), (http://dx.doi.org/10.1002/adom.201300027)

[304] L. Bischoff, Nucl. Instr. Meth. in Phys. Res. B **266**, 1846 (2008), (http://dx.doi.org/10.1016/j.nimb.2007.12.008)

[305] R. Böttger, L. Bischoff, B. Schmidt, and M. Krause, *Characterization of Si nanowires fabricated by Ga^+ FIB implantation and subsequent selective wet etching*, J. Micromech. Microeng. **21,** 095025 (2011), (http://dx.doi.org/10.1088/0960-1317/21/9/095025)

[306] L. Bischoff, and B. Schmidt, Solid State Electronics **47**, 989 (2003), (http://dx.doi.org/10.1016/S0038-1101(02)00456-2)

[307] Ch. Akhmadaliev, L. Bischoff, and B. Schmidt, Materials Science and Engineering **C 26**, 818 (2006), (http://dx.doi.org/10.1016/j.msec.2005.09.026)

[308] P. Philipp, L. Bischoff, U. Treske, B. Schmidt, J. Fiedler, R. Hübner, F. Klein, A. Koitzsch, and T. Mühl, „The origin of conductivity in ion-irradiated diamond-like carbon – Phase transformation and atomic ordering", Carbon **80**, 677 (2014), (http://dx.doi.org/10.1016/j.carbon.2014.09.012)

[309] F. Ghaleh, R. Köster, H. Hövel, L. Bruchhaus, S. Bauerdick, J. Thiel, and R.. Jede, J. Appl. Phys. **101**, 044301 (2007), (http://dx.doi.org/10.1063/1.2450677)

[310] F. Ghaleh, PhD thesis, TU Dortmund (2008), (http://dx.doi.org/10.17877/DE290R-8610)

[311] J. Gierak, E. Bourhis, R. Jede, L. Bruchhaus, B. Beaumont, and P. Gibart, Microelectr. Eng. 73-74, 610 (2004), (http://hdl.handle.net/2003/29512)

[312] R. Kometani , K. Kanada, Y. Haruyama, T. Kaito, and S. Matsui, Jap. J. Appl. Phys. **45**, L711 (2006), (http://dx.doi.org/10.1143/JJAP.45.L711)

[313] J. Fujita, M. Ishida, T. Sakamoto, Y. Ochiai, T. Kaito, and S. Matsui, J. Vac. Sci. Technol. B **19**, 2834 (2001), (http://dx.doi.org/10.1116/1.1417545)

[314] T. Liang, A. Stivers, R. Livengood, P.-Y. Yan, G. Zhang, and F.-C. Lo, J. Vac. Sci. Technol. B **18**, 3216 (2000), (http://dx.doi.org/10.1116/1.1319687)

[315] R. Kometani, T. Hoshino, K. Kondo, K. Kanda, Y. Haruyama, T. Kaito, J. Fujita, M. Ishida, Y. Ochiai, and S. Matsui, J. Vac. Sci. Technol. B **23**, 298 (2005), (http://dx.doi.org/10.1116/1.1849211)

[316] J. Igaki, R. Kometani, K. Nakamatsu, K. Kanda, Y. Haruyama, Y. Ochiai, J. Fujita, T.Kaito, and S. Matsui, Microelec. Eng. **83**, 1221 (2006), (http://dx.doi.org/10.1016/j.mee.2005.12.022)

[317] J. Nilsson, J. R. I. Lee, T. V. Ratto, and S. E. Létant, Adv. Mat. **18**, 427 (2006), (http://dx.doi.org/10.1002/adma.200501991)

[318] T. Hoshino, A. Ozasa, R. Kometani, T. Suzuki, S. Matsui, and K. Mabuchi, J. Vac. Sci. Technol. B **24**, 2538 (2006), (http://dx.doi.org/10.1116/1.2359730)

[319] Chan 2007 - W. L. Chan, and E. Chason, J. Appl. Phys. **101**, 121301 (2007), (http://dx.doi.org/10.1063/1.2749198)

[320] L. Bischoff, K.-H. Heinig, B. Schmidt, S. Facsko, and W. Pilz, Nucl. Instrum. Meth. i. Phys. Res. B **272**, 198 (2012), (http://dx.doi.org/10.1016/j.nimb.2011.01.064)

[321] S. Ichim, and M. J. Aziz, J. Vac. Sci. Technol. B **23**. 1068 (2005),(http://dx.doi.org/10.1116/1.1897711)

[322] Q. Wei, X. Zhou, B. Joshi, Y. Chen, K.-D. Li, Qihuo Wei, K. Sun, and L. Wang, , Adv. Mat. **21**, 2865 (2009), (http://dx.doi.org/10.1002/adma.200803258)

[323] S.T. Purcell, Y.T. Binh, and P. Thevenard, Nanotechnology **12**, 168 (2001), (http://dx.doi.org/10.1088/0957-4484/12/2/320)

[324] C. Perez-Martinez, S. Guilet, N. Gogneau, and Pascale Jegou, J. Gierak and P. Lozano, J. Vac. Sci. Technol. B **28**, L25 (2010), (http://dx.doi.org/10.1116/1.3432125)

[325] F. Ullmann, F. Großmann, V. P. Ovsyannikov, J. Gierak, G. Zschornack,Appl. Phys. Lett. **90**, 083112 (2007), (http://dx.doi.org/10.1063/1.2454699)

[326] B. Knuffman, A. V. Steele, and J. J. McClelland, J. Appl. Phys. **114**, 044303 (2013), (http://dx.doi.org/10.1063/1.4816248)

[327] V. Z.-H. Chan, J. Hoffman, V. Y. Lee, H. Iatrou, A. Avgeropoulos, N. Hadjichristidis, R. D.Miller, and E. L. Thomas, Science **286**, 1716 (1999), (http://dx.doi.org/10.1126/science.286.5445.1716)

[328] J. Y. Cheng, A. M. Mayes, and C. A. Ross, Nature Mat. **3**, 823 (2004), (http://dx.doi.org/10.1038/nmat1211)

[329] A. F. Hannon, K. W. Gotrik, C. A. Ross, and A. Alexander-Katz, ACS macro Lett. **2**, 251 (2013), (http://dx.doi.org/10.1021/mz400038b)

[330] R. A. Mickiewicz, J. K. W. Yang, A. F. Hannon, Y.-S. Jung, A. Alexander-Katz, K. K. Berggren, and C. A. Ross, Macromolecules **43**, 8290 (2010), (http://dx.doi.org/10.1021/ma101360f)

[331] L.. Qin, S. Park, L. Huang, and C. A. Mirkin, Science **309**, 113 (http://dx.doi.org/10.1126/science.1112666)

[332] R. Behrisch, W. Eckstein (ed.), in *sputtering by particle bombardment*, Springer Berlin, Germany, ISBN 978-3540445005 (2007)